A RELATIVISTIC APPROACH TO STRUCTURE FORMATION AND EVOLUTION IN A FRIEDMANN UNIVERSE

KENNEDY KAMUREN KONGA

A Thesis Submitted in Partial Fulfillment for Conferment of Degree of Master of Science in Physics of Meru University of Science and Technology

2025

DECLARATION

This thesis is my original work and has not been presented for the award of a degree in any other university.

Signature: ……. Date: 24th May, 2025

Kennedy Kamuren Konga, B.Sc

SC409/201101/20

DECLARATION BY SUPERVISORS

This thesis has been submitted with our approval as the University Supervisors.

Signature…… Date……..

Dr. Dismas Simiyu Wamalwa, PhD

Meru University of Science & Technology, Kenya

Signature…… Date……..

Dr. Dickson Mwenda Kinyua, PhD

Kirinyaga University, Kenya

Signature…… Date……..

Dr. Daniel Maitethia Memeu, PhD

Meru University of Science & Technology, Kenya

ACKNOWLEDGEMENT

I am deeply grateful for the invaluable support provided by Meru University of Science and Technology during the course of this research. I extend my heartfelt appreciation to the Department of Physical Sciences, including both the faculty and fellow M.Sc students, for their insightful contributions.

A special acknowledgment goes to my esteemed supervisors, Dr. Dismas Simiyu Wamalwa, Dr. Dickson Mwenda Kinyua, and Dr. Daniel Memeu Maitethia. Their guidance and unwavering support have been instrumental in the success of this work, and for that, I am sincerely thankful.

TABLE OF CONTENTS

LIST OF FIGURES

LISTOF APPENDICES

ACRONYMNS AND ABBREVIATIONS

BAO	Baryonic acoustic oscillations
R(t)	Cosmic scale factor
CMBR	Cosmic Microwave Background Radiation
COBE	Cosmic Background Explorer
CDDR	Cosmic distance duality relation
λ	Cosmological constant
DE	Dark energy
DESI	Dark Energy Spectroscopic Instrument
DM	Dark matter
ρ	Density of the universe
EFE	Einstein field equations
$G_{\mu\nu}$	Einstein Tensor
$T_{\mu\nu}$	Energy-Momentum Tensor
ESA	European Space Agency
eBOSS	extended Baryonic Oscillation Spectroscopic Survey
FLRW	Friedmann Lemaitre Robertson Walker
G	Gravitational constant
H	Hubble constant
IAU	International Astronomical Union
ΛCDM	Lambda cold dark matter
LTB	Lemaitre-Tolman-Bondi
I	Light intensity
$g_{\mu\nu}$	Metric Tensor
n(z)	Number density
R	Radius of the universe
z	Redshift
RSD	Redshift-space distortions
$R_{\mu\nu}$	Ricci Tensor
SCM	Standard Cosmological Model
c	Speed of light
SDSS	Sloan Digital Sky Survey

ABSTRACT

The advent of modern satellite technology has transformed observational astronomy and astrophysics, offering unprecedented insights into the large-scale behavior of gravitation and challenging established cosmological models. This technological progress has reinvigorated the study of relativistic cosmology, leading to a critical reassessment of foundational assumptions, particularly the cosmological principle, which posits that the universe is homogeneous and isotropic on large scales. While this principle underpins the Standard Cosmological Model (SCM) and the Friedmann-Lemaitre-Robertson-Walker (FLRW) metric, emerging data has increasingly been challenging its validity. Central to this investigation are the redshift-distance and light intensity-distance relations, essential for testing cosmological models. The integration of both parametric and nonparametric redshift models provides a more comprehensive analysis, addressing discrepancies in our understanding of the universe's structure and evolution. However, unresolved mysteries, particularly concerning dark matter and dark energy, complicate these models. This research critically examines the cosmological principle using the latest observational data and scrutinizes the Friedmann model's assumptions. The study reveals that galaxy formation occurred most rapidly in the early universe, particularly within the redshift range of $0 < z < 0.4$, peaking around $z \approx 0.8$. It also highlights that dark matter plays a significantly more critical role than dark energy in this process. While dark energy primarily affects the large-scale expansion of the universe, dark matter seems to dominate local galaxy formation and the evolution of cosmic structures. These findings underscore the limitations of current models and contribute to the ongoing refinement of cosmological theories, offering a clearer understanding of the universe’s evolution.

CHAPTER 1: INTRODUCTION

1.1 Background

The advent of modern satellite technology in observational astronomy has revolutionized astrophysics, enabling unprecedented insights into the large-scale behavior of gravitation and pushing the boundaries of cosmological research. This technological leap has reinvigorated the study of relativistic cosmology, compelling the scientific community to reconsider several foundational models that have long guided our understanding of the universe (Ijjas et al., 2013, 2017; Tucker et al., 2019). At the heart of these models lies the cosmological principle, which posits that the universe, when viewed on sufficiently large scales, is both homogeneous and isotropic—a cornerstone assumption rooted in Einstein's 1917 geometrical framework (Einstein, 1917). Despite this principle's foundational role in the Standard Cosmological Model (SCM), emerging data increasingly challenges its validity, raising profound questions about our understanding of the universe's true nature.

The cosmological principle asserts that, beyond a certain scale, the universe's matter distribution becomes statistically uniform, smoothing out the apparent inhomogeneities and anisotropies observed at smaller scales (Park et al., 2017). This principle underpins the Friedmann-Lemaitre-Robertson-Walker (FLRW) metric, the standard model used in contemporary cosmology to describe the universe's large-scale structure and evolution (Melia, 2022b).

$$G^{\mu\nu} + \lambda\, g^{\mu\nu} = \frac{8\pi G}{c^4} T^{\mu\nu} \tag{1.1}$$

where $G^{\mu\nu}$ is the Einstein tensor, $g^{\mu\nu}$ is the metric tensor, λ is the cosmological constant, c is the speed of light, G is the Newton's universal gravitational constant, and $T^{\mu\nu}$ is the energy-momentum tensor (Fomin & Chervon, 2017).

Distinctions among these models arise not from the solutions to Einstein's equations (see equation (1.1)) but from the selection of the stress-energy tensor ($T_{\mu\nu}$), specifically influencing the expansion factor, R(t), in the spatial line element (Melia, 2022a).

The SCM, which relies heavily on the FLRW metric and the principles of general relativity, assumes statistical homogeneity and isotropy at large scales, thereby simplifying the complex dynamics of the universe into a model that has generally aligned with observational evidence (Wang et al., 2023).

However, recent findings, such as the Hubble tension and the fine-tuning problems, have exposed cracks in this model, suggesting that the universe may not adhere as closely to these assumptions as previously thought (Díaz-Pachón et al., 2023; Krishnan et al., 2021; S. Weinberg, 1989).

Key to this discussion are the redshift-distance and light intensity-distance relations, which are fundamental tools in observational cosmology. The redshift-distance relation provides critical insights into the universe's expansion rate, serving as a direct test of cosmological models.

Accurate measurements of redshift and corresponding distances allow cosmologists to map the large-scale structure of the universe, revealing patterns that either support or challenge the assumptions of homogeneity and isotropy. Similarly, the light intensity-distance relation, which describes how the observed brightness of an object diminishes with distance, is crucial for determining cosmological distances and, by extension, for understanding the universe's expansion history. Both relations are integral to testing the validity of the Friedmann model and the cosmological principle, particularly in light of the growing complexity observed in deep-space surveys.

To refine the understanding of these relations, recent studies have employed both parametric and nonparametric redshift models. Parametric models rely on predefined functional forms and assumptions about the universe's expansion history, such as the commonly used lambda cold dark matter (ΛCDM) model, which assumes a specific functional form for the expansion rate and matter density (Bassett et al., 2015).

Nonparametric models, on the other hand, do not assume a particular functional form and instead use data-driven approaches to infer the redshift-distance relation directly from observations (Wojtak & Prada, 2017). These models offer greater flexibility and can capture deviations from the standard parametric assumptions, providing a more nuanced view of the universe's structure and evolution (Nyagisera et al., 2024). The integration of both parametric and nonparametric approaches allows for a more comprehensive analysis of the redshift-distance relation, potentially addressing discrepancies and refining our understanding of the cosmological principle.

Compounding these theoretical challenges are the enigmatic dark matter (DM) and dark energy (DE), which together make up 95% of the universe's total mass-energy content. While DM is crucial for explaining the flat rotation curves of galaxies and the formation of large-scale structures, DE is invoked to account for the observed acceleration in the universe's expansion—a phenomenon first detected through observations of Supernovae Type Ia (Jeakel et al., 2024). Yet the physical nature of these two phenomena remains a mystery.

Einstein suggested a long-forgotten solution: gravitationally repulsive negative masses, which drive cosmic expansion and cannot coalesce into light-emitting structures (Farnes, 2018). In addition, a type of cold dark matter in the universe is needed to explain the formation of the cosmic structure and galaxy dynamics. So far, it has been claimed that the cosmological

constant is the best candidate to explain the so-called dark energy (Wang et al., 2023). These unresolved issues further complicate the cosmological models, demanding more precise observational data and innovative theoretical approaches.

The Cosmological Principle (CP) assumes uniformity on large scales, but limited observations prevent definite confirmation or refutation. While we see structures suggesting unevenness, we can't determine if this persists at the largest scales. Until observational methods improve, the CP remains an assumption.

Three-dimensional redshift surveys, despite their sophistication, often produce limited and potentially misleading data due to inherent uncertainties in cosmic distance measurements and the complexity of interpreting large-scale structures. For instance, while observational evidence generally supports isotropy on large scales—demonstrated by the Cosmic Microwave Background Radiation (CMBR), and isotropic distributions of radio sources, gamma-ray bursts, and supernovae (Blake & Wall, 2002; Penzias & Wilson, 1967).

These findings do not unequivocally confirm large-scale homogeneity. Notably, quasar distribution studies suggest homogeneity only beyond scales of $250\,h^{-1}$ Mpc (Pandey & Sarkar, 2016), , highlighting the need for more rigorous testing.

This research aims to address these critical issues by critically examining the cosmological principle in the context of the most precise observational data as per current technology. By scrutinizing the underlying assumptions of the Friedmann model, this study seeks to determine whether the universe's large-scale structure truly conforms to the principles of homogeneity and isotropy, or if these concepts require revision in light of new evidence.

Moreover, recent efforts to apply the Einstein field equations (EFE) to describe the universe's relativistic dynamics during the current matter-dominated era have highlighted discrepancies between theoretical models and observations (Langa et al., 2017).

This research builds on these efforts, aiming to refine our understanding of the universe's evolution and reconcile theoretical predictions with empirical data. By bridging the gap between observation and theory, this study endeavors to contribute to the ongoing refinement of cosmological models, potentially leading to a more accurate and comprehensive understanding of the universe's structure and dynamics.

1.2 Problem statement

The Friedmann model, a key framework in cosmology, has traditionally been supported by observational evidence in explaining the structure and evolution of the universe. However, as redshift surveys delve deeper, they revealed cosmic structures of increasing complexity that challenged the model's foundational assumption of large-scale homogeneity.

The persistent uncertainty in cosmic distance measurements, despite advanced technology, coupled with limited observational data that were prone to misinterpretations further undermined the model's precision in describing the distribution of luminous matter. This compelled us to reconsider the adequacy of the Friedmann model if it can truly account for the observed structures in the universe. We therefore, considered a critical examination of the model's assumptions in light of the most recent observational data based on three astronomical quantities: redshift, light intensity and number density.

1.3 Objectives

1.3.1 General objective

To describe relativistic dynamics and structure formation in the Friedmann Universe

1.3.2 Specific objectives

i. To review Einstein's field equations relevant to relativistic dynamics and structure formation in the Friedmann Universe.

ii. To derive the inter-relationship between redshift and light intensity for the Friedmann Universe.

iii. To determine the inter-relationship between redshift and the number density of galaxies in the Friedmann Universe.

iv. To describe structure formation and evolution in the Friedmann Universe based on variation of redshift with light intensity and on redshift with the number density.

1.4 Justification of the study

Astronomical investigations play a crucial role in understanding the formation and distribution of structures across vast length scales in the universe. The presence of inhomogeneities offers a potential explanation for global cosmic acceleration without necessitating an extra cosmological principle, has effectively explained the process of structure formation in the universe, becoming an indispensable tool for astrophysicists.

Consequently, the recognition of large-scale inhomogeneity in the formation and distribution of celestial objects, contrary to the homogeneous universe supported by the cosmological principle, would represent a groundbreaking shift not only in physics but also in the broader realm of science.

CHAPTER 2: LITERATURE REVIEW

2.1 Evolution of the Universe

The field of cosmology, like the construction of a monumental pyramid, has been an ongoing endeavor characterized by continuous growth and expansion, with its ultimate height remaining uncertain. This analogy aptly captures the essence of cosmology as a scientific discipline that has evolved, adapting to the challenges and questions that emerge with each discovery.

Much like the pyramid's base must be robust enough to support additional layers; cosmological theories have had to be fortified with new elements to address the ever-evolving puzzles of the universe. In doing so, these theories have propelled us toward a deeper understanding of the physical world, often leading us into uncharted territories of knowledge. Yet, a fundamental and perplexing question persists: how strong is the foundation of cosmology, and can it withstand the weight of incorporating new aspects and confronting fresh challenges? This question, while lacking a definitive answer at present, lies at the heart of cosmological exploration and drives researchers to delve into new dimensions of the physical universe.

Gamow (1946) laid the groundwork for the expanding universe concept and delved into the origins of chemical elements. Building upon this, Alpher, Bethe, and Gamow extended the narrative, contributing significantly to the formulation of the Big Bang theory (Alpher et al., 1948). Their work provided critical insights into the synthesis of elements during the early stages of the universe, marking a pivotal moment in our understanding of cosmological evolution and the events that shaped the universe into what we observe today.

Peebles (1980) offered a profound exploration of the large-scale structure of the universe, elucidating the organizational principles governing cosmic components. Guth's (1981) proposal of inflationary cosmology was a breakthrough in addressing cosmological problems like the horizon and flatness issues. Extending this line of thought, Linde's (1982) scenario offered a compelling solution to additional challenges, such as homogeneity, isotropy, and the overabundance of primordial monopoles in the early universe. These contributions significantly enriched our comprehension of the early universe, providing a coherent framework that explained its rapid expansion and various observed characteristics.

Kolb and Turner's (1990) book seamlessly connected the standard model of particle physics with the early universe, providing an accessible yet detailed exploration of the theoretical foundations. Complementing this, S. Weinberg's (1972) work elucidated the principles and applications of general relativity, contributing to the broader understanding of how fundamental forces shape the cosmic landscape.

Mather et al.'s (1990) study was a milestone, presenting a preliminary measurement of the Cosmic Microwave Background (CMB) spectrum using the Cosmic Background Explorer (COBE) satellite. Subsequently, Smoot et al. (1992) scrutinized the first-year COBE differential microwave radiometer maps, revealing intricate structures in the CMB. These observations confirmed the existence of the cosmic microwave background, a crucial piece of evidence supporting the Big Bang theory and our understanding of the universe's early phases.

Cohen, Kaplan, and Nelson's 1993 review marked progress in electroweak baryogenesis, providing a comprehensive examination of the mechanisms behind the origin of baryonic matter in the universe (Cohen et al., 1993) . Sakharov (1998), in revision of his 1967 seminal paper, introduced the Sakharov conditions for baryogenesis, addressing critical issues like the

violation of cosmological principle invariance and the asymmetry between matter and antimatter .These works advanced our understanding of the fundamental processes that led to the predominance of matter over antimatter in the cosmos.

Peebles and Ratra's comprehensive review in 2003 explored the cosmological constant and the enigmatic concept of dark energy (Peebles & Ratra, 2003). In parallel, Bertone, Hooper, and Silk's 2005 study delved into the complex realm of particle dark matter, presenting evidence, potential candidates, and constraints (Bertone et al., 2005). These works collectively navigated the mysteries surrounding dark matter and dark energy, pivotal components in the standard model, offering insights into their roles and implications for the large-scale structure and expansion of the universe.

Parallelly, Springel et al. (2005) study employed sophisticated simulations to analyze the formation, evolution, and clustering of galaxies and quasars. Together, these works not only provided theoretical frameworks but also laid the groundwork for understanding the intricate dance of cosmic structures, offering a glimpse into the dynamic evolution of the universe on a grand scale.

2.2 Review of homogeneity and fractality in the Universe

The history of cosmological thought has been marked by a persistent debate between the concepts of homogeneity and fractality in describing the structure of the universe. This debate has deep roots, dating back to the pioneering work of Isaac Newton and evolving through subsequent centuries. In this review, we will explore the historical progression of these ideas and the key figures who contributed to this ongoing discourse, highlighting the significance of their contributions.

Carl Charlier, in a significant departure from the notion of homogeneity, proposed a hierarchical model of the universe (Charlier, 1908, 1922). In Charlier's model, stars were arranged in a manner such that their densities, as perceived from any given star, decreased with increasing distance. This hierarchical arrangement marked a pivotal moment in cosmological thought, as it represented the first fractal model of the universe. This model challenged the prevailing view of cosmic uniformity and introduced the idea of self-similarity at different scales- fractality.

The introduction of the Einstein equations and their application to cosmology by Einstein, Friedmann, de Sitter, and Lemaitre in the early 20th century elevated the cosmological principle—a notion of homogeneity and isotropy when averaged over some scale to a central tenet in cosmology (Friedmann, 1922; Lemaitre, 1925). These equations provided a mathematical framework for describing the evolution of the universe. The cosmological models based on Friedmann's equations gained remarkable success in explaining observed phenomena and predicting discoveries.

However, in the 1980s, with the completion of the redshift campaign, it became apparent that the universe displayed significant non-uniformities (Peebles, 1980). The data indicated that the assumptions of the Friedmann equations may only be valid on cosmological scales of up to about thirty mega-parsecs. This revelation marked a significant shift in our understanding of the cosmos, emphasizing the need to incorporate inhomogeneous structures into our cosmological models.

Isaac Newton made one of the earliest proposals regarding the structure of the cosmos. Newton posited that a system of stars could resist gravitational collapse if they were initially arranged in a manner that ensured equal spacing among them. In this configuration, each star

would experience uniform gravitational attraction from all directions, maintaining their relative positions (Newton, 1993).

This concept is fundamentally homogeneous, with its underlying premise relying on uniformity. Newton also proposed that stars possess equal intrinsic brightness and are arranged by magnitude in a manner consistent with their distance from an observer, further reinforcing the notion of homogeneity (Amendola, 1998).

Eisenstein and Hu (1998) explored baryonic effects on the matter power spectrum using cosmological perturbation theory and numerical simulations. They identified baryonic acoustic oscillations (BAO) as significant features influenced by early universe physics and baryon-photon interactions. These oscillations imprint distinct patterns on the matter transfer function, crucial for understanding structure formation and cosmological parameter estimation.

The study emphasized damping effects on small scales due to baryon interactions, impacting observational strategies like galaxy surveys and cosmic microwave background measurements. While insightful, the theoretical framework assumes ideal conditions and simplifications, requiring validation against observational data to address uncertainties and ensure robust cosmological interpretations.

Conn et al. (2013) discovered that while the satellites of M31 as a whole do not exhibit any more planar alignment than expected randomly, approximately half of the sample forms a remarkably thin disk. This distinct plane of satellites was a prominent feature in their analysis. They also noted a significant degree of asymmetry in the satellite distribution, particularly noteworthy for its strong alignment with the direction of the Milky Way.

The orthogonal arrangement observed between the Milky Way's disk and M31's satellite distribution suggests a possible coupling between the two halos. This plane of satellites contradicts expectations from ΛCDM cosmology, suggesting the existence of thin satellite disks in galaxy halos challenging the standard model's predictions. The study underscores the need for further investigation into whether current cosmological models can fully explain such structures.

Alam et al. (2021) analyzed data from the Sloan Digital Sky Survey (SDSS) and the extended Baryon Oscillation Spectroscopic Survey (eBOSS) to investigate the large-scale structure of the universe. Using baryon acoustic oscillations (BAO) and redshift-space distortions (RSD), they measured cosmological parameters such as the matter density (Ω_m) and the Hubble parameter (H_o), providing strong support for the ΛCDM model.

The study's results were consistent with previous measurements and highlighted the importance of combining different cosmological probes. However, the reliance on the ΛCDM model, potential observational biases, and cosmic variance present limitations. Overall, the study reinforced the homogeneity and isotropy of the universe on large scales while contributing to the ongoing debate on dark energy and the Hubble constant.

Pastén & Cárdenas (2023) revisited the issue of describing an average fractal distribution of matter using a Lemaitre–Tolman–Bondi (LTB) solution. They focused on the fractal structure of the local universe, considering its fractal dimension and scale transition, while ensuring a homogeneous bang-time function.

The model was tested against the latest type Ia supernova data from the Pantheon compilation. They discussed the model's challenges and potential improvements, concluding that a fractal transition in LTB cosmology cannot explain the effects of dark energy without necessitating

an inhomogeneous big bang. However, the approach remains valuable for studying structures at smaller scales.

Wang et al. (2023) proposed two types of parametrizations for deviations from the FLRW metric and tested the FLRW metric using specific sound horizon scale priors. To avoid bias from these priors, they performed a consistency test with a flat prior for the sound horizon scale. Their findings indicated a concordance between the FLRW metric and observational data using both parametric and nonparametric methods. These parametrizations offer a new, sound horizon scale-independent approach to testing the FLRW metric.

Langa et al. (2017) proposed a framework of determining the dynamics and evolution of the universe by deriving and modeling Einstein field equations relevant to the matter-dominated universe in the presence of dark energy. He found a connection between redshift and the distribution of matter within the framework of the Friedmann universe.

However, the results was not compared with observations. Nyagisera et al., (2024) extended the groundwork laid by this research. They introduced a modification of the conventional redshift adopting parametric and nonparametric models, providing a fresh perspective on the Friedmann equations.

From their work, a critical observation emerged concerning the differential impact of the cosmological constant on structure formation. The study posited that the cosmological constant within the standard redshift model exhibited a less pronounced effect on late-time structure formation growth compared to the modified model in agreement with some observational evidence. Their work was also purely theoretical without any retrieved observational data for comparison.

This motivates our study as we depart from invoking the conservation principle as used in earlier studies (Langa et al., 2017; Nyagisera et al., 2024) and acquisition of observational data to effectively describe the universe's structure and dynamics.

2.3 Review of cosmic distance measurements

Edwin Hubble, a luminary in the realm of cosmology, occupies an indelible place in the annals of scientific history for his pioneering work that reshaped our comprehension of the cosmos. His revolutionary contribution, famously known as the Hubble Law, served as a seismic shift in the world of astrophysics and fundamentally altered our perspective on the universe's workings (Hubble, 1929).

Hubble's profound insights were grounded in the meticulous observational data painstakingly amassed by Vesto Slipher, data that focused on the spectral signatures of celestial systems (Slipher, 1915). The collation and analysis of this data by Hubble precipitated a momentous realization—an epiphany that rippled through the corridors of cosmology—that the universe was indeed expanding .

The 3-dimensional catalogs compiled by these ambitious astronomical projects offer a panoramic view of the cosmos, providing a wealth of information about the spatial distribution of galaxies and their distances from our vantage point. These comprehensive catalogs reveal a strikingly inhomogeneous distribution of galaxies, both at smaller and larger distances, casting doubts upon the long-held cosmological assumption of statistical isotropy and homogeneity on cosmic scales exceeding $150^{-1}Mpc$ (Labini et al., 1998).

In our contemporary epoch, astronomers find themselves immersed in an era of relentless exploration and research, as they endeavor to understand cosmic landscape that extends far beyond the confines of our immediate cosmic neighborhood. This quest for cosmic

understanding has witnessed monumental milestones, and one of the most noteworthy achievements in this quest was the launch of the Hipparcos satellite by the European Space Agency (ESA).

The inception of this groundbreaking spacecraft heralded the creation of the first comprehensive star chart, a pivotal moment that unfurled new vistas for astronomers, enabling them to precisely gauge the distances to celestial objects situated hundreds of parsecs away from Earth (Heck & Caputo, 1999).

In the contemporary landscape of observational cosmology, one project stands as a testament to human ambition and technological prowess—the Sloan Digital Sky Survey (SDSS). This monumental undertaking aspires to chart the most extensive map of the universe ever conceived. It is essential to recognize, however, that despite its grandeur, the SDSS covers only a fraction of the three-dimensional celestial sphere. Nonetheless, the data emanating from the SDSS, when scrutinized within the confines of a volume-limited context, has unveiled astonishing revelations (Yamamoto, 2003)..

It has specifically laid bare a pattern of clustering among galaxies that extends to the largest scales, challenging the bedrock assumption of cosmic homogeneity on vast scales. This discovery beckons us to reevaluate our previous conceptions and delve deeper into the complex web of cosmic structures (Joyce et al., 2005).

Labini (2011) presented strategies to test the most common standard model assumptions and found evidence that, in the available samples, galaxy distribution is spatially inhomogeneous for $r < 100\ Mpc\ h^{-1}$ but statistically homogeneous and isotropic. They concluded that the observed inhomogeneities not only pose a fundamental challenge to the standard picture of

cosmology but also present an important opportunity that may open new directions for many cosmological puzzles.

Within the precincts of the scientific community, the International Astronomical Union (IAU) symposium 289 dedicated focus on the physics underpinning the methodologies utilized in determining cosmic distances throughout the vast cosmic expanse. This symposium was a place where scientists shared ideas and explored different ways to tackle the tough challenge of measuring cosmic distances (de Grijs, 2012; Freedman, 2012).

Importantly, it was a testament to the uncharted territory that still looms large in our understanding of cosmic distances. Despite considerable progress, it underscored the fact that each method employed thus far was fraught with its own unique set of uncertainties, thus making the pursuit of cosmic distance determination a profoundly formidable endeavor.

Damjanov et al. (2014) used BOSS spectroscopic data to identify around 200 compact galaxy candidates at $0.2 < z < 0.6$, exhibiting spectral characteristics typical of quiescent systems. They analyzed 14 of these candidates using CFHT MegaCam images to measure their sizes and structural properties.

The study confirmed that all selected BOSS-CFHT targets were compact, suggesting that at least 82% of the parent BOSS sample (approximately 160 galaxies) are also compact. Their findings indicated that these intermediate-redshift compact galaxies vary in velocity dispersion ($100\,km\,s^{-1}\ to\ 320\,km\,s^{-1}$), with a minority in a post-starburst phase and a significant fraction dominated by old stellar populations formed at $z > 2$.

The galaxies' small sizes resembled those of high-redshift compact systems and were significantly smaller than typical massive galaxies at $z \sim 0$ in size-velocity dispersion parameter space. Furthermore, the study derived dynamical masses for these galaxies,

revealing a size-dynamical mass relation distinct from that of $z \sim 0$ galaxies with similar masses. The research underscored the importance of intermediate-redshift compact galaxies in understanding their structure, evolution, and environmental dependence, offering insights not easily attainable at higher redshifts.

Ntelis (2016) examined the homogeneity scale of our universe using the BOSS CMASS galaxy sample in the redshift region of $0.43 \leq z \leq 0.7$. By measuring the fractal correlation dimension, $D_2(r) = \frac{dln\, N(<r)}{dlnr} + 3$ and its scale dependence, they found that $D_2(r)$ approaches the homogeneous value asymptotically, indicating a homogeneous distribution on scales larger than $R_H = 64.3 \pm 1.6h^{-1}\, Mpc$ for redshifts $0.538 \leq z \leq 0.592$. Below this scale, the distribution exhibited fractal behavior.

The discovery of inhomogeneities or fractal patterns on cosmic scales carries profound implications for our understanding of the universe's physical properties as delineated by general relativity. These inhomogeneities offer an alternative explanation for the phenomenon of global cosmic acceleration, without necessitating the introduction of a dark energy component (Ellis, 2011). This revelation compels us to scrutinize the very foundations of the cosmological principle and the standard theory of cosmology, which have long been regarded as pillars of our cosmic understanding.

However, this requires a huge amount of accurate data, which our current technology cannot yet collect. Even the largest of endeavors, such as the Sloan Digital Sky Survey (SDSS), covers only a minuscule fraction of the celestial sphere (Pâris et al., 2017).

Wojtak and Prada (2017) integrated cosmological probes including CMB data from Planck, Type Ia supernovae, Baryon Acoustic Oscillations (BAO), cosmic chronometers, and local Hubble constant measurements to propose a new cosmological model with redshift remapping

between observed redshift z and cosmic scale factor $R(t)$. This model successfully addressed discrepancies in the standard ΛCDM framework, particularly anomalous BAO signals and Hubble constant inconsistencies. It supports a nearly flat universe $\Omega_m = 0.87 \pm 0.03$ when including all data, aligning with an Einstein-de-Sitter model if excluding cosmic chronometer data.

The reconstructed redshift remapping shows deviations from the standard relation decreasing with redshift, suggesting late-time cosmic evolution effects. Predictions include significant differences in Hubble constant measurements and a power spectrum shape similar to ΛCDM, with adjustments to the lensing template consistent with Planck observations.

The future of observational cosmology promises even more spectacular revelations with the imminent launch of the Vera Rubin Observatory in Chile. Equipped with a state-of-the-art 3.6-gigapixel camera, this observatory is poised to image the entire visible night sky in exquisite detail. Its mission transcends the boundaries of our solar system, delving deep into the extragalactic universe to capture cosmic explosions and unveil the elusive effects of dark matter (Brough et al., 2020).

Xu et al. (2022) proposed a new model-independent test for the cosmic distance duality relation (CDDR) using the Pantheon SNIa sample and the latest BAO measurements, including the eBOSS DR16 quasar sample at $z = 1.48$. Three parameterizations of $\eta(z)$ were used to describe potential CDDR violations: $\eta(z, \eta 1) = 1 + \eta 1 z, \eta(z, \eta 2) = 1 + \eta 2 z/(1+z)$, and $\eta(z, \eta 3) = 1 + \eta 3 ln(1+z)$.

To address the redshift-matching problem; a mismatch between observed and expected redshift-distance relations, two methods were employed to derive m_B values at BAO measurement redshifts: a compressed form of the Pantheon SNIa sample using a piecewise

linear function of $ln(z)$ and the binning SNIa method for $z < 1$ combined with the ANN method at $z = 1.48$. Results indicated that CDDR tests are insensitive to $\eta(z)$ parameterization, showing no significant CDDR violations.

High-redshift BAO and SNIa data improved parameter constraints, reducing confidence intervals by 33%, 21%, and 26% (first method) and 36%, 22%, and 29% (second method). The compressed Pantheon sample method provided more precise m_B values and stricter constraints. The study noted the difficulty of testing CDDR at higher redshifts due to the limited high-redshift SNIa sample. Future observations from the Euclid satellite and DESI could offer better CDDR validation. The compressed observation method could also be extended to other high-redshift standard candles, such as gamma-ray bursts and H II galaxies, for further CDDR testing.

The magnitude of the challenge before us is nothing short of monumental, requiring a profound shift in our approach to cosmic exploration. It hinges on the premise that addressing the intricate complexities of the universe calls for a departure from traditional reliance on distance measurements alone. A novel paradigm is beginning to take shape, one that revolves around the accumulation of vast, direct observational data. This emerging approach aspires to discern the fundamental nature of the universe, particularly the distribution of galaxies, within the framework of the Friedmann universe.

The assumption of the universe's density and the cosmic scale factor as constant in these works (Langa et al., 2017; Nyagisera et al., 2024) cast doubts on their compatibility with observations. This motivated an investigation of the dynamics and evolution of the universe by treating these parameters as variables in the current study. This is intended to generate an

appropriate model for effectively describing the structure formation and evolution of the universe.

CHAPTER THREE: METHODOLOGY

3.1 Einstein field equations based on the Friedmann metric

We examined the Einstein field equations within the Friedmann-Lemaitre-Robertson-Walker space-time framework.

Our primary objective was to deduce the specific Einstein field equations that are pertinent to our exploration of the universe's dynamics and evolution, leveraging on the FLRW metric as the foundation for our analysis;

$$g = c^2dt^2 - \frac{R^2(t)}{(1+\kappa r^2)^2}dr^2 \tag{3.1}$$

where $dr^2 = dx^2 + dy^2 + dz^2$ and the parameter$R(t)$, denoting the scale factor governing the time-dependent evolution of the spatial portion of the metric (specifically, the surfaces corresponding to constant time, t), alongside the parameter $\kappa = (-1,0,+1)$, which defines the geometry of these spatial sections as negatively curved, positively curved, or flat, respectively. Equation (3.1) remains the pivotal cosmological space-time metric, characterizing a universe that is isotropic, homogeneous, and undergoing cosmic expansion.

The rank 2 covariant metric tensor $g_{\mu\nu}$ was obtained as

$$g_{\mu\nu} = \begin{pmatrix} c^2 & 0 & 0 & 0 \\ 0 & \frac{-R^2(t)}{(1+\kappa r^2)^2} & 0 & 0 \\ 0 & 0 & \frac{-R^2(t)}{(1+\kappa r^2)^2} & 0 \\ 0 & 0 & 0 & \frac{-R^2(t)}{(1+\kappa r^2)^2} \end{pmatrix} \tag{3.2}$$

From equation (3.2), it has been shown in earlier work (Wamalwa, 2016) that;

$g_{00} = c^2$

and

$$g_{11} = g_{22} = g_{33} = -\frac{R^2(t)}{(1+\kappa r^2)^2}$$

leads to

$$g^{00} = \frac{1}{c^2} \tag{3.3}$$

and

$$g^{11} = g^{22} = g^{33} = -\frac{(1+\kappa r^2)^2}{R(t)^2} \tag{3.4}$$

The study also have the already derived curvature scalar and non-vanishing components of the Ricci tensor (Wamalwa, 2016) in the form;

$$R^{00} = -\frac{3R''(t)}{c^4 R(t)}$$

together with

$$R^{11} = R^{22} = R^{33} = -\frac{R(t)R''(t) + 2R'(t)^2 + 8\kappa c^2}{c^2 R(t)^4}(1+\kappa r^2)^2$$

The curvature scalar derived from the above equations became;

$$R = R^{\mu}_{\mu} = -\frac{3(2R(t)R''(t) + 2R'(t)^2 + 8\kappa c^2)}{c^2 R(t)^2} \tag{3.5}$$

Focusing on the dynamics and evolution of the universe, the Einstein field equations were considered as;

$$G^{\mu\nu} + \lambda\, g^{\mu\nu} = \frac{8\pi G}{C^4} T^{\mu\nu} \tag{3.6}$$

with

$$G^{\mu\nu} = R^{\mu\nu} - \frac{1}{2} R g^{\mu\nu}$$

where $R^{\mu\nu}$ is the Ricci tensor, $G^{\mu\nu}$ is the Einstein tensor, R is the Ricci scalar, $g^{\mu\nu}$ is the metric tensor, λ is the cosmological constant, and $T^{\mu\nu}$ is the energy-momentum tensor (Fomin & Chervon, 2017).

Just like the Ricci tensor components above, the stress-energy tensor also had the components with raised indices (Wamalwa, 2016) of the form;

$$T^{00} = \rho(t) \tag{3.7}$$

and

$$T^{11} = T^{22} = T^{33} = \frac{(1+\kappa r^2)^2}{R(t)^2} P(t) \tag{3.8}$$

where $\rho(t)$ and $P(t)$ are mass density and pressure of the universe respectively.

It has been shown from earlier studies (Langa et al., 2017; Nyagisera et al., 2024) that these equations lead to;

$$12\kappa c^2 + 3R'(t)^2 = \beta c^4 \rho(t)\, R(t)^2 - \lambda c^2 R(t)^2 \tag{3.9}$$

$$4\kappa c^2 + 2R(t)R''(t) + R'(t)^2 = \beta c^2 p(t) R(t)^2 - \lambda c^2 R(t)^2, \tag{3.10}$$

where $\beta = \frac{8\pi G}{c^4}$, $R'(t) = \frac{dR(t)}{dt}$ and $R''(t) = \frac{d^2R(t)}{dt^2}$

Equations (3.1) to (3.10) laid a foundational groundwork for this project.

In contrast to these existing works, this study used Friedmann equations without invoking the conservation principle $(\rho(t)R(t) = constant, \alpha)$ to derive relevant relativistic field equations to describe relativistic dynamics and structure formation in the Friedmann universe. In the next chapter, these equations yielded our specific Einstein field equations for describing the dynamics and evolution in a Friedmann universe in comparison with previous studies by Langa et al. (2017) and Nyagisera et al. (2024).

3.2 Variation of light intensity and number density with redshift

We took the assumption that we were given a substantial and direct dataset of astronomical objects i.e., galaxies. Importantly, this dataset was assumed free from assumptions about the background geometry or uncertainties associated with distance measurements. Here, the specific astronomical quantities we had at our disposal included:

i. Light intensity (I) from an astronomical object e.g., galaxy

ii. Measured redshift (z) of the light intensity from the given astronomical object in (i) above in a given direction

iii. The number density (n) per solid angle of a class of objects in a given direction.

In order to derive a relation between light intensity and redshift parameter at the beginning of light photon (emission) to the end of light photon (observation), light from an astronomical object located at $r(t_e)$ that emitted light at time t_e that was received by an observer positioned at $r(t_o)$ at time $t = 0$ was considered.

For null geodesic, $g = 0$ from equation (3.1) expressed as

$$0 = c^2\dot{t}^2 - \frac{R^2(t)}{(1+\kappa r^2)^2}\,\dot{r}^2 \tag{3.11}$$

or

$$c\dot{t} = \pm\frac{R(t)}{1+\kappa r^2}\,\dot{r} \tag{3.12}$$

where $dt/d\tau = \dot{t}, dr/d\tau = \dot{r}$

Applying the principle of reversibility of light, equation (3.12) becomes

$$\frac{c}{R(t)}\,dt = -\frac{1}{1+\kappa r^2}\,dr \tag{3.13}$$

Performing integration of equation (3.13) over (t_e, t_o) and $\big(r(t_e), r(t_o)\big)$, we get

$$\int_{t_e}^{t_o} \frac{c}{R(t)} dt = -\int_{r(t_e)}^{r(t_o)} \frac{1}{1+\kappa r^2}\, dr \tag{3.14}$$

Here, dr is the comoving distance that photons travel at time dt. Equation (3.14) is the general Equation for describing dynamics and evolution of the Universe. In the next chapter, a solution for dr is derived based on this equation for different geometry of the Universe. Combining this solution with derived results of the Einstein field equation based on the Friedmann equation (3.9), a general analytical solution on how light intensity and number density of galaxies vary with redshift will be formulated in the next chapter for describing dynamics, structure formation and evolution of observable Universe.

3.3 Assumptions

It was assumed that as this light transverses space, its wavelength is stretched hand hence is redshifted. Furthermore, the light intensity has measured redshift z and solid angle θ. It was again assumed that during this observation time; no new galaxies appeared or disappeared and that the luminosity of every star/galaxy remained constant. The astronomical objects were also assumed to be uniformly distributed in the universe such that the number of stars/galaxies observed in a given redshift could be counted.

3.4 Software used for analysis

The study employed MATLAB program to model the interrelation of redshift with light intensity and also that of redshift with number density from our analytical results. For comparison of our theoretical predictions (models) with existing models as well as with observational data, we retrieved datasets from NASA/IPAC Extragalactic Database (NED) for observed redshift range $0 \leq z \leq 5$ of galaxies (https://ned.ipac.caltech.edu/). A histogram plot of the observational data of galactic number count against redshift was

performed (see Figure 29). Each bin in the histogram represented the number of galaxies distributed with redshift.

CHAPTER FOUR: RESULTS AND DISCUSSIONS

In the last chapter, we introduced our method adopted for use in this work. This chapter proceeded to derive Einstein field equations describing the dynamics and evolution in a Friedmann universe.

4.1 Review of Einstein field equations based on the Friedmann model

Einstein's field equations specific to the Friedmann Universe were obtained by considering equation (3.9).

Earlier studies (Langa et al., 2017; Nyagisera et al., 2024) used equations (3.9) and (3.10) to derive a conservation principle pertinent to a matter-dominated Friedmann universe;

$\rho(t)R(t)^3 = \alpha$

This principle was used to deduce Einstein field equations relation of the form;

$$\mathrm{dt} = \frac{\mathrm{dR(t)}}{\sqrt{\frac{(\beta c^4 \rho(t) - \lambda c^2)\alpha}{3\rho R(t)} - 4\kappa c^2}} \tag{4.1}$$

In contrast to these studies, this project treated the density and the cosmic scale factor as variables thus rearranged equation (3.9) to yield;

$3R'(t)^2 = (\beta c^4 \rho(t) - \lambda c^2)R(t)^2 - 12\kappa c^2$

or

$$R'(t)^2 = \frac{(\beta c^4 \rho(t) - \lambda c^2)R(t)^2}{3} - 4\kappa c^2 \tag{4.2}$$

so that equation (4.2) yields

$$\left(\frac{\mathrm{dR(t)}}{\mathrm{dt}}\right)^2 = \frac{(\beta c^4 \rho(t) - \lambda c^2)R(t)^2}{3} - 4\kappa c^2$$

or

$$\mathrm{dt} = \frac{\mathrm{dR(t)}}{\sqrt{\frac{(\beta c^4 \rho(\mathrm{t}) - \lambda c^2) R(\mathrm{t})^2}{3} - 4\kappa c^2}} \tag{4.3}$$

Equation (4.1) and equation (4.3) are the Friedmann model relations representing time taken by a light photon to travel at a distance dr, describing the Friedmann Universe.

Equation (4.3) brings a clearer description of the dynamics, structure formation and evolution of the universe as compared to equation (4.1) obtained through conservation theorem in existing works (Langa et al., 2017; Nyagisera et al., 2024) and consequently meets our objective one. Equation (4.3) will be applied in deriving the light intensity-redshift and the number density-redshift relations in this work.

4.2 Analytical Results

4.2.1. Light intensity redshift relation

The relationship between light intensity and the redshift parameter of a photon at point of emission and at its observation point is derived. Here equation (3.14) is considered

Substituting equation (4.3) into equation (3.14), we get

$$\int_{\mathrm{R(t_e)}}^{\mathrm{R(t_o)}} \frac{\mathrm{cdR(t)}}{\mathrm{R(t)}\sqrt{\frac{(\beta c^4 \rho(\mathrm{t}) - \lambda c^2)\mathrm{R}(t)^2}{3} - 4\kappa c^2}} = -\int_{\mathrm{r(t_e)}}^{\mathrm{r(t_o)}} \frac{\mathrm{dr}}{1 + \kappa \mathrm{r}^2} \tag{4.4}$$

or

$$\int_{\mathrm{R(t_e)}}^{\mathrm{R(t_o)}} \frac{\mathrm{dR(t)}}{\mathrm{R}(t)^2\sqrt{\frac{\beta c^2 \rho(\mathrm{t}) - \lambda}{3} - \frac{4\kappa}{\mathrm{R}(t)^2}}} = -\int_{\mathrm{r(t_e)}}^{\mathrm{r(t_o)}} \frac{\mathrm{dr}}{1 + \kappa \mathrm{r}^2} \tag{4.5}$$

Equation (4.5) is more general and is suitable for describing the evolution and dynamics of the universe as it contains an extra cosmological term on its L.H.S earlier present in equation (4.3).

We then solved equation (4.5) for three different cases of κ for open universe($\kappa = -1$), flat universe($\kappa = 0$), and for a closed universe($\kappa = 1$)

a. $\kappa = 0$ (flat universe)

Equation (4.5) becomes

$$\int_{R(t_e)}^{R(t_o)} \frac{dR(t)}{R(t)^2\sqrt{\frac{\beta c^2 \rho(t) - \lambda}{3}}} = -\int_{r(t_e)}^{r(t_o)} dr$$

or

$$\int_{R(t_e)}^{R(t_o)} \frac{dR(t)}{aR(t)^2} = -\int_{r(t_e)}^{r(t_o)} dr \tag{4.6}$$

where $a = \sqrt{\frac{\beta c^2 \rho(t) - \lambda}{3}}$

Solving equation (4.6), we get

$$-r|_{r(t_e)}^{r(t_0)} = \frac{1}{aR(t)}|_{R(t_e)}^{R(t_o)}$$

$$r(t_e) - r(t_o) = \frac{1}{aR(t_e)} - \frac{1}{aR(t_o)} \tag{4.7}$$

Using the Hubble law relation $R(t_e) = \frac{R(t_o)}{1+z}$ and setting, $r(t_o) = 0$, equation (4.7) becomes

$$r(t_e) = \frac{1+z}{aR(t_o)} - \frac{1}{aR(t_o)}$$

or

$$r(t_e) = \frac{z}{aR(t_o)} \tag{4.8}$$

b. $\kappa = 1$ (closed universe)

Here, equation (4.5) becomes

$$\int_{R(t_e)}^{R(t_o)} \frac{dR(t)}{R^2(t)\sqrt{\frac{(\beta c^2\rho(t)-\lambda)}{3}-\frac{4}{R(t)^2}}} = -\int_{r(t_e)}^{r(t_o)} \frac{dr}{1+r^2} \tag{4.9}$$

Equation (4.9) is solved as follows:

$$-\int_{r(t_e)}^{r(t_o)} \frac{dr}{1+r^2} = \int_{R(t_e)}^{R(t_o)} \frac{dR(t)}{R(t)^2\sqrt{\frac{(\beta c^2\rho(t)-\lambda)}{3}}\sqrt{1-\frac{12}{(\beta c^2\rho(t)-\lambda)R(t)^2}}} \tag{4.10}$$

or

$$-\tan^{-1} r(t_e)\,|_{r(t_e)}^{r(t_o)} = \int_{R(t_e)}^{R(t_o)} \frac{dR(t)}{aR(t)^2\sqrt{1-\frac{4}{a^2R(t)^2}}} \tag{4.11}$$

where $a = \sqrt{\frac{(\beta c^2\rho(t)-\lambda)}{3}}$

Now let

$\frac{4}{a^2R(t)^2} = \sin^2\theta$,

so that

$R(t)^2 = \frac{4}{a^2\sin^2\theta}$

and

$dR(t) = \frac{-2\cos\theta\, d\theta}{a\sin^2\theta}$

Substituting the above equations into equation (4.11), we have

$$-\tan^{-1} r(t_e)\,|_{r(t_e)}^{r(t_o)} = \int_{\theta(t_e)}^{\theta(t_o)} \frac{-2a^2\sin^2\theta\cos\theta}{4a^2\sin^2\theta\cos\theta}\,d\theta$$

$$-\tan^{-1} r(t_e)\,|_{r(t_e)}^{r(t_o)} = -\frac{1}{2}\theta|_{\theta(t_e)}^{\theta(t_o)} \tag{4.12}$$

but $\theta = \sin^{-1}\frac{2}{aR(t)}$

$$-\frac{1}{2}\theta = -\frac{1}{2}\sin^{-1}\frac{2}{aR(t)} \tag{4.13}$$

Therefore,

$$-\tan^{-1} r(t_e)\,|_{r(t_e)}^{r(t_o)} = -\tfrac{1}{2}\sin^{-1}\tfrac{2}{aR(t)}\,\Big|\,_{R(t_e)}^{R(t_o)} = \tfrac{1}{2}\sin^{-1}\tfrac{2}{aR(t_e)} - \tfrac{1}{2}\sin^{-1}\tfrac{2}{aR(t_o)} \tag{4.14}$$

Applying the Hubble law relation, $R(t_e) = \frac{R(t_o)}{1+z}$ and setting, $r(t_o) = 0$, equation (4.14) becomes

$$\tan^{-1} r(t_e) = \frac{1}{2}\sin^{-1}\frac{2(1+z)}{aR(t_o)} - \frac{1}{2}\sin^{-1}\frac{2}{aR(t_o)} \tag{4.15}$$

Taking the tangent of both sides of equation (4.15) and using the trigonometric identity $\tan(A \pm B) = \frac{\tan A \pm \tan B}{1 \mp \tan A \tan B}$, we get

$$r(t_e) = \frac{\tan\frac{1}{2}\sin^{-1}\frac{2(1+z)}{aR(t_o)} - \tan\frac{1}{2}\sin^{-1}\frac{2}{aR(t_o)}}{1 + \tan\frac{1}{2}\sin^{-1}\frac{2(1+z)}{aR(t_o)}\tan\frac{1}{2}\sin^{-1}\frac{2}{aR(t_o)}} \tag{4.16}$$

Further using the identities

$\tan\frac{A}{2} = \frac{\sin A}{1+\cos A} = \frac{\sin A}{1+\sqrt{1-\sin^2 A}}$, equation (4.16) becomes

$$r(t_e) = \frac{\dfrac{2(1+z)}{aR(t_o) + \sqrt{(aR(t_o))^2 - 4(1+z)^2}} - \dfrac{2}{aR(t_o) + \sqrt{(aR(t_o))^2 - 4}}}{1 + \left(\dfrac{2(1+z)}{aR(t_o) + \sqrt{(aR(t_o))^2 - 4(1+z)^2}}\right)\left(\dfrac{2}{aR(t_o) + \sqrt{(aR(t_o))^2 - 4}}\right)} \tag{4.17}$$

which simplifies as

$$r(t_e) = \frac{2(1+z)\left(aR(t_o) + \sqrt{(aR(t_o))^2 - 4}\right) - 2\left(aR(t_o) + \sqrt{(aR(t_o))^2 - 4(1+z)^2}\right)}{\left(aR(t_o) + \sqrt{(aR(t_o))^2 - 4(1+z)^2}\right)\left(aR(t_o) + \sqrt{(aR(t_o))^2 - 4}\right) + 4(1+z)} \tag{4.18}$$

c. $\kappa = -1$(open universe)

In this case, equation (4.5) becomes

$$\int_{R(t_e)}^{R(t_o)} \frac{dR(t)}{\sqrt{\frac{\beta c^2 \rho(t) - \lambda}{3} + \frac{4}{R(t)^2}}} = -\int_{r(t_e)}^{r(t_o)} \frac{1}{1-r^2}\,dr \tag{4.19}$$

Equation (4.19) is solved as follows

$$-\int_{r(t_e)}^{r(t_o)} \frac{1}{1-r^2}\,dr = \int_{R(t_e)}^{R(t_o)} \frac{dR(t)}{R(t)^2\sqrt{\frac{\beta c^2 \rho(t) - \lambda}{3}}\sqrt{1 + \frac{12}{\beta c^2 \rho(t) - \lambda)\, R(t)^2}}} \tag{4.20}$$

or

$$-\int_{r(t_e)}^{r(t_o)} \frac{1}{1-r^2}\,dr = \int_{R(t_e)}^{R(t_o)} \frac{dR(t)}{aR(t)^2\sqrt{1 + \frac{4}{a^2 R(t)^2}}} \tag{4.21}$$

where $a^2 = \frac{\beta c^2 \rho(t) - \lambda}{3}$

Let

$$\frac{4}{a^2 R^2(t)} = \sinh^2\theta$$

such that

$R(t)^2 = \frac{4}{a^2 \sinh^2\theta}$,

then,

$R(t) = \frac{2}{a \sinh\theta}$

and

$$dR(t) = \frac{-2\cosh\theta\, d\theta}{a\sinh^2\theta}$$

Therefore,

$$\sqrt{1+\frac{4}{a^2R(t_o)^2}}=\sqrt{1+\sinh^2\theta}=\sqrt{\cosh^2\theta}=\cosh\theta$$

Substituting the above equations into equation (4.21), we get

$$-\int_{r(t_e)}^{r(t_o)}\frac{1}{1-r^2}\,dr=\ -\frac{1}{2}\int_{\theta(t_e)}^{\theta(t_o)}d\theta$$

$$-\tanh^{-1}r(t_e)\,|_{r(t_e)}^{r(t_o)}=\ -\frac{1}{2}\theta|_{\theta(t_e)}^{\theta(t_o)} \qquad (4.22)$$

or

$$\theta=\sinh^{-1}\frac{2}{aR(t)} \qquad (4.23)$$

Thus

$$-\tanh^{-1}r(t_e)\,|_{r(t_e)}^{r(t_o)}=\ -\frac{1}{2}\sinh^{-1}\frac{2}{aR(t)}\,|_{R(t_e)}^{R(t_o)}=\frac{1}{2}\sinh^{-1}\frac{2}{aR(t_e)}-\frac{1}{2}\sinh^{-1}\frac{2}{aR(t_o)} \qquad (4.24)$$

Applying the Hubble law relation $R(t_e)=\ \frac{R(t_o)}{1+z}$ and setting $r(t_o)=0$, on equation (4.24), we achieve

$$\tanh^{-1}r(t_e)=\ \frac{1}{2}\sinh^{-1}\frac{2(1+z)}{aR(t_o)}-\frac{1}{2}\sinh^{-1}\frac{2}{aR(t_o)} \qquad (4.25)$$

We now apply the trigonometric identity $\tanh(A\pm B)=\frac{\tanh A\pm\tanh B}{1\pm\tanh A\tanh B}$ on equation (4.25) to obtain

$$r(t_e)=\frac{\tanh\frac{1}{2}\sinh^{-1}\frac{2(1+z)}{aR(t_o)}-\tanh\frac{1}{2}\sinh^{-1}\frac{2}{aR(t_o)}}{1-\ \tanh\frac{1}{2}\sinh^{-1}\frac{2}{aR(t_o)}.\tanh\frac{1}{2}\sinh^{-1}\frac{2(1+z)}{aR(t_o)}}. \qquad (4.26)$$

Using the identity $\tanh\frac{A}{2}=\frac{\sinh A}{1+\cosh A}=\frac{\sinh A}{1+\sqrt{1+\sinh^2 A}}$, we rewrite and simplify equation (4.26) as

$$r\,(t_e) = \frac{\frac{2(1+z)}{aR(t_o)}\cdot\frac{1}{1+\sqrt{1+\frac{4(1+z)^2}{a^2R(t_o)^2}}} - \frac{2}{aR(t_o)}\cdot\frac{1}{1+\sqrt{1+\frac{4}{a^2R(t_o)^2}}}}{1-\frac{2}{aR(t_o)}\cdot\frac{1}{1+\sqrt{1+\frac{4}{a^2R(t_o)^2}}}\frac{2(1+z)}{aR(t_o)}\cdot\frac{1}{1+\sqrt{1+\frac{4(1+z)^2}{a^2R(t_o)^2}}}}$$

$$r(t_e) = \frac{2\left[(1+z)\left(aR(t_o)+\sqrt{a^2R(t_o)^2+4}\right)-\left(aR(t_o)+\sqrt{a^2R(t_o)^2+4(1+z)^2}\right)\right]}{\left(aR(t_o)+\sqrt{a^2R(t_o)^2+4}\right)\left(aR(t_o)+\sqrt{a^2R(t_o)^2+4(1+z)^2}\right)-4(1+z)} \quad (4.27)$$

All the three cases, that is, equations (4.8), (4.18), and (4.27) can be compacted as:

$$r(t_e) = \frac{2\left[(1+z)\left(aR(t_o)+\sqrt{a^2R(t_o)^2-4\kappa}\right)-\left(aR(t_o)+\sqrt{a^2R(t_o)^2-4\kappa(1+z)^2}\right)\right]}{\left(aR(t_o)+\sqrt{a^2R(t_o)^2-4\kappa}\right)\left(aR(t_o)+\sqrt{a^2R(t_o)^2-4\kappa(1+z)^2}\right)+4\kappa(1+z)} \quad (4.28)$$

where $\kappa = -1,0,1$

Let us now define

$$p = aR(t_o)+\sqrt{a^2R(t_o)^2-4\kappa} \quad (4.29)$$

$$q = aR(t_o)+\sqrt{a^2R(t_o)^2-4\kappa(1+z)^2} \quad (4.30)$$

We consider $r(t_e)$ as a function of z since t_e depends on z, then equation (4.28) becomes

$$r(z) = \frac{2(p(1+z)-q)}{pq+4\kappa(1+z)} \quad (4.31)$$

Consider an astronomical object (star or a galaxy) positioned at the origin, $r = 0$, radiating light with a luminosity, L. Over a time span of emission, t_e we contemplate the emission of light, each increment of which is encapsulated by dt_e. Subsequently, at a distinct moment of observation, t_o, an observer gauges the intensity of the emitted light, quantified as I, which is inevitably subject to a redshift z. The spatial coordinates of the observer are captured by Equation (4.28). This intricate interplay of emission, transmission, and observation culminates

in Equation (4.32), where the luminosity of the radiant matter within the universe manifests as a decisive determinant in the computation of light intensity, expressed as

$$I(z) = \frac{L dt_e}{(1+z) S_{r(z)}} \tag{4.32}$$

where $S_{r(z)} = \frac{4\pi r(z)^2 R(t_o)^2}{(1+\kappa r^2)^2}$ - the surface area of the sphere of radius $r = r(z)$ at time $t = t_o$ (Langa et al., 2017) .

Substituting equation (4.31) into equation (4.32), we finally achieve

$$I(z) = \frac{L\left[1+\kappa\left(\frac{2(p(1+z)-q)}{pq+4\kappa(1+z)}\right)^2\right]^2}{4\pi\left(\frac{2(p(1+z)-q)}{pq+4\kappa(1+z)}\right)^2 R(t_o)^2(1+z)^2} \tag{4.33}$$

Equation (4.33), based on the Friedmann Universe, shows an important link between redshift z and luminous intensity $I(z)$. This equation helps explore the relationship between cosmic radiation and luminosity, providing insight into the evolution of the universe. It also addresses objective 2.

4.2.2. Number density redshift relation

In our exploration, we shall direct our focus toward celestial entities, e.g galaxies, which exhibit a uniform distribution across the universe within a specific range of redshift. In this context, let N symbolize the number of galaxies existing per unit volume within a spatial metric denoted as $\frac{(dr^2+r^2d\theta^2+r^2\sin^2\theta d\theta)}{(1+\kappa r^2)^2}$.

Additionally, the volume element $r^2\sin\theta d\theta d\varphi dr/(1+\kappa r^2)^3$ encapsulates the spatial dimensions. This framework enables us to delineate the population of galaxies spanning the range from r to dr, expressed as $4\pi r^2 dr/(1+\kappa r^2)^3$, as expounded by Langa et al. in 2017.

By adhering to this conceptual groundwork, we embark on an illuminating journey into the intricacies of cosmic distribution and structure.

Differentiating equation (4.31) with respect to z we get

$$r'(z) = \frac{2(x(x - aR(t_o)) - y(y - aR(t_o))}{(q - aR(t_o)x^2} \tag{4.34}$$

where $x = pq + 4\kappa(1 + z)$ and $y = p(1 + z) - q$

Again, we can assume that the number of astronomical objects bounded in a hyperspherical coordinates $r(z)$ and $r(z + dz)$ as

$$n(z)dz = \frac{4\pi r(z)^2 N r'(z)dz}{(1 + \kappa r(z)^2)^3} \tag{4.35}$$

Substituting equations (4.31) and (4.34) into equation (4.35) yields

$$n(z) = \frac{32\pi(p(1 + z) - q)^2 N\left(x(x - aR(t_o)) - y(y - aR(t_o))\right)}{\left(pq + 4k(1 + z)\right)^2 ((q - aR(t_o)x^2)\left(1 + \kappa\left(\frac{2(p(1 + z) - q)}{pq + 4\kappa(1 + z)}\right)^2\right)^3} \tag{4.36}$$

Expressed as Equation (4.36), $n(z)$ encapsulates a profound revelation: the intricate interplay between redshift and the evolving density of astronomical objects and it consequently meets our objective 3.

This equation relates to how the number density $n(z)$ of galaxies evolves with redshift. Together with equation (4.33), they constitute important results of this project. The equations reveal the delicate balance between factors like the curvature parameter, energy density, and cosmological constants. Together, they provide a deep understanding of the universe's evolution. The combination of these equations forms a key foundation for our exploration, driving us toward valuable insights and discoveries.

4.3 Graphical results

Let us now employ our findings to facilitate the determination or approximation of the galactic population within the observable universe. Moreover, our approach allows us to gauge the extent of their distribution scales and to deduce suitable methodologies governing the evolutionary patterns of galactic number densities. A pivotal achievement of this is the acquisition of theoretical and mathematical insights into the dynamics and evolution of galactic number densities, extending up to a redshift of $z = 5$.

In the preceding section, we derived the interrelationships between galactic number density with redshift, and light intensity with redshift through analytical methods. We shall now transition to the exploration of our established outcomes, achieved through the development and execution of straightforward MATLAB programs. By implementing these programs, we generate graphical representations that illustrate the relationships between light intensity and redshift, as well as between number density and redshift, as dictated by equations (4.33) and (4.36) correspondingly. The range of redshift values employed in our MATLAB simulations spans from $z = 0$ to $z = 5$, a spectrum that aligns harmoniously with existing statistical data and observations.

The program encompasses a range of universe energy densities, spanning from $\rho(t) = 6.99 \times 10^{-23}\text{kg/m}^3$ to $\rho(t) = 5 \times 10^{-27}\text{kg/m}^3$. The velocity of light, c remains constant at $c = 3 \times 10^8$ m/s. The cosmic scale factor, $R(t_o) = 9 \times 10^{25}$m while the gravitational constant $G = 6.67 \times 10^{-11}\text{m}^3/\text{kg/s}^2$. The universe's curvature, κ assumes values of -1, 0, and 1, and the cosmological constant $\lambda = 1.19 \times 10^{-52}\text{m}^{-2}$. To enhance accuracy, logarithms of light intensity and number density are employed.

For our exploration, we assign arbitrary values of 1 to the parameters N (number of galaxies per unit volume) and L (absolute power of a galaxy or star) since we implore that no galaxies (or stars) are destroyed or created during this epoch. This approach facilitates the determination of parameter combinations $\rho(t)$ and $\mathrm{R(t_o)}$ that best align with experimental data without presuming assumptions about background geometry, thereby enabling the creation of a well-fitted curve based on comprehensive observational information.

The analysis reinterprets simulation results by considering $z = 0$ as the universe's inception, with increasing z values representing the progression of cosmic time. The comparison includes our model (standard Friedmann redshift model), the approximate standard Friedmann redshift model (Langa et al., 2017), and the modified standard Friedmann redshift model (Nyagisera et al., 2024).

4.3.1 Light intensity redshift relation

Executing our program using equation (4.33) for different $\rho(\mathrm{t})(\mathrm{kg/m^3})$ and κ values yields the ensuing outcomes (refer to figures 1 to 14 and see Appendix I to V for the MATLAB programs) pertinent to light intensity.

Figures 1 to 14 show the relationship between light intensity and redshift. The Y-axis (Log I) shows the logarithm of light intensity, where lower values correspond to low intensity. The X-axis (Redshift z) tracks the evolution of the universe from its inception at $z = 0$. Different initial values of log(I) across the curves indicate varying light intensities based on the universe's density (ρ) and curvature (κ).

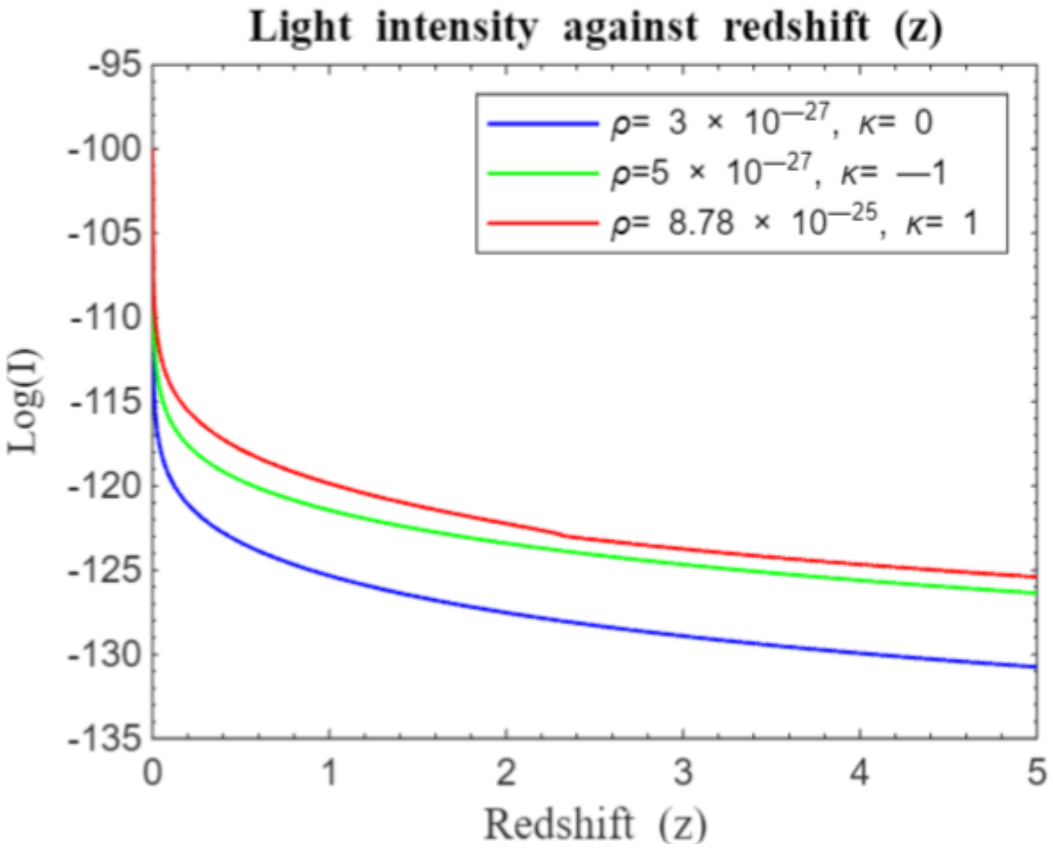

Figure 1: Simulation result for log (n) against redshift z for $z = 0$ to $z = 5$ of the standard Friedmann redshift model without λ.

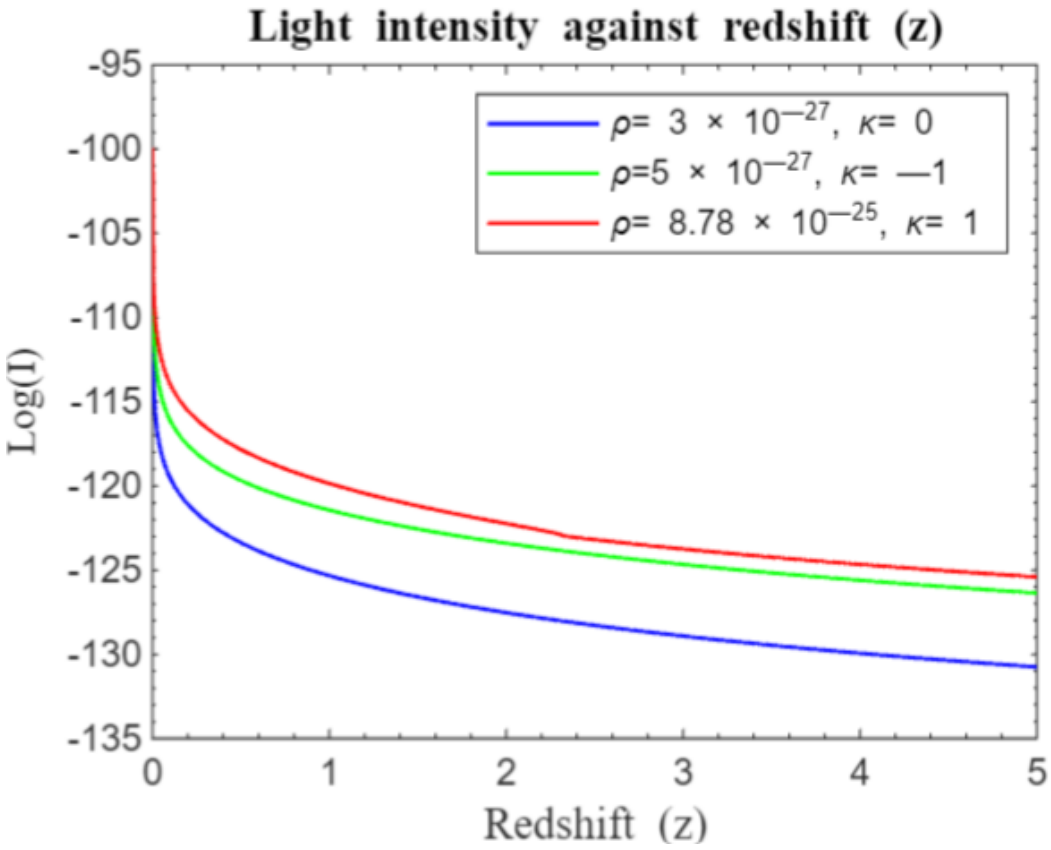

Figure 2: Simulation result for log (n) against redshift z for $z = 0$ to $z = 5$ of the standard Friedmann redshift model with λ.

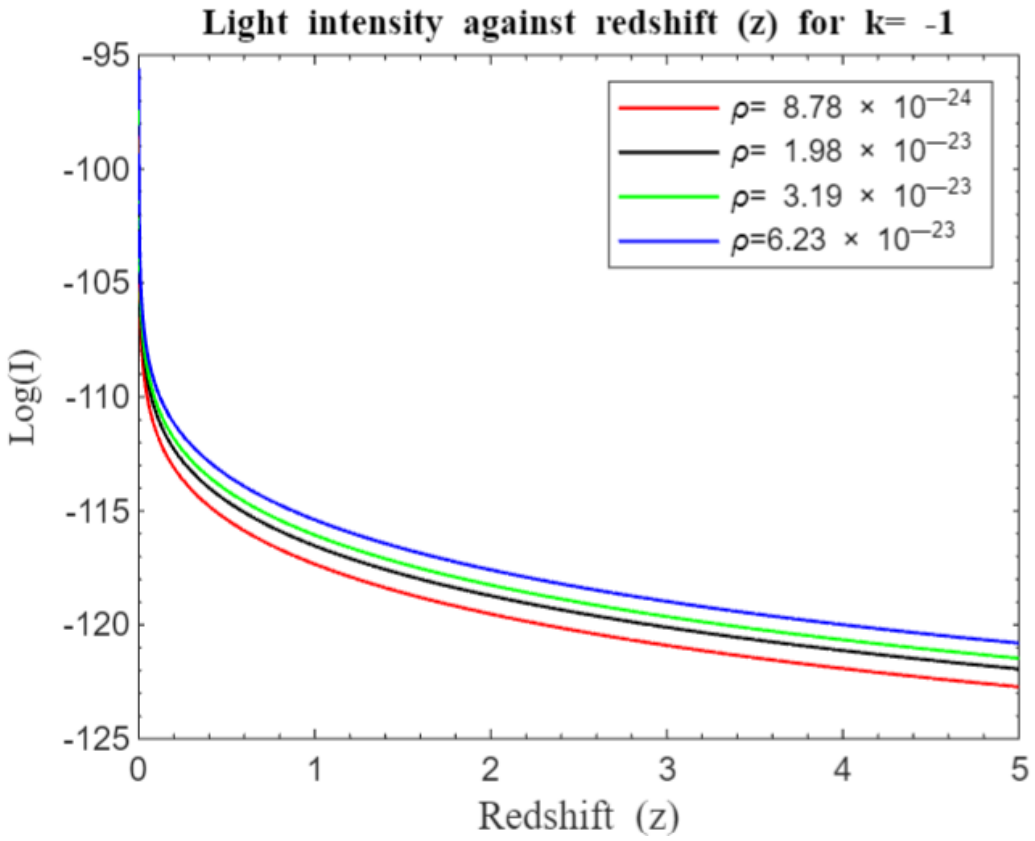

Figure 3: Simulation result for log (n) against redshift z for $z = 0$ to $z = 5$ of the standard Friedmann redshift model for an open universe without λ.

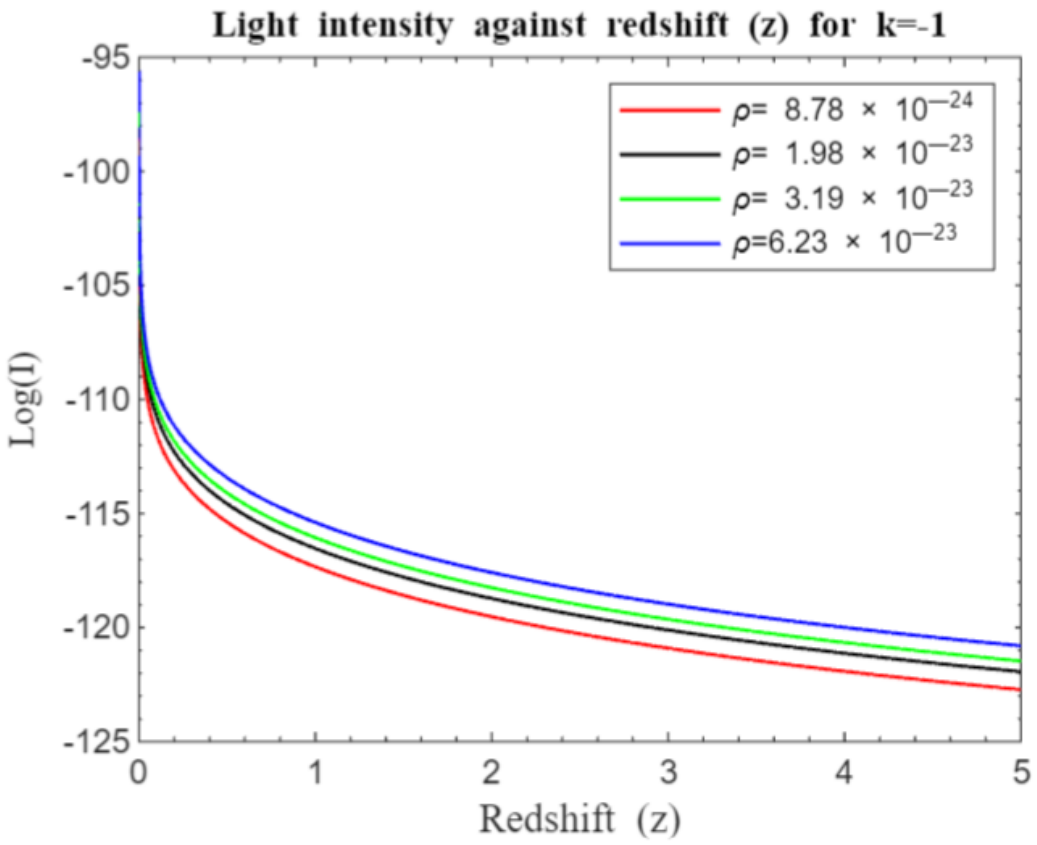

Figure 4: Simulation result for log (n) against redshift z for $z = 0$ to $z = 5$ of the standard Friedmann redshift model for an open universe with λ.

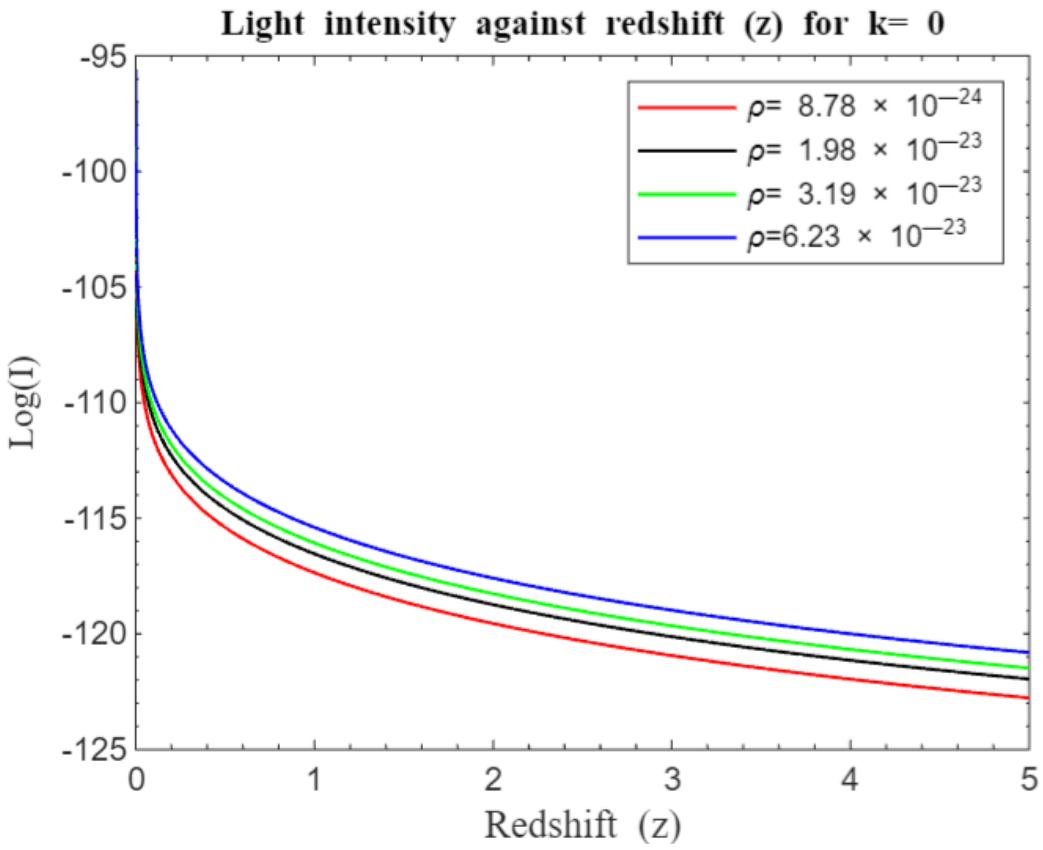

Figure 5: Simulation result for log (n) against redshift z for $z = 0$ to $z = 5$ of the standard Friedmann redshift model for a flat universe without λ.

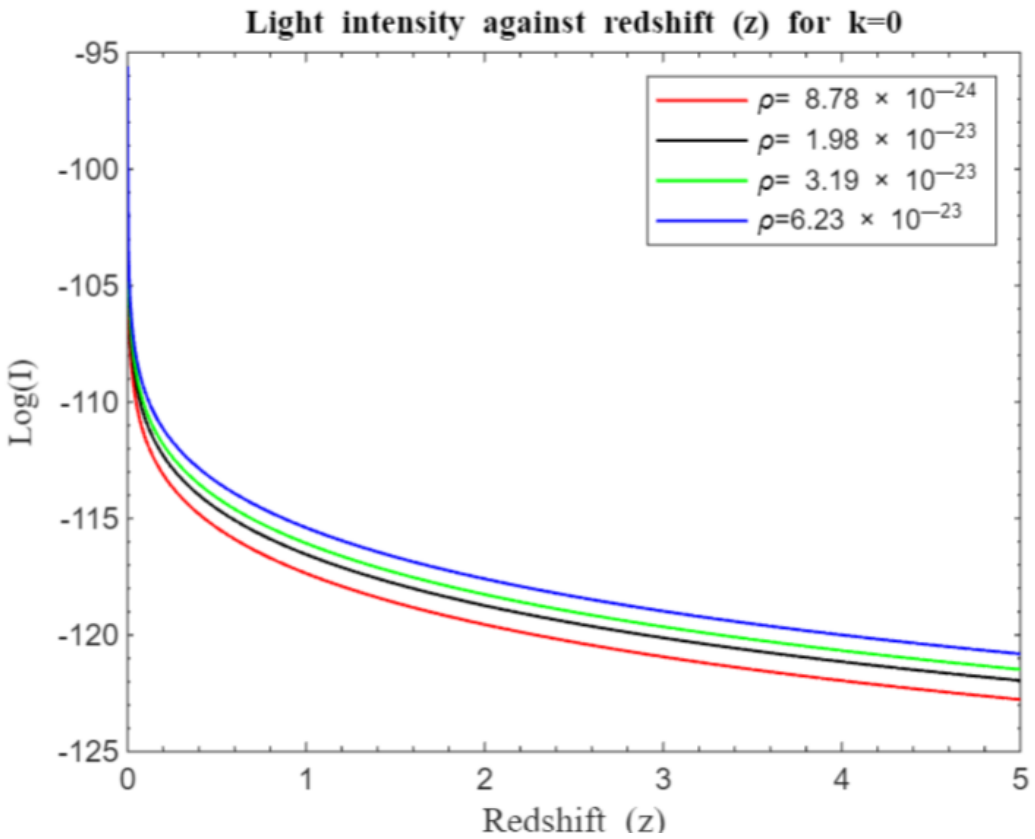

Figure 6: Simulation result for log (n) against redshift z for z=0 to z=5 of the standard Friedmann redshift model for a flat universe with λ.

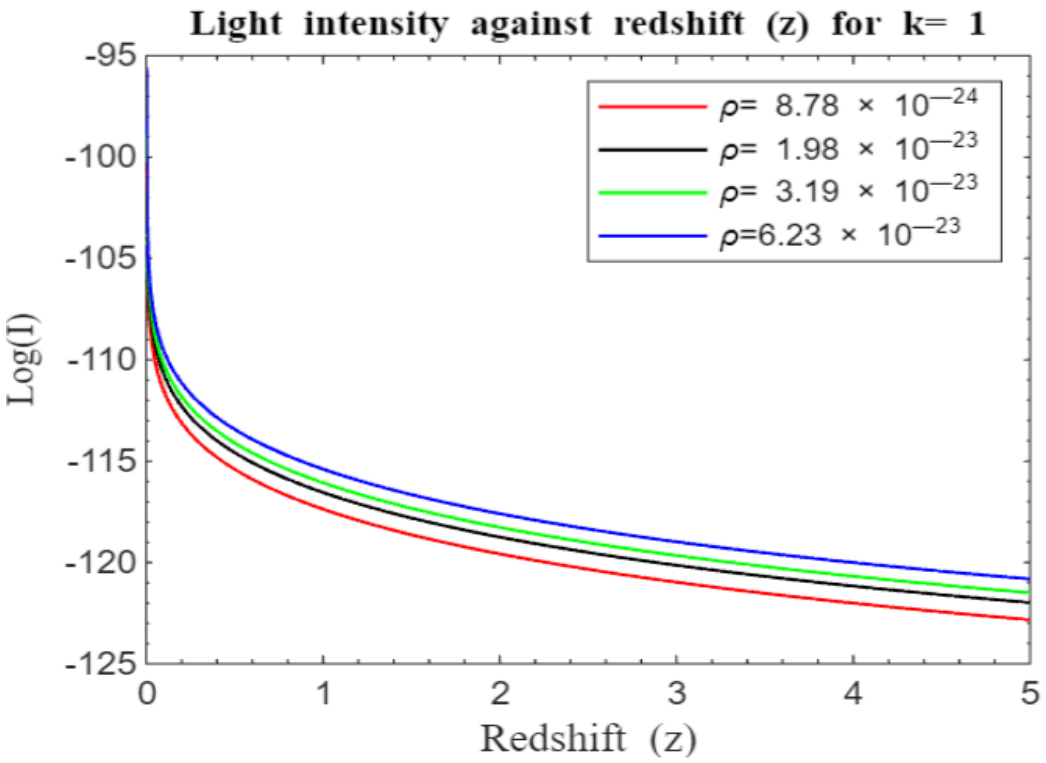

Figure 7: Simulation result for log (n) against redshift z for z=0 to z=5 of the Standard Friedmann redshift model for a closed universe without λ.

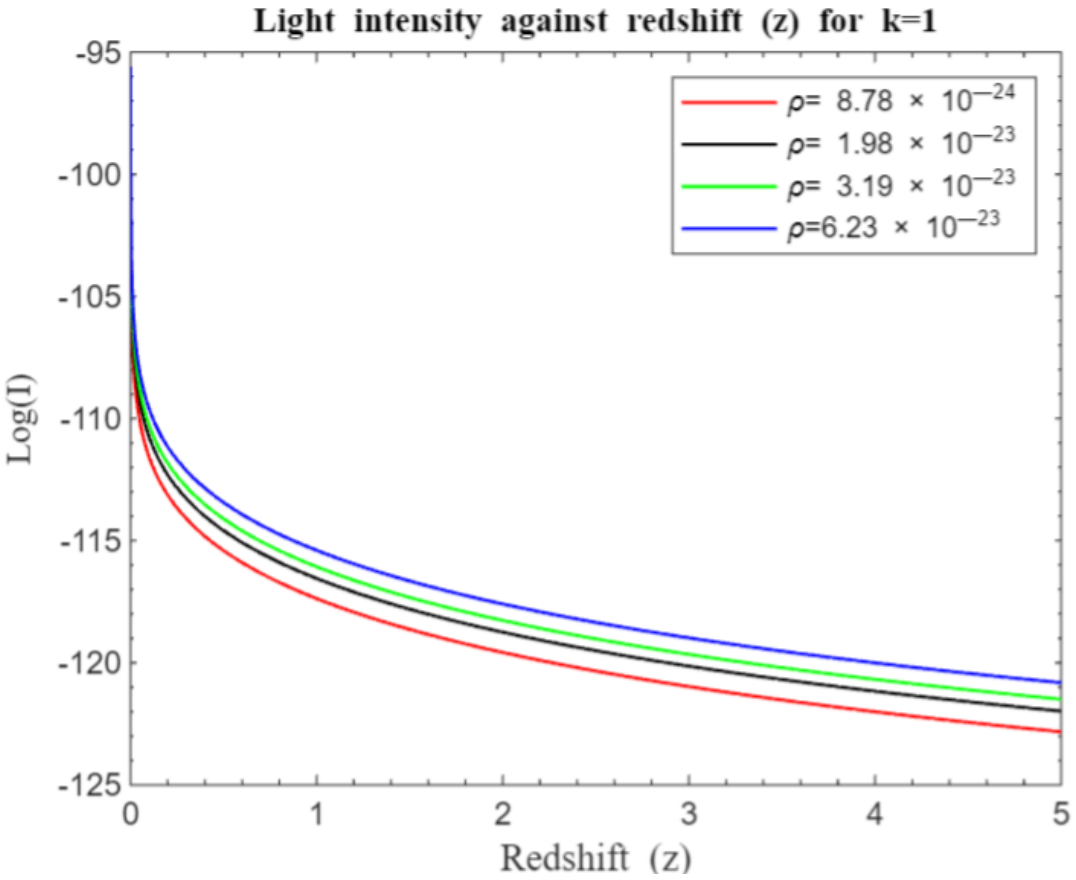

Figure 8: Simulation result for log (n) against redshift z for z=0 to z=5 of the standard Friedmann redshift model for a closed universe with λ.

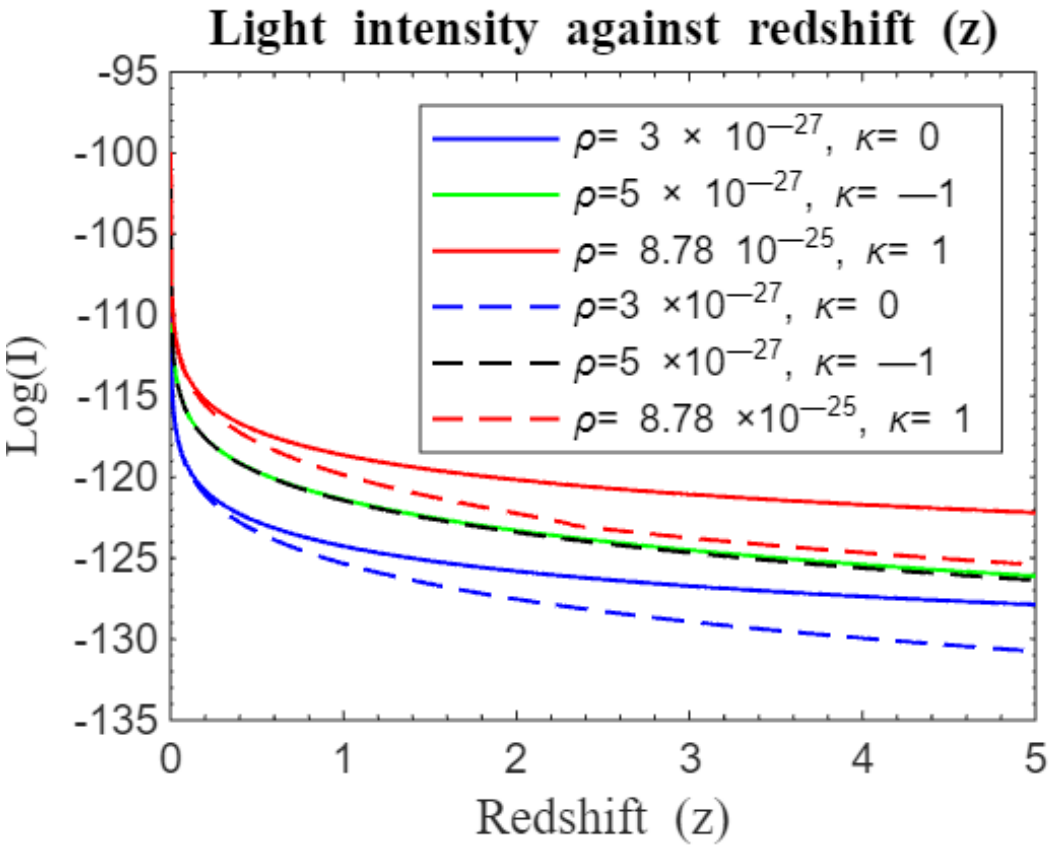

Figure 9: Simulation result for log (I) against redshift z for $z = 0$ to $z = 5$ of the standard Friedmann redshift and the approximate standard Friedmann redshift model.
The solid curves represent the approximate standard Friedmann redshift model while dotted curves represent the standard Friedmann redshift model. Both models without λ

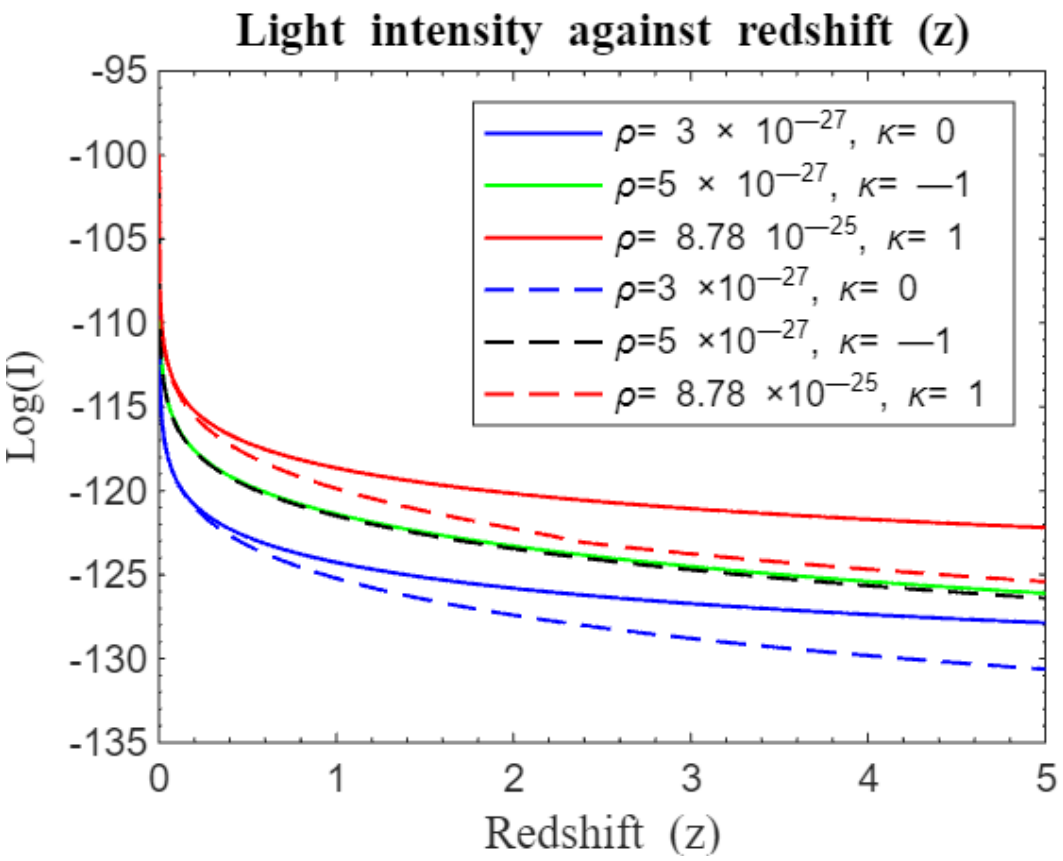

Figure 10: Simulation result for log (I) against redshift z for $z = 0$ to $z = 5$ of the standard Friedmann redshift and the approximate standard Friedmann redshift model.
The solid curves represent the approximate standard Friedmann redshift model without λ while dotted curves represent the standard Friedmann redshift model with λ.

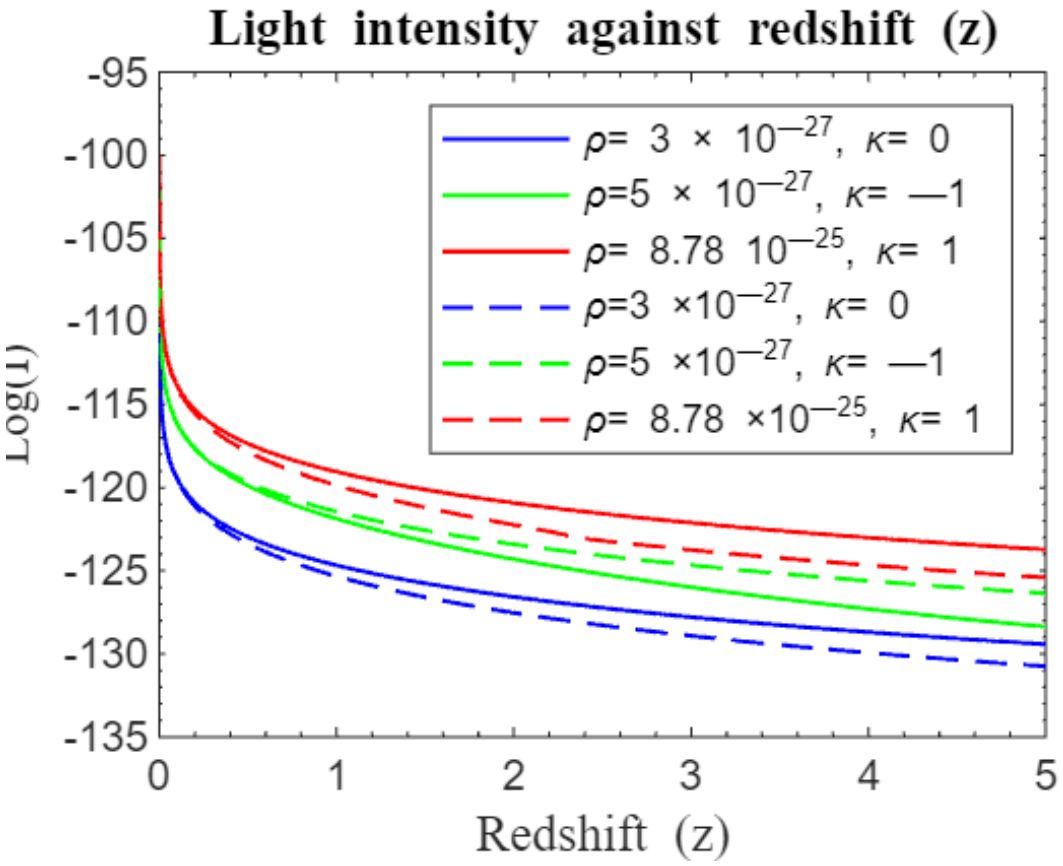

Figure 11: Simulation result for log (I) against redshift z for $z = 0$ to $z = 5$ of the standard Friedmann redshift model and the nonparametric model.
The solid curves represent the modified standard Friedmann redshift model $f(z) = z + \gamma(z)^2$ with $\gamma = 0.45$ while the dotted curves represent the Standard Friedmann Redshift Model. Both models without λ.

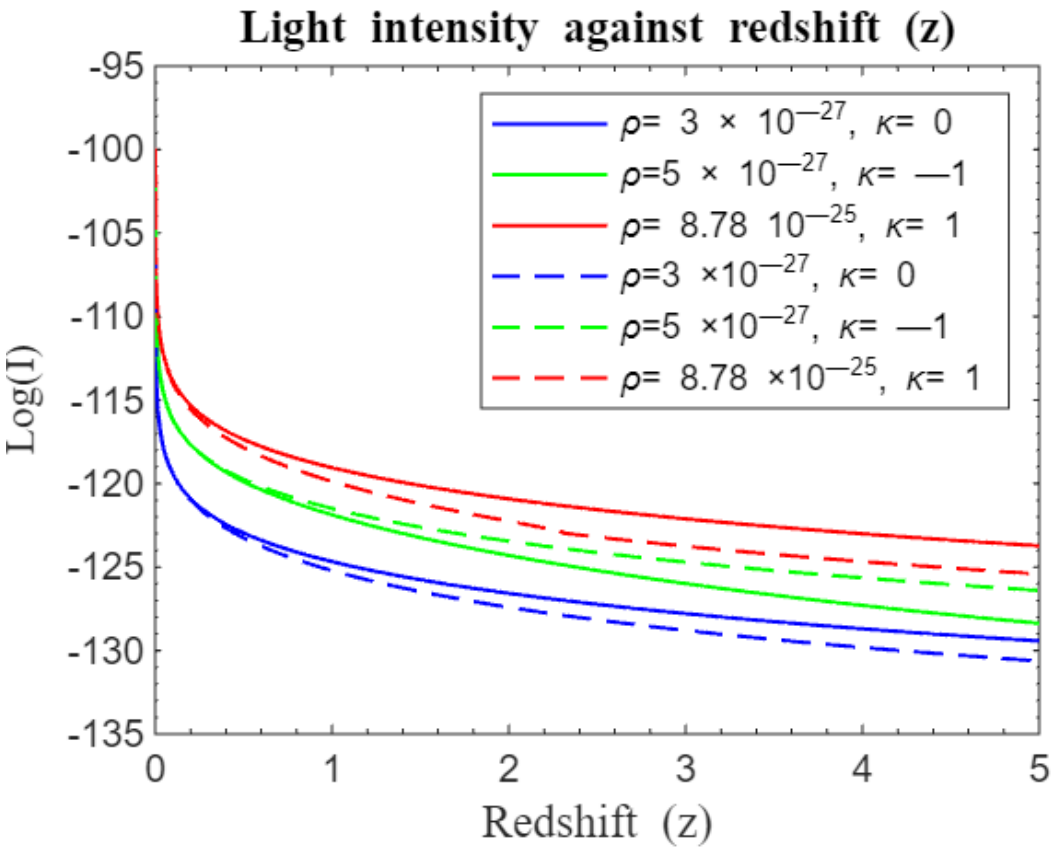

Figure 12: Simulation result for log (I) against redshift z for $z = 0$ to $z = 5$ of the standard Friedmann redshift model and the nonparametric model.
The solid curves represent the modified standard Friedmann redshift model $f(z) = z + \gamma(z)^2$ with $\gamma = 0.45$ without λ while dotted curves represent the standard Friedmann redshift model with λ.

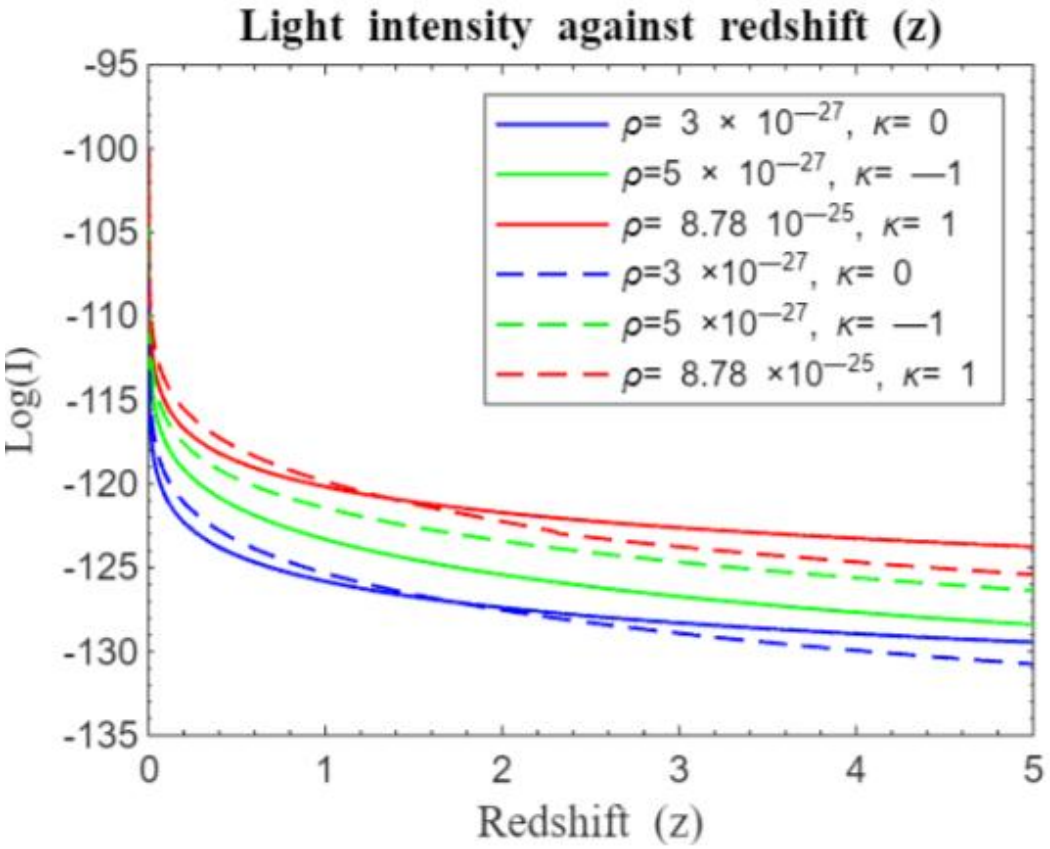

Figure 13: Simulation result for log (I) against redshift z for $z = 0$ to $z = 5$ of the standard Friedmann redshift model and the parametric model.
The solid curves represent the modified standard Friedmann redshift model $f(z) = \alpha_1 z + \alpha_2 z^2$ with $\alpha_1 = 2.005$ and $\alpha_2 = 0.005$ while dotted curves represent the standard Friedmann redshift model. Both models without λ.

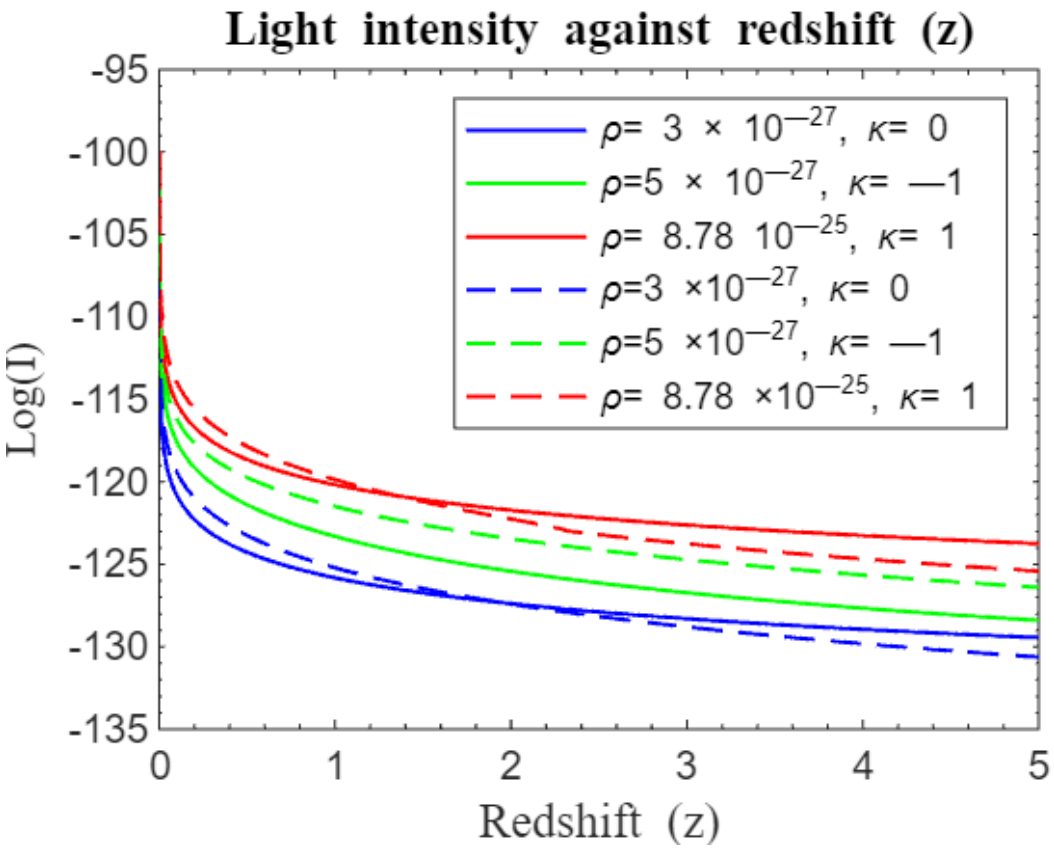

Figure 14: Simulation result for log (I) against redshift z for $z = 0$ to $z = 5$ of the standard Friedmann redshift model and the parametric model.
The solid curves represent the modified standard Friedmann redshift model $f(z) = \alpha_1 z + \alpha_2 z^2$ with $\alpha_1 = 2.005$ and $\alpha_2 = 0.005$ without λ while dotted curves represent the standard Friedmann redshift models with λ

4.3.2 Number density redshift relation

Figures 15 to 28 show the evolution of galaxy number density, $n(z)$, in relation to redshift z, as described by equation (4.36). The Y-axis (Log n) shows the logarithm of number density, where lower values correspond to reduced number density. The X-axis (Redshift, z) tracks the evolution of the universe from its inception at $z = 0$. Different initial values of Log(n) across the curves indicate varying number densities based on the density (ρ) of the universe and its curvature, κ (see Appendix VI to X for the MATLAB programs).

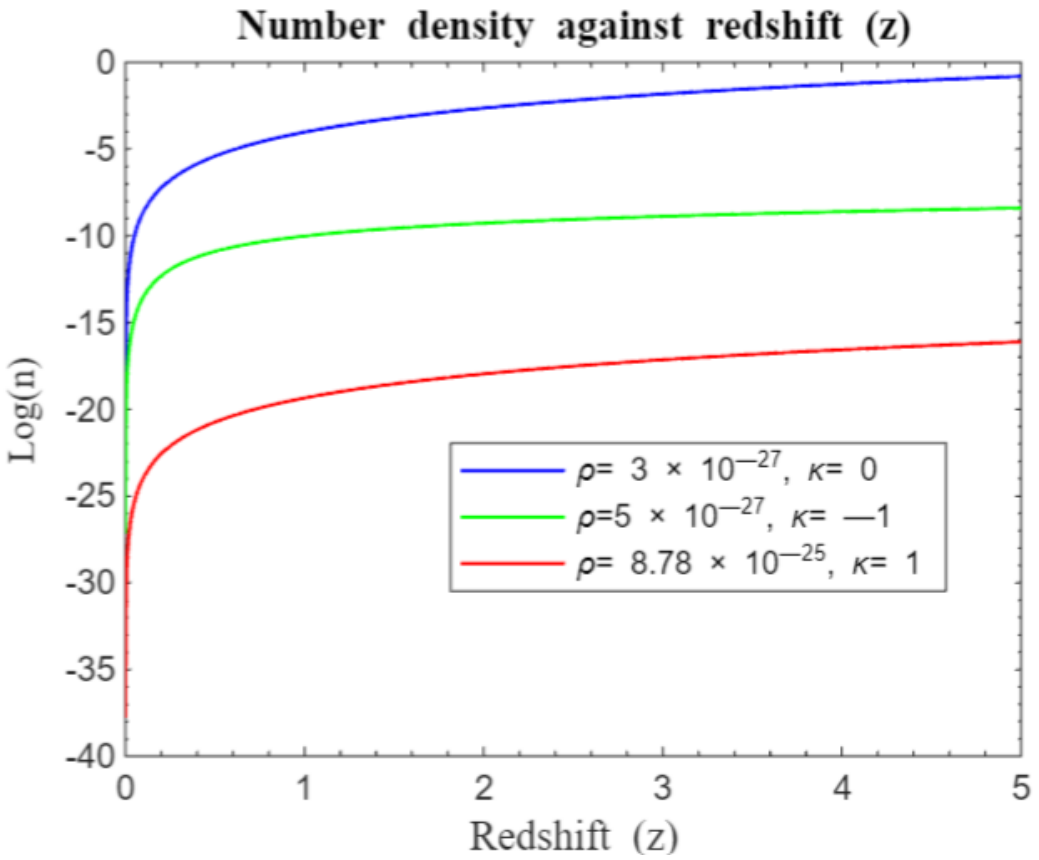

Figure 15: Simulation result for log (n) against redshift z for $z = 0$ to $z = 5$ of the standard Friedmann redshift model without λ.

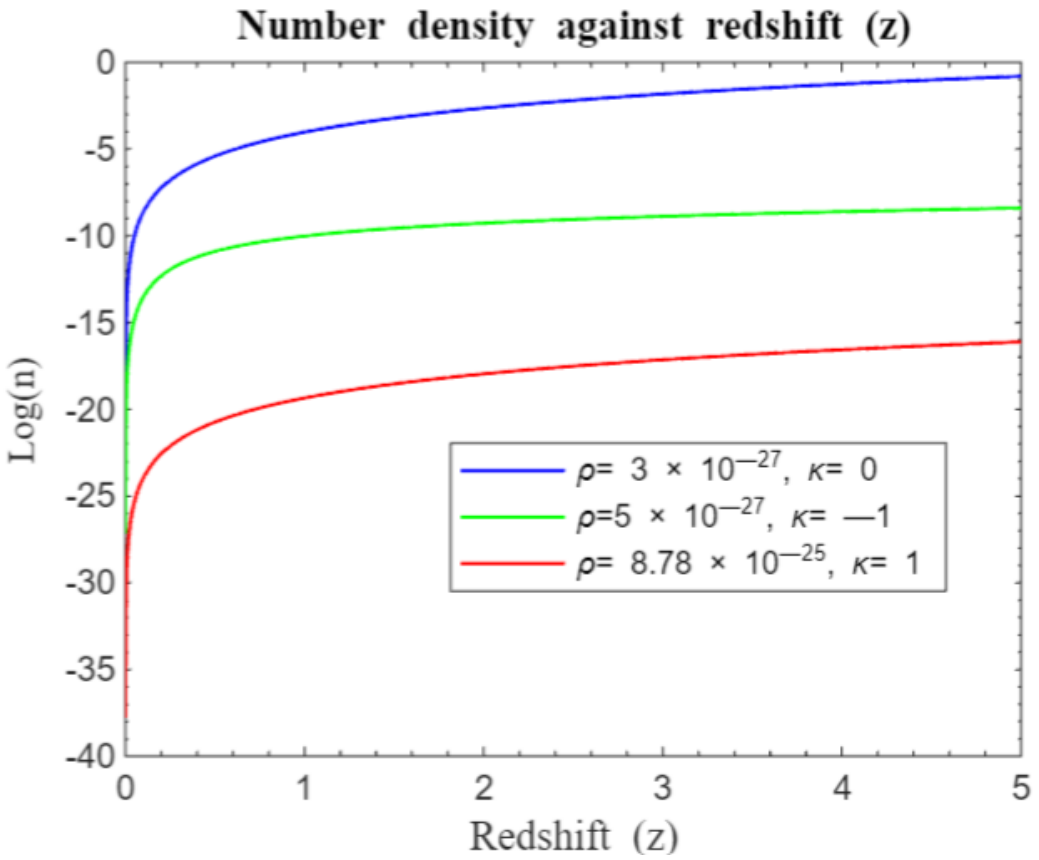

Figure 16: Simulation result for log (n) against redshift z for $z = 0$ to $z = 5$ of the standard Friedmann redshift model with λ.

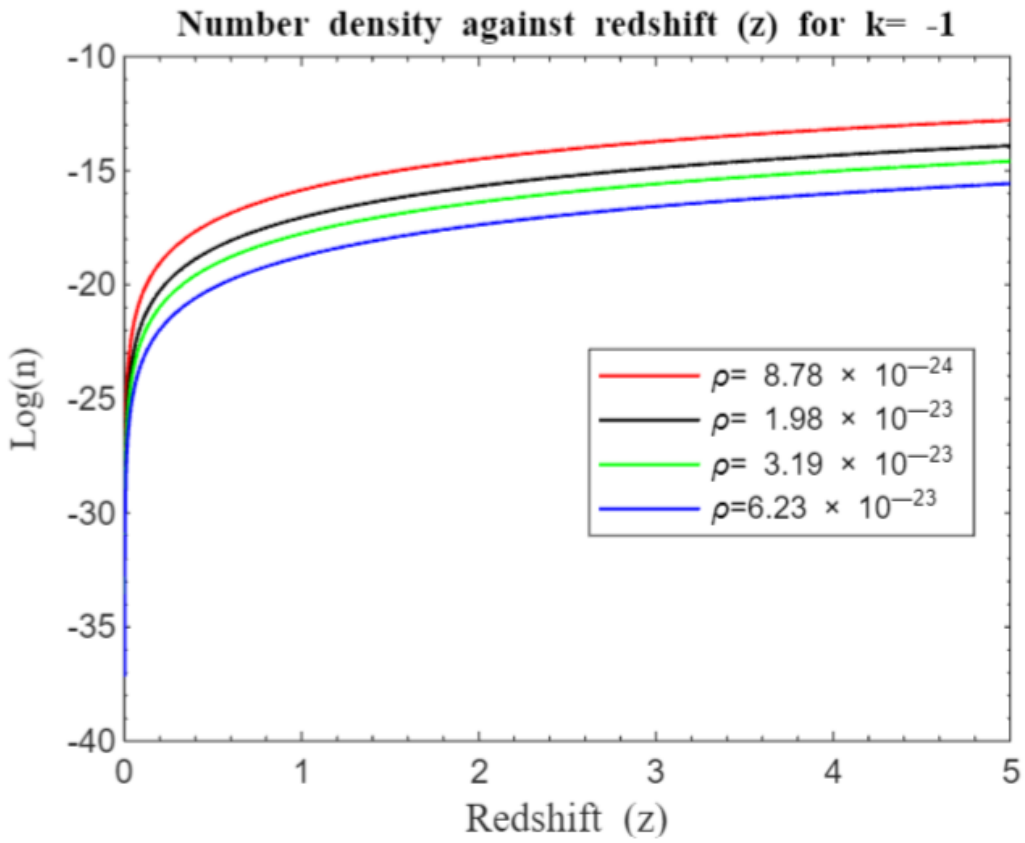

Figure 17: Simulation result for log (n) against redshift z for $z = 0$ to $z = 5$ of the standard Friedmann redshift model for an open universe without λ.

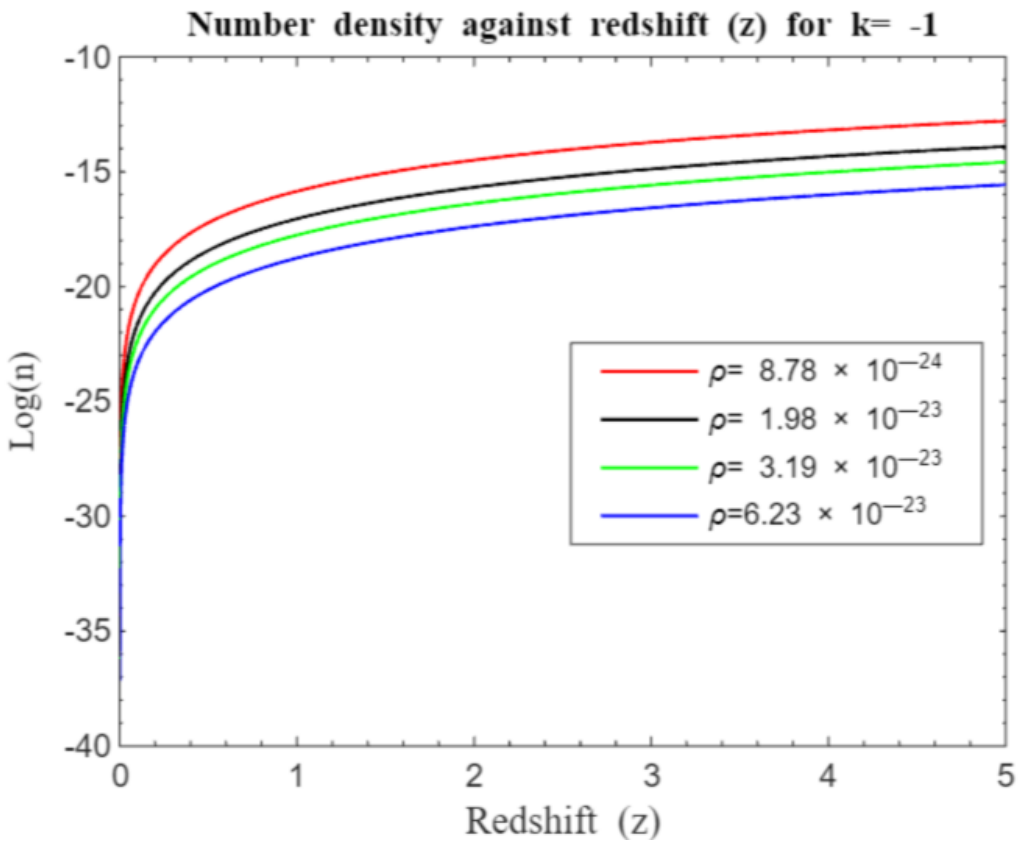

Figure 18: Simulation result for log (n) against redshift z for $z = 0$ to $z = 5$ of the standard Friedmann redshift model for an open universe with λ.

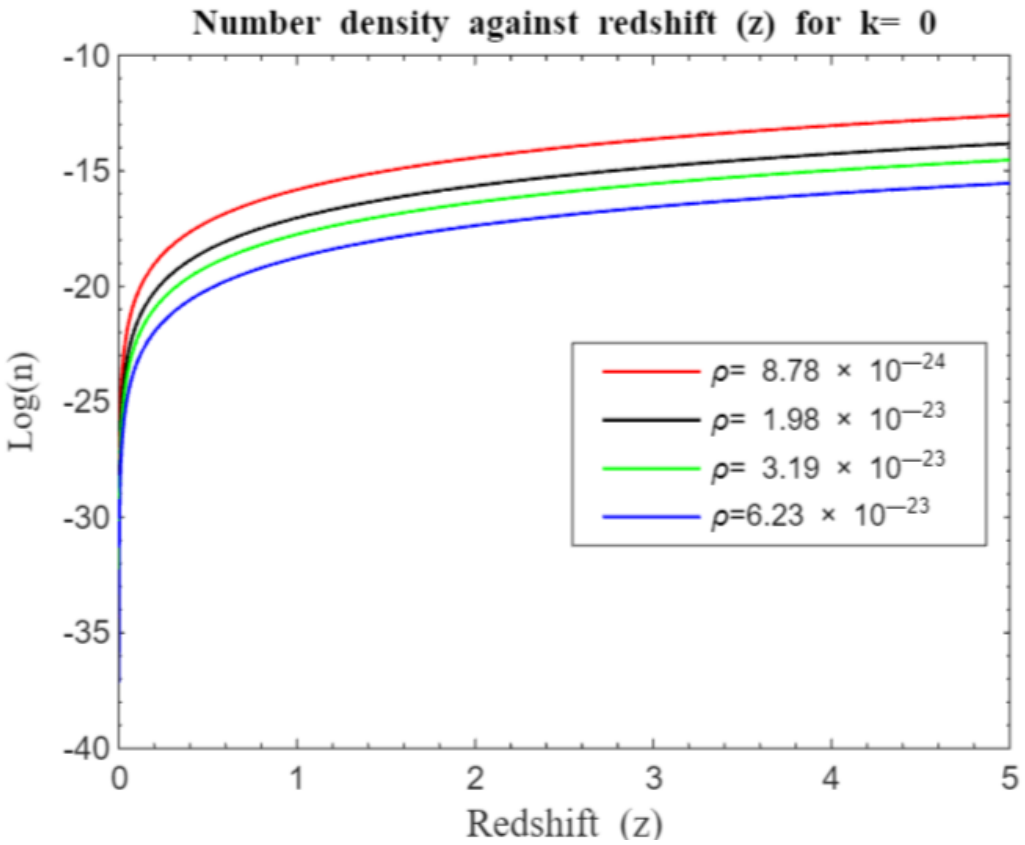

Figure 19: Simulation result for log (n) against redshift z for $z = 0$ to $z = 5$ of the standard Friedmann redshift model for a flat universe without λ.

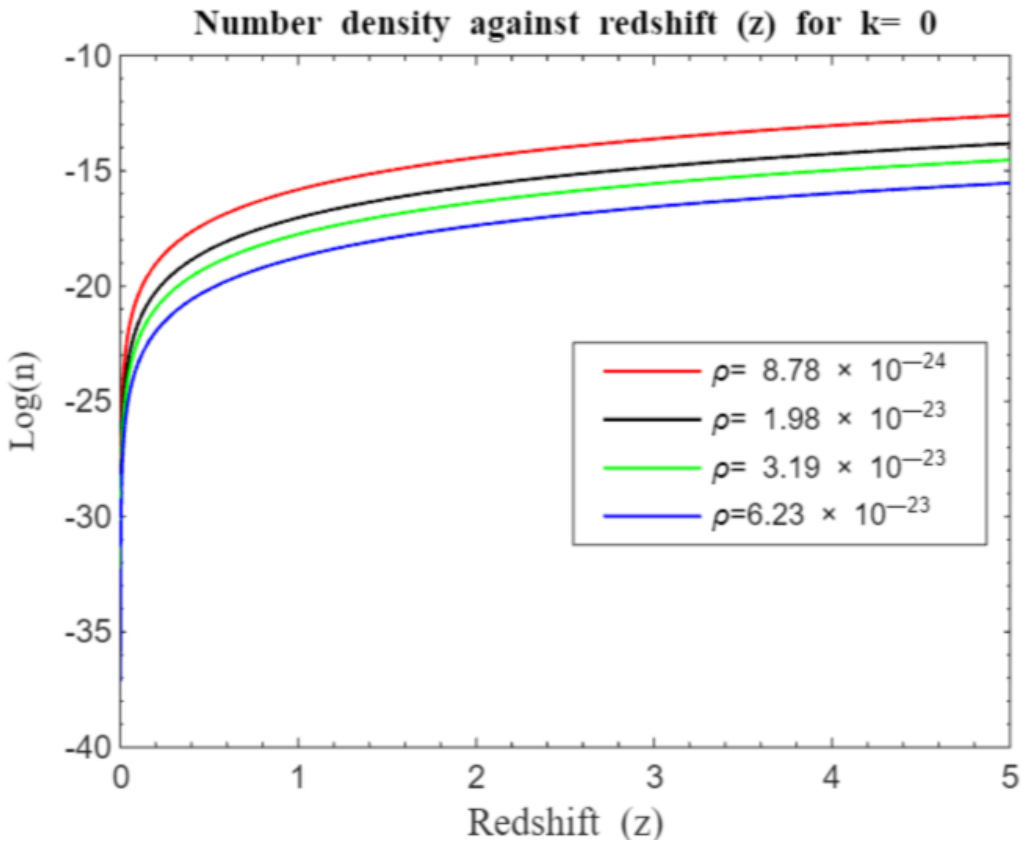

Figure 20: Simulation result for log (n) against redshift z for $z = 0$ to $z = 5$ of the standard Friedmann redshift model for a flat universe with λ.

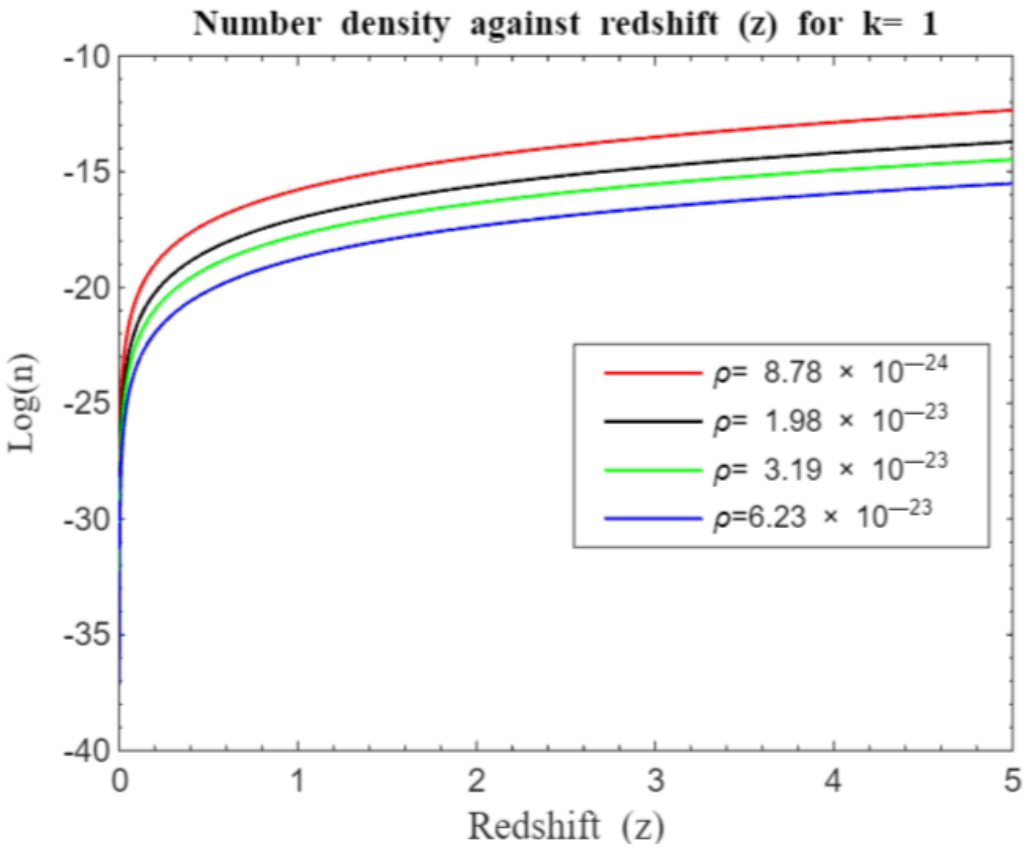

Figure 21: Simulation result for log (n) against redshift z for $z = 0$ to $z = 5$ of the standard Friedmann redshift model for a closed universe without λ.

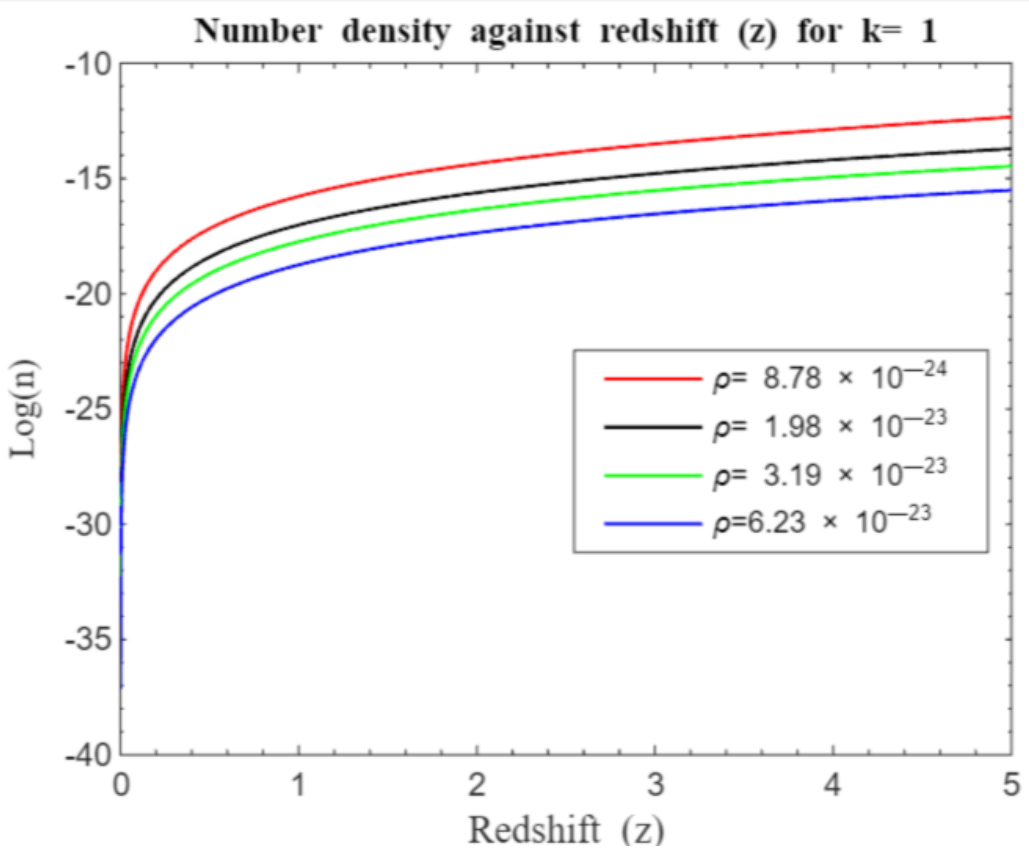

Figure 22: Simulation result for log (n) against redshift z for $z = 0$ to $z = 5$ of the standard Friedmann redshift model for a closed universe with λ.

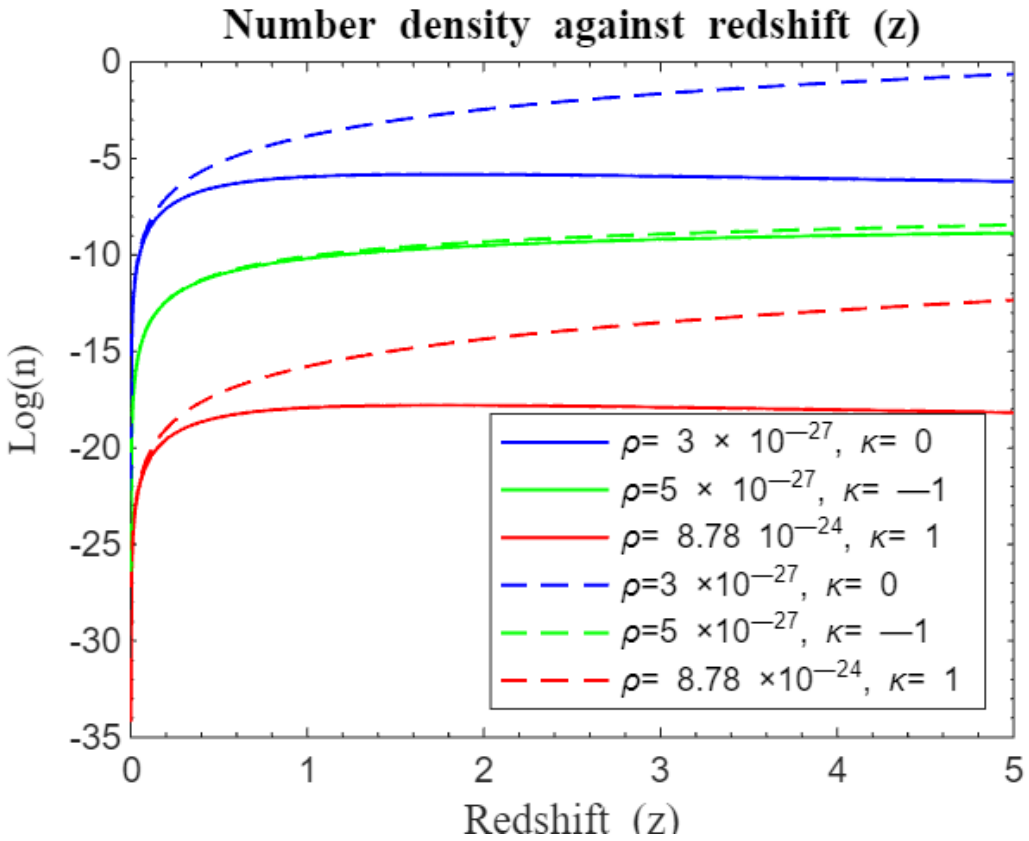

Figure 23: Simulation result for log (n) against redshift z for $z = 0$ to $z = 5$ of the standard Friedmann redshift and the approximate standard Friedmann redshift model.
The solid curves represent the approximate standard Friedmann redshift model while dotted curves represent the standard Friedmann redshift model. Both models without λ.

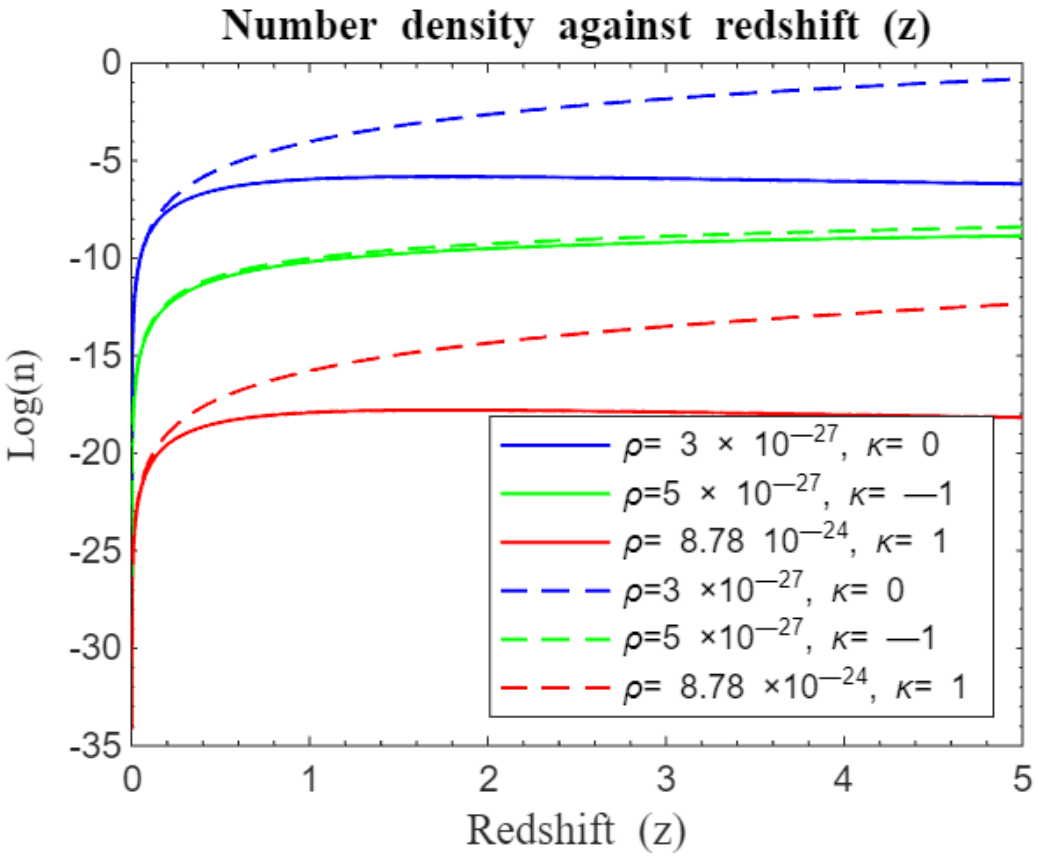

Figure 24: Simulation result for log (n) against redshift z for $z = 0$ to $z = 5$ of the standard Friedmann redshift and the approximate standard Friedmann redshift model.
The solid curves represent the approximate standard Friedmann redshift model without λ while dotted curves represent the standard Friedmann redshift model with λ.

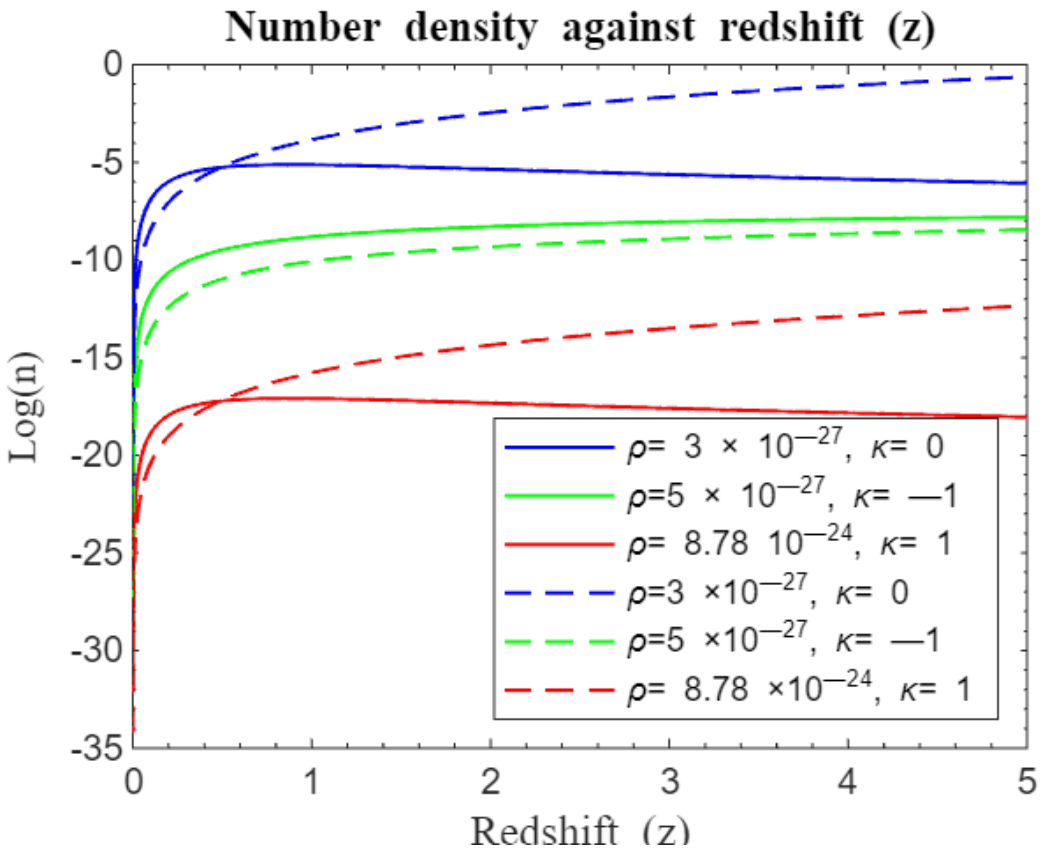

Figure 25: Simulation result for log (n) against redshift z for $z = 0$ to $z = 5$ of the standard Friedmann redshift model and the parametric model.
The solid curves represent the modified standard Friedmann redshift $f(z) = \alpha_1 z + \alpha_2 z^2$ with $\alpha_1 = 2.005$ and $\alpha_2 = 0.005$ of the approximate standard Friedmann model while dotted curves represent the standard Friedmann redshift model. Both models without λ.

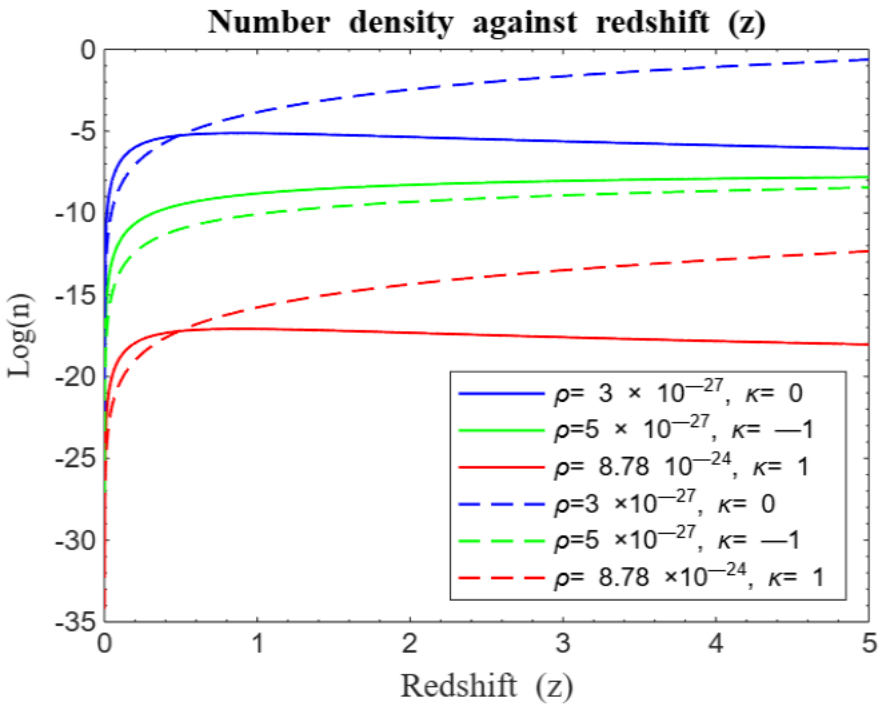

Figure 26: Simulation result for log (n) against redshift z for $z = 0$ to $z = 5$ of the standard Friedmann redshift model and the parametric model.

The solid curves represent the modified standard Friedmann redshift $f(z) = \alpha_1 z + \alpha_2 z^2$ with $\alpha_1 = 2.005$ and $\alpha_2 = 0.005$ of the approximate standard Friedmann redshift model without λ in a matter dominated universe while dotted curves represent the standard Friedmann redshift model with λ.

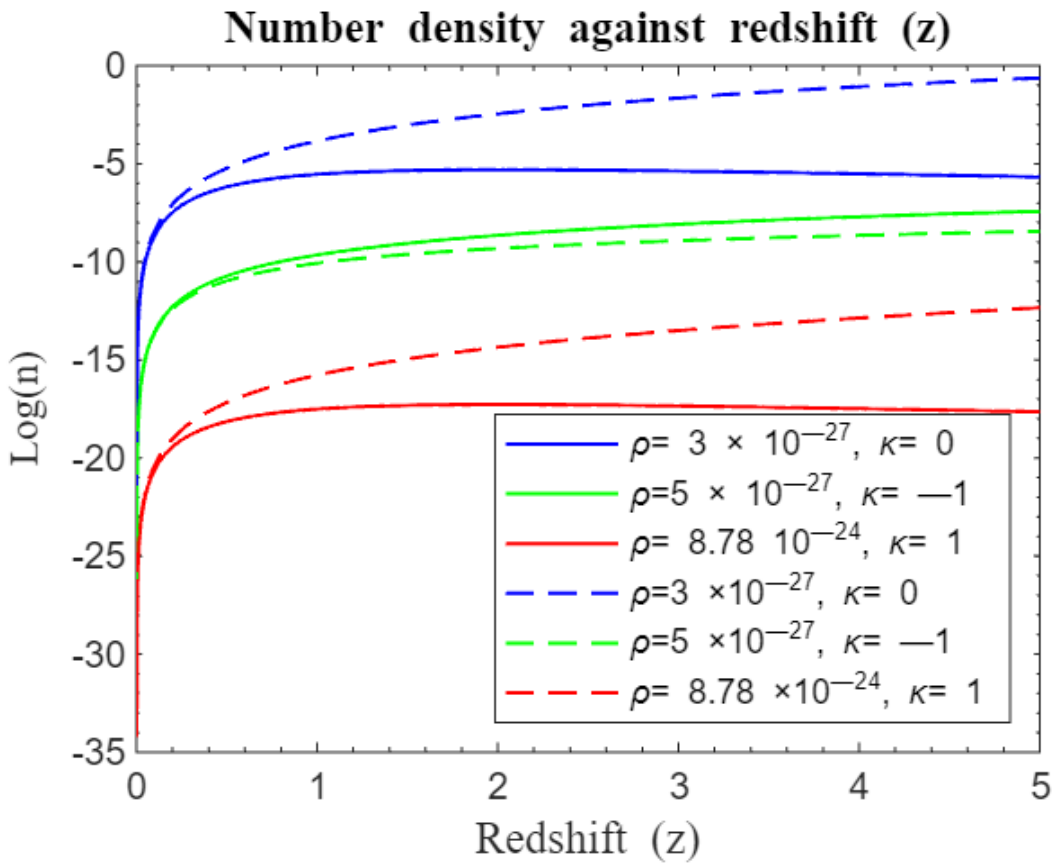

Figure 27: Simulation result for log (n) against redshift z for $z = 0$ to $z = 5$ of the standard Friedmann redshift model and the nonparametric model.
The solid curves represent the modified standard Friedmann redshift $f(z) = z + \gamma(z)^2$ with $\gamma = 0.45$ of the approximate standard Friedmann redshift model while dotted curves represent the standard Friedmann redshift model. Both models without λ.

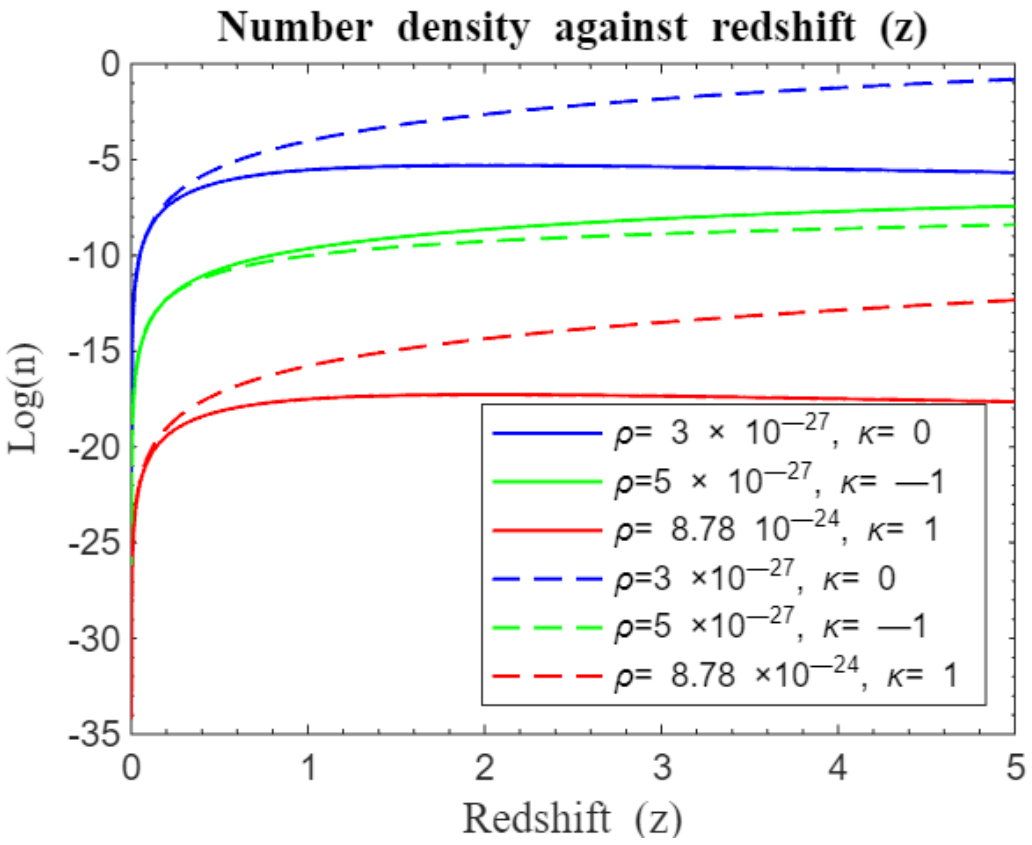

Figure 28: Simulation result for log (n) against redshift z for $z = 0$ to $z = 5$ of the standard Friedmann redshift model and the nonparametric model.
The solid curves represent the modified standard Friedmann redshift $f(z) = z + \gamma(z)^2$ with $\gamma = 0.45$ of the approximate standard Friedmann redshift model without λ while dotted curves represent the standard Friedmann redshift model with λ.

4.4 Discussion

4.4.1 Light intensity redshift relation

In cosmological studies, the relationship between light intensity and redshift is a crucial indicator of galaxy formation and the evolution of large-scale structures.

Figures 1 to 14 demonstrates an exponential decay in light intensity with increasing redshift, consistent with classical theory. This decay results from the dilution of photons as the universe expands. As the universe grows, the wavelengths of photons stretch, causing a decrease in

their energy density. This effect arises because the number of photons remains constant while they are distributed over an increasingly larger volume (Ryden, 2003; S. Weinberg, 2008).

Figures 1 and 2 compare light intensity-redshift relationships under different geometries, both without and with the cosmological constant. These figures reveal that in a flat universe, light intensity decays more rapidly compared to an open or closed universe. The figures also show no significant effect of the cosmological constant on the expansion of the universe.

Figures 3 to 8 illustrate how light intensity changes with redshift across various densities and curvatures. A significant drop in intensity is observed at redshifts $0 < z < 0.5$, with a more gradual decline at higher redshifts. At lower redshifts, the universe is relatively young, which influences intensity. As redshift increases, light comes from increasingly distant regions. The slower intensity decay at higher redshifts may result from cumulative factors like distance, cosmic expansion, and the evolving structure of the universe, reflecting the intricate interplay of spatial distance, temporal evolution, and cosmic morphology (Riess et al., 1998).

In a universe with positive curvature, a closed model akin to a spherical structure is represented. Here, we still observe light attenuation with increase in redshift. A case of positive curvature points to a closed universe whose 3-D space is similar to the surface of a sphere in which the r-sphere wipes out the entire universe leaving it unbounded as the coordinates of the sphere varies from 1 to 0. We observe that light curves seem not to converge for positive curvature according to our model in contrast to earlier works (Langa et al., 2017). As the redshift parameter (z) increases, these geometric differences become more pronounced, showing how curvature affects light behavior. In all geometries, light intensity curves decay more rapidly at lower densities compared to higher densities.

Figures 9 to 14 compare our model with those from previous studies (Langa et al., 2017; Nyagisera et al., 2024). These figures show that high-density universes consistently exhibit higher initial light intensity at early times, regardless of the model. This implies that a denser universe leads to stronger early cosmic structures with higher light intensity.

The gradual decline over time in such models suggests that denser universes, with stronger gravitational influences, retain light longer due to slower expansion rates. In contrast, a flat universe ($\kappa = 0$) shows moderate initial intensity and a steady decrease, while an open universe ($\kappa = -1$) exhibits a lower initial intensity and rapid decline, indicating that accelerated expansion reduces observable light intensity quickly. A closed universe ($\kappa = 1$) shows higher initial intensity and a more prolonged decline, reflecting a slower expansion rate.

Figures 9 and 10 compares our standard Friedmann redshift model with the approximate standard Friedmann redshift model proposed by Langa et al. (2017). Figure 10, which includes the cosmological constant, highlights the role of dark energy. Dark energy is known to accelerate the universe's expansion (Perlmutter et al., 1999; Riess et al., 1998).

The approximate standard Friedmann redshift model suggests that early cosmic structures had higher initial light intensities with a slower decline, indicating that matter's gravitational influence moderate expansion and preserves light intensity. In contrast, the standard Friedmann redshift model shows lower initial light intensity and a more rapid decline, implying that insufficient matter to stabilize the expansion leads to faster reduction in light from early structures.

Further comparison with Nyagisera et al. (2024), who modified the approximate standard Friedmann redshift model with non-parametric (Figures 11 and 12) and parametric (Figures

13 and 14) redshift functions, provides additional insights. Figures 11 and 12 show that light attenuation is more pronounced in the standard Friedmann redshift model compared to the modified standard Friedmann redshift nonparametric model. Even without dark energy, as indicated by the absence of a cosmological constant, the universe still experiences accelerated expansion, suggesting a significant role for dark matter in driving this expansion and redshifting of light (Nyagisera et al., 2024).

Figures 13 and 14 exhibit similar trends in light attenuation with increasing redshift, particularly between redshifts 0 and 1, where attenuation is rapid for flat and closed geometries except in open geometry where our model attenuates slower than parametric model. The standard Friedmann redshift model shows faster attenuation compared to the modified standard Friedmann redshift parametric model, potentially due to factors like photon-electron recombination, Thomson scattering, or accelerated expansion. The absence of a cosmological constant in Figure 13 implies that dark matter may primarily drive accelerated expansion, overshadowing the cosmological constant's effects.

The analytical and graphical simulations as discussed for redshift-light intensity in respective Figures 1 to 8 answers part I of our objective 4. However, for complete picture of the dynamics and evolution of the universe, we proceeded to compare our model with earlier works.

4.4.2 Number density redshift relation

The number density redshift relation helps astronomers understand how the number of galaxies changes over time. By studying how galaxy number density evolves with redshift, scientists can infer the processes of galaxy formation, growth, and the effects of cosmic expansion on galactic structures.

We shall, in particular, focus on the processes of galaxy formation and evolution. Our overall simulations show that the number density of galaxies generally rises at the beginning from $z = 0$ and grows at uneven rate until a plateau before declining, leveling or showing slight rate of increase regardless of the model used.

In particular, our model in Figures 15 to 22 show that there is rapid structure formation at the beginning of the universe for $0 < z < 0.4$ which gradually rises up to around $z \approx 0.8$ before structure formation proceeds at a slower rate regardless of the curvature and density of the universe. However, our model shows that the presence of a cosmological constant seems not to impact structure formation showing that dark energy presence seem to have negligible effects on galaxy formation in contrast to earlier works (Langa et al., 2017). This may probably be because dark energy primarily affects the large-scale expansion of the universe rather than local gravitationally bound systems like galaxies or galaxy clusters.

On small scales, gravity, driven by dark matter and ordinary matter, dominates over the effects of dark energy. We compared our simulations on structure formation with earlier works of Langa et al. (2017) as depicted by Figures 23 and 24. It is clear from these simulations that structure formation for both approximate standard Friedmann redshift model and standard Friedmann redshift model experienced similar rapid galaxy formation rate for both closed and flat universes at early times until $z \approx 0.1$ before our model (standard Friedmann redshift model) made a sharp departure from approximate standard Friedmann model (Langa et al., 2017).

It is also noted that for both models, the open universe curves do not deviate from each other at early times and tend to follow similar structure formation trajectories with our model slightly having an edge over its counterpart in terms of galaxy formation rate at late times.

After the point of departure, structure formation for both closed and flat universes in our model continued steadily but at reduced rate unlike its counterpart that reached a plateau around $z \approx 0.4$ then after this, they started to decline while open universe leveled off in growth.

It is again clear that the effect of a cosmological constant that is associated with dark energy is less impactful as demonstrated by results of Figures 23 and 24. This shows that structural growth of galaxies is influenced by dark matter much more than dark energy. This emphasizes the fact that dark matter is associated with accelerated expansion of the universe and arises as an emergent phenomenon as posited by phenomenological models (Bassett et al., 2015; Nyagisera et al., 2024; Wojtak & Prada, 2016, 2017) .

We again proceeded to compare our model with Nyagisera et al. (2024) as depicted by simulation results in Figures 25 to 28. Our model was compared with the modified standard Friedmann redshift model for parametric and nonparametric functions as shown in Figures 25 to 26 and 27 to 28 respectively.

It is evident from Figures 25 and 26 that there was rapid structure formation at the beginning of the universe for the modified standard Friedmann redshift parametric models than our standard Friedmann redshift model until redshift $z \approx 0.5$ when formation rate was now same and divergent of curves followed hereafter. Structure formation consequently changed with our model maintaining a stead but less rapid galaxy formation for both closed and flat universe after $z \approx 0.5$. However, there is obvious departure for curves of open universe right from the onset of structure formation with our model trailing in number density at early epoch but trying to catch up at later times.

On the other hand, modified standard Friedmann redshift nonparametric model in Figures 27 and 28 compares with our standard Friedmann redshift model in such a way that structure

formation rate is similar at the beginning of the universe for both closed and flat universe only diverging after $z \approx 0.2$. Hereafter, curves from our model depict steady galaxy formation for both closed and flat universe. However, the green curves depicting an open universe follow a similar trajectory to the modified parametric curves, starting together and only differing at later times with ours slightly below the modified parametric green curve. The two universes reaches a plateau at $z \approx 0.4$ before structure formation proceeds at a constant rate.

From figures 15 to 28, we observe high activity in galaxy formation rate at the beginning of the universe than at later times. Formation of cosmic structures seem to have been faster at redshifts up to $0 < z < 0.5$ after which it slowed down.

Galaxy formation is influenced by a variety of factors including the density fluctuations in the early universe and the nature of dark matter. In the early universe, density fluctuations provided the seeds for the formation of structures like galaxies. These fluctuations were more pronounced at smaller redshifts, corresponding to earlier times in the universe's history. As the universe expanded, the density of matter decreased, leading to slower galaxy formation over time (Aghanim et al., 2020).

Dark matter, which constitutes a significant portion of the universe's mass, plays a crucial role in galaxy formation by gravitationally attracting ordinary matter. Studies have shown that dark matter halos, which host galaxies, grow more rapidly at smaller redshifts due to the higher density of matter in the early universe (Wechsler et al., 2006). This observation is in agreement with our results. Also feedback processes, including supernova explosions and black hole activity, regulate the rate of star formation within galaxies.

As the universe ages and galaxies evolve, these feedback mechanisms become more efficient, leading to a slowdown in the formation of new stars. Observations and simulations, like those

conducted by Péroux et al. (2020), highlight the importance of feedback in shaping galaxy properties over cosmic time.

Recent observational studies, such as those analyzed by Huterer & Shafer (2017), indicate that as the universe expands, the gravitational pull between galaxies weakens, contributing to a slowdown in the formation of new galaxies at higher redshifts. These factors collectively contribute to the observed trend of faster galaxy formation at smaller redshifts and a gradual decrease in the rate of formation as redshifts increase or as the universe expands. This balanced expansion results in a relatively stable number density of objects over cosmic time (D. H. Weinberg et al., 2004).

In an open universe with negative curvature, the spatial geometry is hyperbolic, and the expansion continues indefinitely without a collapse. Similarly, in the flat universe, the expansion may decelerate due to matter density, but the presence of dark matter again may lead to an accelerated expansion. This continuous expansion results in a gradual decrease in the growth rate of large-scale structure, leading to a flattening of the number density vs redshift curve (Bond, 1986).

In a universe with positive curvature, the spatial geometry resembles that of a hypersphere. As the universe evolves, the gravitational attraction due to the matter density eventually overcomes the expansion driven by dark energy, leading to a collapse of the universe. This collapse results in a rapid decrease in the observed number density of objects (such as galaxies) as redshift increases (Peebles, 2020). In our case, we did not observe substantial impact of dark energy so that its effect may have been overshadowed by dark matter effects.

The analytical and graphical simulations as discussed for redshift-number density in respect to Figures 15 to 22 answers part II of our objective 4. However, for a comprehensive picture

of the dynamics and evolution of the universe, we proceeded with comparison of our model with other works.

4.5 Comparison with observational data

The study of redshift in galaxies stands as a cornerstone in our quest to understand the processes of structure formation, and evolutionary in the universe. Central to our task, we embarked on the utilization of vast and accurate astronomical datasets of our present time, teeming with measurements of redshift and number density. These datasets are curated to ensure accuracy and freedom from the effects of background geometry or cosmic distance measurement anomalies as much as possible. Leveraging on these datasets, we embarked on comparative analysis, extracting plots that mirrored the parameters of our analytical models. This alignment in scale facilitates a direct comparison between the theoretical constructs delineated by our model and the empirical realities captured by observational data.

We collected observed redshifts between 0 and 5, specifically, for extragalactic galaxies in the infrared spectral region, using Planck 2015 cosmological parameters from the NASA/IPAC Extragalactic Database (NED) (Ade et al., 2016). The distribution of these

retrieved redshifts were plotted, with the bin heights indicating the number of galaxies observed at each redshift, as shown in Figure 29.

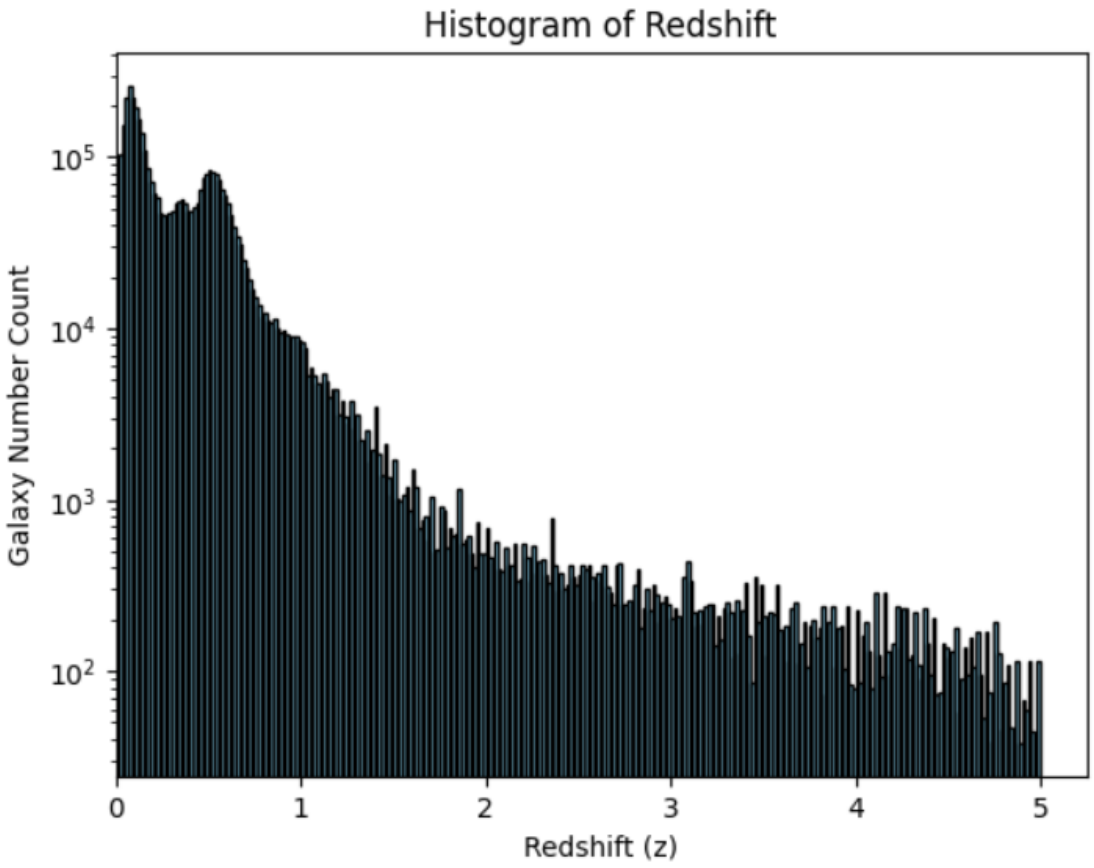

Figure 29: Redshift distribution for NED observed galaxies in infrared spectral region. Source: https://ned.ipac.caltech.edu/

In figure 29, an exponential decrease in the distribution of observed galaxies with increase in redshift was observed. Clearly, there was a burst of galaxy formation in the redshift range $0 < z < 1$ with peak of galaxy formation between $0 < z < 0.8$. This indicated that galaxies were formed at a faster rate in the beginning of the universe $z < 1$ than at later time. This observational data therefore, is in fair agreement with our theoretical model predictions thereby validating the Friedmann model as a valid model for accounting of structure formation and evolution in the universe.

CHAPTER FIVE: CONCLUSION, RECOMMENDATIONS AND PUBLICATION

5.1 Conclusion

The study establishes that light intensity decays exponentially with increasing redshift due to the universe's expansion. This relationship, confirmed by Figures 1 to 14, is in agreement with our classical expectation that attribute the decrease in energy density to photon dilution as the universe expands.

The results highlight that the geometry of the universe significantly impacts light intensity. In a flat universe, light intensity decays more rapidly compared to an open or closed universe, as shown in Figures 1 and 2. For example, a closed universe ($\kappa = 1$) displays higher initial intensity with a slower decline, while an open universe ($\kappa = -1$) shows a faster drop in light intensity. Comparative analysis of models reveals that high-density universes exhibit higher initial light intensities during early times.

Figures 15 to 22 indicate that dark energy has negligible effects on structure formation, contrasting with earlier works. This emphasizes that dark matter, rather than dark energy, drives galaxy formation by influencing local gravitationally bound systems.

Furthermore, the study shows that galaxy formation occurred more rapidly at early times, particularly within the redshift range of $0 < z < 0.5$, as illustrated in Figures 15 to 28. This aligns with the idea that density fluctuations in the early universe, amplified by dark matter, were key in facilitating early galaxy formation (Aghanim et al., 2020).

Observational data from the NASA/IPAC Extragalactic Database, presented in Figure 29, reinforces these findings by showing that there was a galaxy burst between redshifts 0 and 1, which peaked around $z \approx 0.8$. This pattern is consistent with the predictions of our standard Friedmann redshift model used in this work, validating its accuracy in explaining the formation and evolution of cosmic structures.

Together, these conclusions enhance our understanding of the relationship between light intensity, redshift, and structure formation in the universe, while emphasizing the pivotal role of dark matter and cosmic geometry in shaping the universe's evolution.

5.2 Recommendations

The implications of this work extend into several key areas for future research. First, a more subtle approach is needed to model the structure and evolution of the universe, one that better accounts for the complexities of dark energy’s and dark matter's influence on galaxy formation. Second, our results call for more detailed observational campaigns targeting the redshift ranges identified in this study to further investigate the underlying mechanisms driving these processes.

Furthermore, the growing challenges to the cosmological principle suggest that alternative models of the universe, potentially those that allow for more variation on large scales, should be considered.

Lastly, the evidence of rapid galaxy formation at specific redshifts and the crucial role of dark matter in shaping cosmic structures point to gaps in our current understanding that require further exploration.

5.3 Publication

Konga, K., Wamalwa, D., Mwenda, D., & Maitethia, D. (2025). Probing Cosmic Expansion: The Cosmological Implications of Redshift. European Journal of Applied Physics, 7(2), 32–39. https://doi.org/10.24018/ejphysics.2025.7.2.355.

REFERENCES

Ade, P.A., Aghanim, N., Arnaud, M., Ashdown, M., Aumont, J., Baccigalupi, C., Banday, A.J., Barreiro, R.B., Bartlett, J.G., & Bartolo, N. (2016). Planck 2015 results-xiii. Cosmologicalparameters.*Astronomy&Astrophysics*,*594*,A13. https://www.aanda.org/articles/aa/abs/2016/10/aa25830-15/aa25830-15.html

Aghanim, N., Akrami, Y., Ashdown, M., Aumont, J., Baccigalupi, C., Ballardini, M., Banday, A.J., Barreiro, R.B., Bartolo, N., & Basak, S. (2020). Planck 2018 results-VI. Cosmologicalparameters.*Astronomy&Astrophysics*,*641*,A6. https://www.aanda.org/articles/aa/abs/2020/09/aa33910-18/aa33910-18.html

Alam, S., Aubert, M., Avila, S., Balland, C., Bautista, J. E., Bershady, M. A., Bizyaev, D., Blanton, M. R., Bolton, A. S., Bovy, J., Brinkmann, J., Brownstein, J. R., Burtin, E., Chabanier, S., Chapman, M. J., Choi, P. D., Chuang, C.-H., Comparat, J., Cousinou, M.-C., … Zheng, Z. (2021). Completed SDSS-IV extended Baryon Oscillation Spectroscopic Survey: Cosmological implications from two decades of spectroscopic surveys at the Apache Point Observatory. *Physical Review D*, *103*(8), 083533. https://doi.org/10.1103/PhysRevD.103.083533

Alpher, R. A., Bethe, H., & Gamow, G. (1948). The Origin of Chemical Elements. *Physical Review*, *73*(7), 803–804. https://doi.org/10.1103/PhysRev.73.803

Amendola, L. (1998). *Homogeneity and Fractality*.

Bassett, B. A., Fantaye, Y., Hlozek, R., Sabiu, C., & Smith, M. (2015). A tale of two redshifts. *arXiv Preprint arXiv:1312.2593*. https://www.researchgate.net/profile/Yabebal-Fantaye/publication/259220250_A_Tale_of_Two_Redshifts/links/546f4ca30cf24af340c082d9/A-Tale-of-Two-Redshifts.pdf

Bertone, G., Hooper, D., & Silk, J. (2005). Particle dark matter: Evidence, candidates and constraints.*PhysicsReports,405*(5–6),279–390. https://www.sciencedirect.com/science/article/pii/S0370157304003515

Blake, C., & Wall, J. (2002). Measurement of the angular correlation function of radio galaxies from the NRAO VLA Sky Survey. *Monthly Notices of the Royal Astronomical Society, 329*(2), L37–L41. https://academic.oup.com/mnras/article-abstract/329/2/L37/997189

Bond, J. R. (1986). Large Scale Structure in Universes Dominated by Cold Dark Matter. In B. F. Madore & R. B. Tully (Eds.), *Galaxy Distances and Deviations from Universal Expansion* (pp. 255–263). Springer Netherlands. https://doi.org/10.1007/978-94-009-4702-3_43

Brough, S., Collins, C., Demarco, R., Ferguson, H. C., Galaz, G., Holwerda, B., Martinez-Lombilla, C., Mihos, C., & Montes, M. (2020). *The Vera Rubin Observatory Legacy Survey of Space and Time and the Low Surface Brightness Universe* (arXiv:2001.11067). arXiv. http://arxiv.org/abs/2001.11067

Charlier, C. V. L. (1908). Das planetarische Rotationsproblem. *Meddelanden Fran Lunds AstronomiskaObservatoriumSerieI,39*,1–14. https://ui.adsabs.harvard.edu/abs/1908MeLuF..39....1C/abstract

Charlier, C. V. L. (1922). How an infinite world may be built up. *Meddelanden Fran Lunds AstronomiskaObservatoriumSerieI,98*,1–37. https://ui.adsabs.harvard.edu/abs/1922MeLuF..98....1C/abstract

Cohen, A. G., Kaplan, D. B., & Nelson, A. E. (1993). Progress in Electroweak Baryogenesis. *AnnualReviewofNuclearandParticleScience*,*43*(1),27–70. https://doi.org/10.1146/annurev.ns.43.120193.000331

Conn, A. R., Lewis, G. F., Ibata, R. A., Parker, Q. A., Zucker, D. B., McConnachie, A. W., Martin, N. F., Valls-Gabaud, D., Tanvir, N., & Irwin, M. J. (2013). The three-dimensional structure of the M31 satellite system; strong evidence for an inhomogeneous distribution of satellites. *The Astrophysical Journal*, *766*(2), 120. https://iopscience.iop.org/article/10.1088/0004-637X/766/2/120/meta

Damjanov, I., Hwang, H. S., Geller, M. J., & Chilingarian, I. (2014). The number density of quiescent compact galaxies at intermediate redshift. *The Astrophysical Journal*, *793*(1), 39. https://iopscience.iop.org/article/10.1088/0004-637X/793/1/39/meta

de Grijs, R. (2012). Advancing the physics of cosmic distances: Conference summary. *Proceedings of the International Astronomical Union*, *8*(S289), 351–360. https://www.cambridge.org/core/journals/proceedings-of-the-international-astronomical-union/article/advancing-the-physics-of-cosmic-distances-conference-summary/0D7887B334539D9FE60E411A818F811C

Díaz-Pachón, D. A., Hössjer, O., & Marks, R. J. (2023). Sometimes size does not matter. *FoundationsofPhysics*,*53*(1),1.https://idp.springer.com/authorize/casa?redirect_uri=https://link.springer.com/article/10.1007/s10701-022-00650-1&casa_token=sVfK4LD0QJ8AAAAA:UUl16jRQrW2QrXcCQliifkrCaxyRPy7RBcsfj0z67h00_JzVOveVrKZ0tjq1tacLotgMTFM7aNSyUTofiO4

Einstein, A. (1917). On the special and general theory of relativity. *CPAE (English Translation)*,*6*,247–

420.http://markpellaton.com/pdf/alberteinstein/The%20Special%20and%20General%20Theory%20of%20Relativity.pdf

Eisenstein, D. J., & Hu, W. (1998). Baryonic features in the matter transfer function. *The AstrophysicalJournal,496*(2),605.https://iopscience.iop.org/article/10.1086/305424/meta

Ellis, G. F. (2011). Inhomogeneity effects in cosmology. *Classical and Quantum Gravity, 28*(16),164001.https://iopscience.iop.org/article/10.1088/0264-9381/28/16/164001/meta?casa_token=tJgjHq-XwbYAAAAA:rQnKtyXYl3ujsdkQaB4JGWZGAU5bNNubYQmIBrrbYD-u91v3P5psh4FiEFHo63rQmTxnvU5wAovIH6jtPK2aiMqdtOky0A

Farnes, J. S. (2018). A unifying theory of dark energy and dark matter: Negative masses and matter creation within a modified ΛCDM framework. *Astronomy & Astrophysics*, *620*, A92. https://www.aanda.org/articles/aa/abs/2018/12/aa32898-18/aa32898-18.html

Fomin, I., & Chervon, S. (2017). Exact and Approximate Solutions in the Friedmann Cosmology. *Russian Physics Journal*, *60*(3).

Freedman, W. L. (2012). The cosmic distance scale and H0: Past, present, and future. *Proceedings of the International Astronomical Union*, *8*(S289), 3–9. https://www.cambridge.org/core/journals/proceedings-of-the-international-astronomical-union/article/cosmic-distance-scale-and-h0-past-present-and-future/D57F717704392324948CFB6B16800ADB

Friedmann, A. (1922). Curvature of the Universe. *Z. Phys*, *10*, 377.

Gamow, G. (1946). Expanding Universe and the Origin of Elements. *Physical Review*, *70*(7–8), 572–573. https://doi.org/10.1103/PhysRev.70.572.2

Heck, A., & Caputo, F. (1999). *Post-Hipparcos cosmic candles* (Vol. 237). Springer Science &BusinessMedia.https://books.google.com/books?hl=en&lr=&id=AO_6rWuG5isC&oi=fnd&pg=PP11&dq=(Heck+%26+Caputo,+1999).&ots=2WmyfKnSVo&sig=cHVQYAl1kzqRUMgF_zXFRi-w0-A

Hubble, E. (1929). A relation between distance and radial velocity among extra-galactic nebulae. *Proceedings of the National Academy of Sciences*, *15*(3), 168–173. https://doi.org/10.1073/pnas.15.3.168

Huterer, D., & Shafer, D. L. (2017). Dark energy two decades after: Observables, probes, consistency tests. *Reports on Progress in Physics*, *81*(1), 016901. https://iopscience.iop.org/article/10.1088/1361-6633/aa997e/meta?casa_token=8sIA1RuujhAAAAAA:ww3wkbU4mUCMVa_ZoH2OcxTBPdlvHoRSfxDRznES_GSFN8t1Msdy3-11nRGFyJOjIQ_IX9KnbXvD0l5EdsKWhFUX25l4Kw

Ijjas, A., Steinhardt, P. J., & Loeb, A. (2013). Inflationary paradigm in trouble after Planck2013. *Physics Letters B*, *723*(4–5), 261–266.

Ijjas, A., Steinhardt, P. J., & Loeb, A. (2017). Pop goes the universe. *Scientific American*, *316*(2),32–39. https://www.jstor.org/stable/26047449?casa_token=Hqr8Ypsec28AAAAA:hZNRAYxB8azaQTKHx9kjYGNAhER_gQUS1eUGYgM1D0MlQsqQhUwQ_caRXQdSrfTxIUjmZ7SrfMuta2E48xjGhZjfzPBzZeRscZS_WhhTahw_2N8nNyXl-A

Jeakel, A. P., da Silva, J. P., & Velten, H. (2024). Revisiting f (R, T) cosmologies. *PhysicsoftheDarkUniverse*,*43*,101401.https://www.sciencedirect.com/science/article/

pii/S2212686423002340?casa_token=amvzMBqa9bQAAAAA:68hK2uzyut9rDNnpi42JFYzP-WKgFMsOieiRnKuRUx5N8I67-7lUj36A2f03eVdKOztpoeT8K-Tp

Joyce, M., Labini, F. S., Gabrielli, A., Montuori, M., & Pietronero, L. (2005). Basic properties of galaxy clustering in the light of recent results from the Sloan Digital Sky Survey. *Astronomy&Astrophysics*,*443*(1),11–16. https://www.aanda.org/articles/aa/abs/2005/43/aa3658-05/aa3658-05.html

Kolb, E. W., & Turner, M. S. (1990). *The Early Universe. Addison-Wesley Publishing Company.*

Krishnan, C., Mohayaee, R., Colgáin, E. Ó., Sheikh-Jabbari, M. M., & Yin, L. (2021). Does Hubble tension signal a breakdown in FLRW cosmology? *Classical and Quantum Gravity*,*38*(18),184001.https://iopscience.iop.org/article/10.1088/1361-6382/ac1a81/meta?casa_token=NBeyyZP17GoAAAAA:nUIKv0alBh0r0rBvrXKuT270dzhXPXtZFIGWW0YBfKdsPWklNoPeKjypECeU8ngWqUh_B81EQjtJxoqjHNRD8mWTHGGgbw

Labini, F. S. (2011). Inhomogeneities in the universe. *Classical and Quantum Gravity*, *28*(16), 164003. https://iopscience.iop.org/article/10.1088/0264-9381/28/16/164003/meta

Labini, F. S., Montuori, M., & Pietronero, L. (1998). Scale-invariance of galaxy clustering. *PhysicsReports*,*293*(2–4),61–226. https://www.sciencedirect.com/science/article/pii/S0370157397000446

Langa, M., Wamalwa, D. S., & Mito, C. (2017). Relativistic Dynamics in a Matter-Dominated Friedmann Universe. *Journal of Astrophysics and Astronomy*, *38*(4), 71. https://doi.org/10.1007/s12036-017-9482-5

Lemaitre, G. (1925). Note on De Sitter's Universe. *Journal of Mathematics and Physics*, *4*(1–4), 188–192. https://doi.org/10.1002/sapm192541188

Linde, A. D. (1982). A new inflationary universe scenario: A possible solution of the horizon, flatness, homogeneity, isotropy and primordial monopole problems. *Physics Letters B*,*108*(6),389–393. https://www.sciencedirect.com/science/article/pii/0370269382912199

Mather, J. C., Cheng, E. S., Eplee Jr, R. E., Isaacman, R. B., Meyer, S. S., Shafer, R. A., Weiss, R., Wright, E. L., Bennett, C. L., & Boggess, N. W. (1990). A preliminary measurement of the cosmic microwave background spectrum by the Cosmic Background Explorer (COBE) satellite. *Astrophysical Journal, Part 2-Letters (ISSN 0004-637X),Vol.354,May10,1990,p.L37-L40.*,*354*,L37–L40. https://adsabs.harvard.edu/full/record/seri/ApJ../0354/1990ApJ...354L..37M.html

Melia, F. (2022a). A candid assessment of standard cosmology. *Publications of the AstronomicalSocietyofthePacific*,*134*(1042),121001.https://iopscience.iop.org/article/10.1088/1538-3873/aca51f/meta?casa_token=pQ3oeYAhY3cAAAAA:Q3wm9MAMMUPM5MUo3OidyvbmQtIpjTgN62Y6tud01weYio7s0ld_GLii8qX21SVVjVudSxFRbOIhtfVNresT7pjGmTynQA

Melia, F. (2022b). The Friedmann–Lemaître–Robertson–Walker metric. *Modern Physics Letters A*, *37*(03), 2250016. https://doi.org/10.1142/S021773232250016X

Newton, I. (1993). A new theory about light and colors. *American Journal of Physics*, *61*(2), 108–112. https://pubs.aip.org/aapt/ajp/article-abstract/61/2/108/1054295

Ntelis, P. (2016). *The Homogeneity Scale of the universe* (arXiv:1607.03418). arXiv. http://arxiv.org/abs/1607.03418

Nyagisera, R. N., Wamalwa, D., Rapando, B., Awino, C., & Mageto, M. (2024). A Critical Examination of the Standard Cosmological Model: Toward a Modified Framework for Explaining Cosmic Structure Formation and Evolution. *Astronomy*, *3*(1), 43–67. https://www.mdpi.com/2674-0346/3/1/5

Nyenje, P. M., Foppen, J. W., Uhlenbrook, S., & Kulabako, R. (2013). Eutrophication and nutrient release in urban areas of sub-Saharan Africa. *Science of the Total Environment*, *408*(3), 447–455.

Pandey, B., & Sarkar, S. (2016). *An information theory based search for homogeneity on the largest accessible scale*. https://vbudspace.lsdiscovery.in/xmlui/handle/123456789/71

Pâris, I., Petitjean, P., Ross, N. P., Myers, A. D., Aubourg, É., Streblyanska, A., Bailey, S., Armengaud, É., Palanque-Delabrouille, N., & Yèche, C. (2017). The sloan digital sky survey quasar catalog: Twelfth data release. *Astronomy & Astrophysics*, *597*, A79. https://www.aanda.org/articles/aa/abs/2017/01/aa27999-15/aa27999-15.html

Park, C.-G., Hyun, H., Noh, H., & Hwang, J. (2017). The cosmological principle is not in the sky. *Monthly Notices of the Royal Astronomical Society*, *469*(2), 1924–1931. https://academic.oup.com/mnras/article-abstract/469/2/1924/3760286

Pastén, E., & Cárdenas, V. H. (2023). A fractal LTB model cannot explain dark energy. *General Relativity and Gravitation*, *55*(7), 79. https://doi.org/10.1007/s10714-023-03127-2

Peebles, P. J. E. (1980). *The large-scale structure of the universe* (Vol. 12). Princeton universitypress.https://books.google.com/books?hl=en&lr=&id=5uQ9DwAAQBAJ

&oi=fnd&pg=PR11&dq=peebles.+The+Large-Scale+Structure+of+the+Universe&ots=3X6LNJkVHU&sig=2f9ct-JeuEVLPw3ylog0spZmk4Q

Peebles, P. J. E. (2020). *The large-scale structure of the universe* (Vol. 98). Princeton universitypress.https://books.google.com/books?hl=en&lr=&id=L5HUDwAAQBAJ&oi=fnd&pg=PR11&dq=Peebles,+P.+J.+E.+(1980).+%22The+Large-Scale+Structure+of+the+Universe.%22+Princeton+University+Press.&ots=BVe8Dmvn6K&sig=xWn--yOWEHUaEHBd3xkGQGpeUKs

Peebles, P. J. E., & Ratra, B. (2003). The cosmological constant and dark energy. *Reviews of Modern Physics*, *75*(2), 559–606. https://doi.org/10.1103/RevModPhys.75.559

Penzias, A. A., & Wilson, R. W. (1967). A measurement of the background temperature at 1415MHz.*AstronomicalJournal*,*Vol.72*,*p.315*,*72*,315.https://adsabs.harvard.edu/pdf/1967AJ.....72S.315P

Perlmutter, S., Turner, M. S., & White, M. (1999). Constraining dark energy with type Ia supernovae and large-scale structure. *Physical Review Letters*, *83*(4), 670. https://journals.aps.org/prl/abstract/10.1103/PhysRevLett.83.670

Péroux, C., Nelson, D., van de Voort, F., Pillepich, A., Marinacci, F., Vogelsberger, M., & Hernquist, L. (2020). Predictions for the angular dependence of gas mass flow rate and metallicity in the circumgalactic medium. *Monthly Notices of the Royal Astronomical Society*,*499*(2),2462–2473.https://academic.oup.com/mnras/article-abstract/499/2/2462/5909619

Riess, A. G., Filippenko, A. V., Challis, P., Clocchiatti, A., Diercks, A., Garnavich, P. M., Gilliland, R. L., Hogan, C. J., Jha, S., & Kirshner, R. P. (1998). Observational evidence

from supernovae for an accelerating universe and a cosmological constant. *The AstronomicalJournal*,*116*(3),1009.https://iopscience.iop.org/article/10.1086/300499/meta

Ryden, B. (2003). Introduction to Cosmology Addison Wesley. *San Francisco, USA.*

Sakharov, A. D. (1998). VIOLATION OF CP-INVARIANCE, C-ASYMMETRY, AND BARYON ASYMMETRY OF THE UNIVERSE. In Y. A. Trutnev, *In the Intermissions…*(pp.84–87).WORLDSCIENTIFIC. https://doi.org/10.1142/9789812815941_0013

Slipher, V. M. (1915). Spectrographic observations of nebulae. *Popular Astronomy, Vol. 23, p. 21-24, 23*, 21–24. https://adsabs.harvard.edu/full/1915PA.....23...21S

Smoot, G. F., Bennett, C. L., Kogut, A., Wright, E. L., Aymon, J., Boggess, N. W., Cheng, E. S., De Amici, G., Gulkis, S., & Hauser, M. G. (1992). Structure in the COBE differential microwave radiometer first-year maps. *Astrophysical Journal, Part 2-Letters (ISSN 0004-637X), Vol. 396, No. 1, Sept. 1, 1992, p. L1-L5. Research SupportedbyNASA.*,*396*,L1–L5. https://adsabs.harvard.edu/full/1992ApJ...396L...1S7

Springel, V., White, S. D., Jenkins, A., Frenk, C. S., Yoshida, N., Gao, L., Navarro, J., Thacker, R., Croton, D., & Helly, J. (2005). Simulations of the formation, evolution and clustering of galaxies and quasars. *Nature*, *435*(7042), 629–636. https://www.nature.com/articles/nature03597

Tucker, R. W., Walton, T. J., Arrayás, M., & Trueba, J. L. (2019). A new paradigm for the dynamics of the early Universe. *Classical and Quantum Gravity*, *36*(24), 245016. https://iopscience.iop.org/article/10.1088/1361-6382/ab4ecc/meta

Wamalwa, D. S. (2016). On the FriedmannCosmology. *International Journal of Pure and Apllied Mathematics*, *107*(4). https://doi.org/10.12732/ijpam.v107i4.2

Wang, M., Fu, X., Xu, B., Yang, Y., & Chen, Z. (2023). *Testing the FLRW metric with the Hubble and transversal BAO measurements* (arXiv:2305.01268). arXiv. http://arxiv.org/abs/2305.01268

Wechsler, R. H., Zentner, A. R., Bullock, J. S., Kravtsov, A. V., & Allgood, B. (2006). The dependence of halo clustering on halo formation history, concentration, and occupation.*TheAstrophysicalJournal*,*652*(1),71.https://iopscience.iop.org/article/10.1086/507120/meta

Weinberg, D. H., Dave, R., Katz, N., & Hernquist, L. (2004). Galaxy clustering and galaxy bias in a ΛCDM universe. *The Astrophysical Journal*, *601*(1), 1. https://iopscience.iop.org/article/10.1086/380481/meta

Weinberg, S. (1972). *Gravitation and cosmology: Principles and applications of the general theory of relativity*. https://philpapers.org/rec/WEIGAC

Weinberg, S. (1989). The cosmological constant problem. *Reviews of Modern Physics*, *61*(1), 1–23. https://doi.org/10.1103/RevModPhys.61.1

Weinberg,S.(2008).*Cosmology*.OUP.Oxford.https://books.google.com/books?hl=en&lr=&id=2wlREAAAQBAJ&oi=fnd&pg=PR11&dq=Weinberg,+S.+(2008).+Cosmology.+Oxford+University+Press&ots=vkS0j65jZB&sig=EKlzKtmrt_SBqiORHRqRK2b-INg

Wojtak, R., & Prada, F. (2016). Testing the mapping between redshift and cosmic scale factor. *MonthlyNoticesoftheRoyalAstronomicalSociety*,*458*(3),3331–3340. https://academic.oup.com/mnras/article-abstract/458/3/3331/2589357

Wojtak, R., & Prada, F. (2017). Redshift remapping and cosmic acceleration in dark-matter-dominated cosmological models. *Monthly Notices of the Royal Astronomical Society, 470*(4),4493–4511.https://academic.oup.com/mnras/article-abstract/470/4/4493/3873958

Xu, B., Wang, Z., Zhang, K., Huang, Q., & Zhang, J. (2022). Model-independent Test for the Cosmic Distance–Duality Relation with Pantheon and eBOSS DR16 Quasar Sample. *TheAstrophysicalJournal*,*939*(2),115.https://iopscience.iop.org/article/10.3847/1538-4357/ac9793/meta

Yamamoto, K. (2003). Measuring cosmological parameters with the SDSS QSO spatial power spectrum analysis to test the cosmological principle. *Monthly Notices of the Royal Astronomical Society*, *341*(4), 1199–1204. https://academic.oup.com/mnras/article-abstract/341/4/1199/1036396

Appendix I: MATLAB code for light against redshift

MATLAB code for plotting graphs of light intensity against redshift comparing how curvature affects the dynamics and evolution of the universe (figure 1 and 2). $\lambda = 1.19 \times 10^{-52}$ *and* 0 was used to represent curves either with or without cosmological constant.

```
% Case 1: k=0, Flat Universe
rho = 3*10^(-27);
sc = 3*10^8;  % speed of light
R = 9*10^25; % cosmic scale factor equal to value of R(to)
G = 6.67*10^-11; % Gravitational constant
z =0:0.0001:5;
L = 1;
lambda = 0;
kappa =0; % the curvature parameter of the universe, gives value of k
beta = 8*pi*G*c^-4;
a=sqrt((beta*c^2*rho-lambda)/3);
a1 =a*R+sqrt(a^2*R^2-4*kappa);
a2 =a*R+sqrt(a^2*R^2-4*kappa*(1+z).^2);
n1 =2*(a1*(1+z)-a2);
d1 =a1*a2+4*kappa*(1+z);
r = n1./d1;
n =L*(1+kappa*r.^2).^2; % Numerator
d = 4*pi.*(1+z).^2*R.^2.*r.^2; % Denominator
I = log(n./d); % Gives values of intensity of light
plot(z,I,'b-','LineWidth',1)
xlabel('\fontname{Times New Roman}Redshift (z)','FontSize',12)
ylabel('\fontname{Times New Roman}Log(I)','FontSize',11)
title('\fontname{Times New Roman}Light intensity against redshift (z)','FontSize',12)
set(gca, 'XMinorTick','on', 'YMinorTick','on')
set(gca,'xtick',0:1:5)
set(gca, 'XMinorTick','on', 'YMinorTick','on')
hold on
% Case 2: k=-1, Open Universe
% Defining constants
rho = 5*10^-27; % Upper density of the universe
c = 3*10^8;  % speed of light
R = 9*10^25; % cosmic scale factor equal to value of R(to)
G = 6.67*10^-11; % Gravitational constant
z =0:0.0001:5;
L = 1;
lambda = 0;
kappa =-1; % the curvature parameter of the universe, gives value of k
beta = 8*pi*G*c^-4;
```

```
a=sqrt((beta*c^2*rho-lambda)/3);
a1 =a*R+sqrt(a^2*R^2-4*kappa);
a2 =a*R+sqrt(a^2*R^2-4*kappa*(1+z).^2);
n1 =2*(a1*(1+z)-a2);
d1 =a1*a2+4*kappa*(1+z);
r = n1./d1;
n =L*(1+kappa*r.^2).^2; % Numerator
d = 4*pi.*(1+z).^2*R.^2.*r.^2; % Denominator
I = log(n./d); % Gives values of intensity of light
plot(z,I,'g-','LineWidth',1)
% Case 3: k=+1, Closed Universe
% Defining constants
rho = 8.78*10^-25; % Upper density of the universe
c = 3*10^8;  % speed of light
R = 9*10^25; % cosmic scale factor equal to value of R(to)
G = 6.67*10^-11; % Gravitational constant
z =0:0.0001:5;
L = 1;
lambda = 0;
kappa =1; % the curvature parameter of the universe, gives value of k
beta = 8*pi*G*c^-4;
a=sqrt((beta*c^2*rho-lambda)/3);
a1 =a*R+sqrt(a^2*R^2-4*kappa);
a2 =a*R+sqrt(a^2*R^2-4*kappa*(1+z).^2);
n1 =2*(a1*(1+z)-a2);
d1 =a1*a2+4*kappa*(1+z);
r = n1./d1;
n =L*(1+kappa*r.^2).^2; % Numerator
d = 4*pi.*(1+z).^2*R.^2.*r.^2; % Denominator
I = log(n./d); % Gives values of intensity of light
plot(z,I,'r-','LineWidth',1)
legend('\rho= 3 × 10^{—27}, \kappa= 0','\rho=5 × 10^{—27}, \kappa= —1','\rho= 8.78 ×
10^{—25}, \kappa= 1','Location','NorthEast')
hold off
```

Appendix II: MATLAB code for light intensity against redshift for each curvature

MATLAB codes for comparing the effects of density on the evolution of light intensity with increasing redshift of each curvature (figures 3 to 8). $kappa = -1, 0, 1$ was used to give graphs for open, flat and closed universe respectively and $\lambda = 1.19 \times 10^{-52}$ and 0 was used to represent curves either with or without cosmological constant.

```
% Case 1: rho=8.78 *10^-24
rho = 8.78*10^(-24);
c = 3*10^8;  % speed of light
R = 9*10^25; % cosmic scale factor equal to value of R(to)
G = 6.67*10^-11; % Gravitational constant
z =0:0.0001:5;
L = 1;
lambda = 0;
kappa = 1; % the curvature parameter of the universe, gives value of k
beta = 8*pi*G*c^-4;
a=sqrt((beta*c^2*rho-lambda)/3);
a1 =a*R+sqrt(a^2*R^2-4*kappa);
a2 =a*R+sqrt(a^2*R^2-4*kappa*(1+z).^2);
n1 =2*(a1*(1+z)-a2);
d1 =a1*a2+4*kappa*(1+z);
r = n1./d1;
n =L*(1+kappa*r.^2).^2; % Numerator
d = 4*pi.*(1+z).^2*R.^2.*r.^2; % Denominator
I = log(n./d); % Gives values of intensity of light
plot(z,I,'r','LineWidth',1)
xlabel('\fontname{Times New Roman}Redshift (z)','FontSize',12)
ylabel('\fontname{Times New Roman}Log(I)','FontSize',11)
title('\fontname{Times New Roman}Light intensity against redshift (z) for k= 1','FontSize',11)
set(gca, 'XMinorTick','on', 'YMinorTick','on')
set(gca,'xtick',0:1:5)
set(gca, 'XMinorTick','on', 'YMinorTick','on')
hold on
% Case 2: rho=1.98e-23,
% Defining constants
rho = 1.98*10^-23; % Upper density of the universe
c = 3*10^8;  % speed of light
R = 9*10^25; % cosmic scale factor equal to value of R(to)
G = 6.67*10^-11; % Gravitational constant
z =0:0.0001:5;
L = 1;
```

```
lambda = 0;
kappa = 1; % the curvature parameter of the universe, gives value of k
beta = 8*pi*G*c^-4;
a=sqrt((beta*c^2*rho-lambda)/3);
a1 =a*R+sqrt(a^2*R^2-4*kappa);
a2 =a*R+sqrt(a^2*R^2-4*kappa*(1+z).^2);
n1 =2*(a1*(1+z)-a2);
d1 =a1*a2+4*kappa*(1+z);
r = n1./d1;
n =L*(1+kappa*r.^2).^2; % Numerator
d = 4*pi.*(1+z).^2*R.^2.*r.^2; % Denominator
I = log(n./d); % Gives values of intensity of light
plot(z,I,'k','LineWidth',1)
% Case 3: rho=3.19*10^-23
% Defining constants
rho = 3.19*10^-23; % Upper density of the universe
c = 3*10^8;  % speed of light
R = 9*10^25; % cosmic scale factor equal to value of R(to)
G = 6.67*10^-11; % Gravitational constant
z =0:0.0001:5;
L = 1;
lambda = 0;
kappa = 1; % the curvature parameter of the universe, gives value of k
beta = 8*pi*G*c^-4;
a=sqrt((beta*c^2*rho-lambda)/3);
a1 =a*R+sqrt(a^2*R^2-4*kappa);
a2 =a*R+sqrt(a^2*R^2-4*kappa*(1+z).^2);
n1 =2*(a1*(1+z)-a2);
d1 =a1*a2+4*kappa*(1+z);
r = n1./d1;
n =L*(1+kappa*r.^2).^2; % Numerator
d = 4*pi.*(1+z).^2*R.^2.*r.^2; % Denominator
I = log(n./d); % Gives values of intensity of light
plot(z,I,'g','LineWidth',1)
hold on
% Case 4: rho=6.23*e-23
% Defining constants
rho = 6.23*10^-23; % Upper density of the universe
c = 3*10^8;  % speed of light
R = 9*10^25; % cosmic scale factor equal to value of R(to)
G = 6.67*10^-11; % Gravitational constant
z =0:0.0001:5;
L = 1;
lambda = 0;
kappa = 1; % the curvature parameter of the universe, gives value of k
beta = 8*pi*G*c^-4;
```

```
a=sqrt((beta*c^2*rho-lambda)/3);
a1 =a*R+sqrt(a^2*R^2-4*kappa);
a2 =a*R+sqrt(a^2*R^2-4*kappa*(1+z).^2);
n1 =2*(a1*(1+z)-a2);
d1 =a1*a2+4*kappa*(1+z);
r = n1./d1;
n =L*(1+kappa*r.^2).^2; % Numerator
d = 4*pi.*(1+z).^2*R.^2.*r.^2; % Denominator
I = log(n./d); % Gives values of intensity of light
plot(z,I,'b','LineWidth',1)
legend('\rho= 8.78 × 10^{—24}','\rho= 1.98 × 10^{—23}','\rho= 3.19 × 10^{—
23}','\rho=6.23 × 10^{—23}','Location','NorthEast')
hold off
```

Appendix III: MATLAB code for light intensity against redshift for standard Friedmann redshift and approximate standard Friedmann redshift models comparison

MATLAB codes for comparing the standard Friedmann redshift model and approximate standard Friedmann redshift model models' effect of density on the evolution of light intensity with redshift (figures 9 and 10). $\lambda = 1.19 \times 10^{-52}$ *and* 0 was used to represent curves either with or without cosmological constant.

```
% Case 1: k=0, Flat Universe
rho = 3*10^(-27);
c = 3*10^8;  % speed of light
R = 9*10^25; % cosmic scale factor equal to value of R(to)
G = 6.67*10^-11; % Gravitational constant
z =0:0.0001:5;
L = 1;
kappa =0; % the curvature parameter of the universe, gives value of k
beta = 8*pi*G*c^-4;
alpha = rho*R^3;
a1 =beta*c^2*alpha-12*kappa*R;
a2 =((beta*c^2*alpha)*(1+z))-(12*kappa*R);
n1=((sqrt(12*R)*(sqrt(a2)-sqrt(a1)))./(sqrt(a1*a2)+(12*kappa*R))).^2;
n =L*(1+kappa*n1).^2; % Numerator
d0 = ((sqrt(12*R)*(sqrt(a2)-sqrt(a1)))./(sqrt(a1*a2)+(12*kappa*R))).^2;
d1 =4*pi*(1+z).^2*R.^2;
d = d0.*d1; % Denominator
I = log(n./d); % Gives values of intensity of light
plot(z,I,'b','LineWidth',1)
xlabel('\fontname{Times New Roman}Redshift (z)','FontSize',12)
ylabel('\fontname{Times New Roman}Log(I)','FontSize',11)
title('\fontname{Times New Roman}Light intensity against redshift (z)','FontSize',12)
set(gca, 'XMinorTick','on', 'YMinorTick','on')
set(gca,'xtick',0:1:5)
set(gca, 'XMinorTick','on', 'YMinorTick','on')
hold on
% Case 2: k=-1, Open Universe
% Defining constants
rho = 5*10^-27; % Upper density of the universe
c = 3*10^8;  % speed of light
R = 9*10^25;  % cosmic scale factor equal to value of R(to)
G = 6.67*10^-11; % Gravitational constant
z =0:0.0001:5;
L = 1;
```

```
kappa=-1;  % the curvature parameter of the universe, gives value of k
beta = 8*pi*G*c^-4;
alpha = rho*R^3;
a1 =(beta*c^2*alpha)-(12*kappa*R);
a2 =((beta*c^2*alpha)*(1+z))-(12*kappa*R);
n1=((sqrt(12*R)*(sqrt(a2)-sqrt(a1)))./(sqrt(a1*a2)+(12*kappa*R))).^2;
n =L*(1+kappa*n1).^2; % Numerator
d0 = ((sqrt(12*R)*(sqrt(a2)-sqrt(a1)))./(sqrt(a1*a2)+(12*kappa*R))).^2;
d1 =(4*pi*(1+z).^2)*R.^2;
d = d0.*d1; % Denominator
I = log(n./d);% Gives values of intensity of light
plot(z,I,'g','LineWidth',1)
% Case 3: k=+1, Closed Universe
% Defining constants
rho = 8.78*10^-25; % Upper density of the universe
c = 3*10^8;  % speed of light
R = 9*10^25;  % cosmic scale factor equal to value of R(to)
G = 6.67*10^-11; % Gravitational constant
z =0:0.0001:5;
L = 1;
kappa=1;  % the curvature parameter of the universe, gives value of k
beta = 8*pi*G*c^-4;
alpha = rho*R^3;
a1 =(beta*c^2*alpha)-(12*kappa*R);
a2 = ((beta*c^2*alpha)*(1+z))-(12*kappa*R);
n1=((sqrt(12*R)*(sqrt(a2)-sqrt(a1)))./(sqrt(a1*a2)+(12*kappa*R))).^2;
n =L*(1+kappa*n1).^2; % Numerator
d0 = ((sqrt(12*R)*(sqrt(a2)-sqrt(a1)))./(sqrt(a1*a2)+(12*kappa*R))).^2;
d1 =(4*pi*(1+z).^2)*R.^2;
d = d0.*d1; % Denominator
I = log(n./d); % Gives values of intensity of light
plot(z,I,'r','LineWidth',1)
%standard
% Case 1: rho=8.78 *10^-24
rho = 3*10^(-27);
c = 3*10^8;  % speed of light
R = 9*10^25; % cosmic scale factor equal to value of R(to)
G = 6.67*10^-11; % Gravitational constant
z =0:0.0001:5;
L = 1;
lambda = 0;
kappa = 0; % the curvature parameter of the universe, gives value of k
beta = 8*pi*G*c^-4;
a=sqrt((beta*c^2*rho-lambda)/3);
a1 =a*R+sqrt(a^2*R^2-4*kappa);
a2 =a*R+sqrt(a^2*R^2-4*kappa*(1+z).^2);
```

```
n1 =2*(a1*(1+z)-a2);
d1 =a1*a2+4*kappa*(1+z);
r = n1./d1;
n =L*(1+kappa*r.^2).^2; % Numerator
d = 4*pi.*(1+z).^2*R.^2.*r.^2; % Denominator
I = log(n./d); % Gives values of intensity of light
plot(z,I,'b--','LineWidth',1)
hold on
% Case 2: rho=1.98e-23,
% Defining constants
rho = 5*10^-27; % Upper density of the universe
c = 3*10^8;  % speed of light
R = 9*10^25; % cosmic scale factor equal to value of R(to)
G = 6.67*10^-11; % Gravitational constant
z =0:0.0001:5;
L = 1;
lambda = 0;
kappa = -1; % the curvature parameter of the universe, gives value of k
beta = 8*pi*G*c^-4;
a=sqrt((beta*c^2*rho-lambda)/3);
a1 =a*R+sqrt(a^2*R^2-4*kappa);
a2 =a*R+sqrt(a^2*R^2-4*kappa*(1+z).^2);
n1 =2*(a1*(1+z)-a2);
d1 =a1*a2+4*kappa*(1+z);
r = n1./d1;
n =L*(1+kappa*r.^2).^2; % Numerator
d = 4*pi.*(1+z).^2*R.^2.*r.^2; % Denominator
I = log(n./d); % Gives values of intensity of light
plot(z,I,'k--','LineWidth',1)
% Case 3: rho=3.19*10^-23
% Defining constants
rho = 8.78*10^-25; % Upper density of the universe
c = 3*10^8;  % speed of light
R = 9*10^25; % cosmic scale factor equal to value of R(to)
G = 6.67*10^-11; % Gravitational constant
z =0:0.0001:5;
L = 1;
lambda = 0;
kappa = 1; % the curvature parameter of the universe, gives value of k
beta = 8*pi*G*c^-4;
a=sqrt((beta*c^2*rho-lambda)/3);
a1 =a*R+sqrt(a^2*R^2-4*kappa);
a2 =a*R+sqrt(a^2*R^2-4*kappa*(1+z).^2);
n1 =2*(a1*(1+z)-a2);
d1 =a1*a2+4*kappa*(1+z);
r = n1./d1;
```

```
n =L*(1+kappa*r.^2).^2; % Numerator
d = 4*pi.*(1+z).^2*R.^2.*r.^2; % Denominator
I = log(n./d); % Gives values of intensity of light
plot(z,I,'r--','LineWidth',1)
legend('\rho= 3 × 10^{—27}, \kappa= 0','\rho=5 × 10^{—27}, \kappa= —1','\rho= 8.78
10^{—25}, \kappa= 1','\rho=3 ×10^{—27}, \kappa= 0','\rho=5 ×10^{—27}, \kappa= —
1','\rho= 8.78 ×10^{—25}, \kappa= 1','Location','NorthEast')
hold off
```

Appendix IV: MATLAB code for light intensity against redshift for standard Friedmann redshift and parametric models comparison

MATLAB codes for comparing the standard redshift model and parametric models' effect of density on the evolution of light intensity with redshift (figures 11 and 12). $\lambda = 1.19 \times 10^{-52}$ *and* 0 was used to represent curves either with or without cosmological constant.

```
% Case 1: k=0, Flat Universe
rho = 3*10^(-27);
c = 3*10^8;  % speed of light
R = 9*10^25; % cosmic scale factor equal to value of R(to)
G = 6.67*10^-11; % Gravitational constant
z =0:0.0001:5;
L = 1;
kappa =0; % the curvature parameter of the universe, gives value of k
beta = 8*pi*G*c^-4;
epsilon1 = 2.005;
epsilon2 = 0.005;
alpha = rho*R^3;
a1 =(beta*c^2*alpha)-(12*kappa*R);
a2 =((beta*c^2*alpha)*(1+epsilon1*z+epsilon2*z.^2))-(12*kappa*R);
n1=((sqrt(12*R)*(sqrt(a2)-sqrt(a1)))./(sqrt(a1*a2)+(12*kappa*R))).^2;
n =L*(1+kappa*n1).^2; % Numerator
d0 =(sqrt(12*R)*(sqrt(a2)-sqrt(a1)))./(sqrt(a1*a2)+(12*kappa*R))).^2;
d1 =4*pi*(1+epsilon1*z+epsilon2*z.^2).^2 *R.^2;
d = d0.*d1; % Denominator
I = log(n./d); % Gives values of intensity of light
plot(z,I,'b','LineWidth',1)
xlabel('\fontname{Times New Roman}Redshift (z)','FontSize',12)
ylabel('\fontname{Times New Roman}Log(I)','FontSize',11)
title('\fontname{Times New Roman}Light intensity against redshift (z)','FontSize',12)
set(gca, 'XMinorTick','on', 'YMinorTick','on')
set(gca,'xtick',0:1:5)
set(gca, 'XMinorTick','on', 'YMinorTick','on')
hold on
% Case 2: k=-1, Open Universe
rho = 5*10^-27;
c = 3*10^8;  % speed of light
R = 9*10^25; % cosmic scale factor equal to value of R(to)
G = 6.67*10^-11; % Gravitational constant
z =0:0.0001:5;
L = 1;
epsilon1 = 2.005;
```

```
epsilon2 = 0.005;
kappa = -1;% the curvature parameter of the universe, gives value of k
beta = 8*pi*G*c^-4;
alpha = rho*R^3;
a1 = ((beta*c^2*alpha)-(12*kappa*R));
a2 = ((beta*c^2*alpha)*(1+epsilon1*z+epsilon2*z.^2))-(12*kappa*R);
n1=(sqrt(12*R)*(sqrt(a2)-sqrt(a1))./(sqrt(a1*a2)+(12*kappa*R))).^2;
n =L*(1+kappa*n1).^2; % Numerator
d0 = (sqrt(12*R)*(sqrt(a2)-sqrt(a1))./(sqrt(a1*a2)+(12*kappa*R))).^2;
d1 =4*pi*(1+epsilon1*z+epsilon2*z.^2).^2 *R.^2;
d = d0.*d1; % Denominator
I = log(n./d); % Gives values of intensity of light
plot(z,I,'g','LineWidth',1)
hold on
% Case 3: k=+1, Closed Universe
rho = 8.78*10^-25;
c = 3*10^8;  % speed of light
R = 9*10^25;% cosmic scale factor equal to value of R(to)
G = 6.67*10^-11; % Gravitational constant
z =0:0.0001:5;
L = 1;
epsilon1 = 2.005;
epsilon2 = 0.005;
kappa =1;% the curvature parameter of the universe, gives value of k
beta = 8*pi*G*c^-4;
alpha = rho*R^3;
a1 = (beta*c^2*alpha)-(12*kappa*R);
a2 = ((beta*c^2*alpha)*(1+epsilon1*z+epsilon2*z.^2))-(12*kappa*R);
n1=(sqrt(12*R)*(sqrt(a2)-sqrt(a1))./(sqrt(a1*a2)+(12*kappa*R))).^2;
n =L*(1+kappa*n1).^2; % Numerator
d0 = (sqrt(12*R)*(sqrt(a2)-sqrt(a1))./(sqrt(a1*a2)+(12*kappa*R))).^2;
d1 =4*pi*(1+epsilon1*z+epsilon2*z.^2).^2 *R.^2;
d = d0.*d1; % Denominator
I = log(n./d); % Gives values of intensity of light
plot(z,I,'r','LineWidth',1)
hold on
%standard
% Case 1: rho=8.78 *10^-24
rho = 3*10^(-27);
c = 3*10^8;  % speed of light
R = 9*10^25; % cosmic scale factor equal to value of R(to)
G = 6.67*10^-11; % Gravitational constant
z =0:0.0001:5;
L = 1;
lambda = 0;
kappa = 0; % the curvature parameter of the universe, gives value of k
```

```
beta = 8*pi*G*c^-4;
a=sqrt((beta*c^2*rho-lambda)/3);
a1 =a*R+sqrt(a^2*R^2-4*kappa);
a2 =a*R+sqrt(a^2*R^2-4*kappa*(1+z).^2);
n1 =2*(a1*(1+z)-a2);
d1 =a1*a2+4*kappa*(1+z);
r = n1./d1;
n =L*(1+kappa*r.^2).^2; % Numerator
d = 4*pi.*(1+z).^2*R.^2.*r.^2; % Denominator
I = log(n./d); % Gives values of intensity of light
plot(z,I,'b--','LineWidth',1)
hold on
% Case 2: rho=1.98e-23,
% Defining constants
rho = 5*10^-27; % Upper density of the universe
c = 3*10^8;  % speed of light
R = 9*10^25; % cosmic scale factor equal to value of R(to)
G = 6.67*10^-11; % Gravitational constant
z =0:0.0001:5;
L = 1;
lambda = 0;
kappa = -1; % the curvature parameter of the universe, gives value of k
beta = 8*pi*G*c^-4;
a=sqrt((beta*c^2*rho-lambda)/3);
a1 =a*R+sqrt(a^2*R^2-4*kappa);
a2 =a*R+sqrt(a^2*R^2-4*kappa*(1+z).^2);
n1 =2*(a1*(1+z)-a2);
d1 =a1*a2+4*kappa*(1+z);
r = n1./d1;
n =L*(1+kappa*r.^2).^2; % Numerator
d = 4*pi.*(1+z).^2*R.^2.*r.^2; % Denominator
I = log(n./d); % Gives values of intensity of light
plot(z,I,'g--','LineWidth',1)
% Case 3: rho=3.19*10^-23
% Defining constants
rho = 8.78*10^-25; % Upper density of the universe
c = 3*10^8;  % speed of light
R = 9*10^25; % cosmic scale factor equal to value of R(to)
G = 6.67*10^-11; % Gravitational constant
z =0:0.0001:5;
L = 1;
lambda = 0;
kappa = 1; % the curvature parameter of the universe, gives value of k
beta = 8*pi*G*c^-4;
a=sqrt((beta*c^2*rho-lambda)/3);
a1 =a*R+sqrt(a^2*R^2-4*kappa);
```

```
a2 =a*R+sqrt(a^2*R^2-4*kappa*(1+z).^2);
n1 =2*(a1*(1+z)-a2);
d1 =a1*a2+4*kappa*(1+z);
r = n1./d1;
n =L*(1+kappa*r.^2).^2; % Numerator
d = 4*pi.*(1+z).^2*R.^2.*r.^2; % Denominator
I = log(n./d); % Gives values of intensity of light
plot(z,I,'r--','LineWidth',1)
legend('\rho= 3 × 10^{—27}, \kappa= 0','\rho=5 × 10^{—27}, \kappa= —1','\rho= 8.78
10^{—25}, \kappa= 1','\rho=3 ×10^{—27}, \kappa= 0','\rho=5 ×10^{—27}, \kappa= —
1','\rho= 8.78 ×10^{—25}, \kappa= 1','Location','NorthEast')
hold off
```

Appendix V: MATLAB code for light intensity against redshift for standard Friedmann redshift and non-parametric models comparison

MATLAB codes for comparing the standard redshift model and non-parametric models' effect of the universe's density on the evolution of light intensity with redshift (figures 13 and 14). $\lambda = 1.19 \times 10^{-52}$ *and* 0 was used to represent curves either with or without cosmological constant.

```
% Case 1: k=0, Flat Universe
rho = 3*10^(-27);
c = 3*10^8;  % speed of light
R = 9*10^25; % cosmic scale factor equal to value of R(to)
G = 6.67*10^-11; % Gravitational constant
z =0:0.0001:5;
L = 1;
kappa =0; % the curvature parameter of the universe, gives value of k
beta = 8*pi*G*c^-4;
alpha = rho*R^3;
delta=0.45;
a1 =beta*c^2*alpha-12*kappa*R;
a2 =((beta*c^2*alpha)*(1+z+delta^2.*z.^2))-(12*kappa*R);
n1=((sqrt(12*R)*(sqrt(a2)-sqrt(a1)))./(sqrt(a1*a2)+(12*kappa*R))).^2;
n =L*(1+kappa*n1).^2; % Numerator
d0 = ((sqrt(12*R)*(sqrt(a2)-sqrt(a1)))./(sqrt(a1*a2)+(12*kappa*R))).^2;
d1 =4*pi*(1+z+delta^2.*z.^2).^2*R.^2;
d = d0.*d1; % Denominator
I = log(n./d); % Gives values of intensity of light
plot(z,I,'b','LineWidth',1)
xlabel('\fontname{Times New Roman}Redshift (z)','FontSize',12)
ylabel('\fontname{Times New Roman}Log(I)','FontSize',11)
title('\fontname{Times New Roman}Light intensity against redshift (z)','FontSize',12)
set(gca, 'XMinorTick','on', 'YMinorTick','on')
set(gca,'xtick',0:1:5)
set(gca, 'XMinorTick','on', 'YMinorTick','on')
hold on
% Case 2: k=-1, Open Universe
% Defining constants
rho = 5*10^-27; % Upper density of the universe
c = 3*10^8;  % speed of light
R = 9*10^25;  % cosmic scale factor equal to value of R(to)
G = 6.67*10^-11; % Gravitational constant
z =0:0.0001:5;
```

```
L = 1;
kappa=-1;  % the curvature parameter of the universe, gives value of k
beta = 8*pi*G*c^-4;
alpha = rho*R^3;
a1 =(beta*c^2*alpha)-(12*kappa*R);
a2 =((beta*c^2*alpha)*(1+z+delta^2.*z.^2))-(12*kappa*R);
n1=((sqrt(12*R)*(sqrt(a2)-sqrt(a1))))./(sqrt(a1*a2)+(12*kappa*R))).^2;
n =L*(1+kappa*n1).^2; % Numerator
d0 = ((sqrt(12*R)*(sqrt(a2)-sqrt(a1))))./(sqrt(a1*a2)+(12*kappa*R))).^2;
d1 =(4*pi*(1+z+delta^2.*z.^2).^2)*R.^2;
d = d0.*d1; % Denominator
I = log(n./d);% Gives values of intensity of light
plot(z,I,'g','LineWidth',1)
% Case 3: k=+1, Closed Universe
% Defining constants
rho = 8.78*10^-25; % Upper density of the universe
c = 3*10^8;  % speed of light
R = 9*10^25;  % cosmic scale factor equal to value of R(to)
G = 6.67*10^-11; % Gravitational constant
z =0:0.0001:5;
L = 1;
kappa=1;  % the curvature parameter of the universe, gives value of k
beta = 8*pi*G*c^-4;
alpha = rho*R^3;
a1 =(beta*c^2*alpha)-(12*kappa*R);
a2 = ((beta*c^2*alpha)*(1+z+delta^2.*z.^2))-(12*kappa*R);
n1=((sqrt(12*R)*(sqrt(a2)-sqrt(a1))))./(sqrt(a1*a2)+(12*kappa*R))).^2;
n =L*(1+kappa*n1).^2; % Numerator
d0 = ((sqrt(12*R)*(sqrt(a2)-sqrt(a1))))./(sqrt(a1*a2)+(12*kappa*R))).^2;
d1 =(4*pi*(1+z+delta^2.*z.^2).^2)*R.^2;
d = d0.*d1; % Denominator
I = log(n./d); % Gives values of intensity of light
plot(z,I,'r','LineWidth',1)
%standard
% Case 1: rho=8.78 *10^-24
rho = 3*10^(-27);
c = 3*10^8;  % speed of light
R = 9*10^25; % cosmic scale factor equal to value of R(to)
G = 6.67*10^-11; % Gravitational constant
z =0:0.0001:5;
L = 1;
lambda = 0;
kappa = 0; % the curvature parameter of the universe, gives value of k
beta = 8*pi*G*c^-4;
a=sqrt((beta*c^2*rho-lambda)/3);
a1 =a*R+sqrt(a^2*R^2-4*kappa);
```

```
a2 =a*R+sqrt(a^2*R^2-4*kappa*(1+z).^2);
n1 =2*(a1*(1+z)-a2);
d1 =a1*a2+4*kappa*(1+z);
r = n1./d1;
n =L*(1+kappa*r.^2).^2; % Numerator
d = 4*pi.*(1+z).^2*R.^2.*r.^2; % Denominator
I = log(n./d); % Gives values of intensity of light
plot(z,I,'b--','LineWidth',1)
hold on
% Case 2: rho=1.98e-23,
rho = 5*10^-27; % Upper density of the universe
c = 3*10^8;  % speed of light
R = 9*10^25; % cosmic scale factor equal to value of R(to)
G = 6.67*10^-11; % Gravitational constant
z =0:0.0001:5;
L = 1;
lambda = 0;
kappa = -1; % the curvature parameter of the universe, gives value of k
beta = 8*pi*G*c^-4;
a=sqrt((beta*c^2*rho-lambda)/3);
a1 =a*R+sqrt(a^2*R^2-4*kappa);
a2 =a*R+sqrt(a^2*R^2-4*kappa*(1+z).^2);
n1 =2*(a1*(1+z)-a2);
d1 =a1*a2+4*kappa*(1+z);
r = n1./d1;
n =L*(1+kappa*r.^2).^2; % Numerator
d = 4*pi.*(1+z).^2*R.^2.*r.^2; % Denominator
I = log(n./d); % Gives values of intensity of light
plot(z,I,'g--','LineWidth',1)
% Case 3: rho=3.19*10^-23
rho = 8.78*10^-25; % Upper density of the universe
c = 3*10^8;  % speed of light
R = 9*10^25; % cosmic scale factor equal to value of R(to)
G = 6.67*10^-11; % Gravitational constant
z =0:0.0001:5;
L = 1;
lambda = 0;
kappa = 1; % the curvature parameter of the universe, gives value of k
beta = 8*pi*G*c^-4;
a=sqrt((beta*c^2*rho-lambda)/3);
a1 =a*R+sqrt(a^2*R^2-4*kappa);
a2 =a*R+sqrt(a^2*R^2-4*kappa*(1+z).^2);
n1 =2*(a1*(1+z)-a2);
d1 =a1*a2+4*kappa*(1+z);
r = n1./d1;
n =L*(1+kappa*r.^2).^2; % Numerator
```

```
d = 4*pi.*(1+z).^2*R.^2.*r.^2; % Denominator
I = log(n./d); % Gives values of intensity of light
plot(z,I,'r--','LineWidth',1)
legend('\rho= 3 × 10^{—27}, \kappa= 0','\rho=5 × 10^{—27}, \kappa= —1','\rho= 8.78
10^{—25}, \kappa= 1','\rho=3 ×10^{—27}, \kappa= 0','\rho=5 ×10^{—27}, \kappa= —
1','\rho= 8.78 ×10^{—25}, \kappa= 1','Location','NorthEast')
hold off
```

Appendix VI: MATLAB code for number density against redshift

MATLAB code for plotting graphs of number density against redshift comparing how curvature affects the dynamics and evolution of the universe (figures 15 and 16). $\lambda = 1.19 \times 10^{-52}$ and 0 was used to represent curves either with or without cosmological constant.

```
% Case 1: k=0, Flat Universe
rho = 3*10^(-27);
c = 3*10^8;  % speed of light
R = 9*10^25; % cosmic scale factor equal to value of R(to)
G = 6.67*10^-11; % Gravitational constant
z =0:0.0001:5;
N = 1;
lambda = 1.19*10^-52;
kappa =0; % the curvature parameter of the universe, gives value of k
beta = 8*pi*G*c^-4;
a=sqrt((beta*c^2*rho-lambda)/3);
a1 =a*R+sqrt(a^2*R^2-4*kappa);
a2 =a*R+sqrt(a^2*R^2-4*kappa*(1+z).^2);
n1 =2*(a1*(1+z)-a2);
d1 =a1*a2+4*kappa*(1+z);
r = n1./d1;
q = diff(r);
p = [0,q];
n2 = 4*pi*N*p.*r.^2; % Numerator
d = (1+kappa*r.^2).^3; % Denominator
n = log(n2./d); % Gives values of number density of galaxies
plot(z,n,'b-','LineWidth',1)
xlabel('\fontname{Times New Roman}Redshift (z)','FontSize',12)
ylabel('\fontname{Times New Roman}Log(n)','FontSize',11)
title('\fontname{Times New Roman}Number density against redshift (z)','FontSize',12)
set(gca, 'XMinorTick','on', 'YMinorTick','on')
set(gca,'xtick',0:1:5)
set(gca, 'XMinorTick','on', 'YMinorTick','on')
hold on
% Case 2: k=-1, Open Universe
% Defining constants
rho = 5*10^-27; % Upper density of the universe
c = 3*10^8;  % speed of light
R = 9*10^25; % cosmic scale factor equal to value of R(to)
G = 6.67*10^-11; % Gravitational constant
z =0:0.0001:5;
N = 1;
lambda = 1.19*10^-52;
```

```
kappa =-1; % the curvature parameter of the universe, gives value of k
beta = 8*pi*G*c^-4;
a=sqrt((beta*c^2*rho-lambda)/3);
a1 =a*R+sqrt(a^2*R^2-4*kappa);
a2 =a*R+sqrt(a^2*R^2-4*kappa*(1+z).^2);
n1 =2*(a1*(1+z)-a2);
d1 =a1*a2+4*kappa*(1+z);
r = n1./d1;
q = diff(r);
p = [0,q];
n2 = 4*pi*N*p.*r.^2; % Numerator
d = (1+kappa*r.^2).^3; % Denominator
n = log(n2./d); % Gives values of number density of galaxies
plot(z,n,'g-','LineWidth',1)
% Case 3: k=+1, Closed Universe
% Defining constants
rho = 9.28*10^-23; % Upper density of the universe
c = 3*10^8;  % speed of light
R = 9*10^25; % cosmic scale factor equal to value of R(to)
G = 6.67*10^-11; % Gravitational constant
z =0:0.0001:5;
L = 1;
lambda = 1.19*10^-52;
kappa =1; % the curvature parameter of the universe, gives value of k
beta = 8*pi*G*c^-4;
a=sqrt((beta*c^2*rho-lambda)/3);
a1 =a*R+sqrt(a^2*R^2-4*kappa);
a2 =a*R+sqrt(a^2*R^2-4*kappa*(1+z).^2);
n1 =2*(a1*(1+z)-a2);
d1 =a1*a2+4*kappa*(1+z);
r = n1./d1;
q = diff(r);
p = [0,q];
n2 = 4*pi*N*p.*r.^2; % Numerator
d = (1+kappa*r.^2).^3; % Denominator
n = log(n2./d); % Gives values of number density of galaxies
plot(z,n,'r-','LineWidth',1)
legend('\rho= 3 × 10^{—27}, \kappa= 0','\rho=5 × 10^{—27}, \kappa= —1','\rho= 8.78 ×
10^{—25}, \kappa= 1','Location','SouthEast')
hold off
```

Appendix VII: MATLAB code for number density against redshift for each curvature

MATLAB codes for comparing the effects of density on the evolution of number density with increasing redshift of each curvature (figures 17 to 22). $kappa = -1, 0, 1$ was used to give graphs for open, flat and closed universe respectively and $\lambda = 1.19 \times 10^{-52}$ and 0 was used to represent curves either with or without cosmological constant.

```
% Case 1: 8.78*10^-24
rho = 8.78*10^(-24);
c = 3*10^8;  % speed of light
R = 9*10^25; % cosmic scale factor equal to value of R(to)
G = 6.67*10^-11; % Gravitational constant
z =0:0.0001:5;
N = 1;
lambda = 1.19*10^-52;
kappa = 1; % the curvature parameter of the universe, gives value of k
beta = 8*pi*G*c^-4;
a=sqrt((beta*c^2*rho-lambda)/3);
a1 =a*R+sqrt(a^2*R^2-4*kappa);
a2 =a*R+sqrt(a^2*R^2-4*kappa*(1+z).^2);
n1 =2*(a1*(1+z)-a2);
d1 =a1*a2+4*kappa*(1+z);
r = n1./d1;
q = diff(r);
p = [0,q];
n2 = 4*pi*N*p.*r.^2; % Numerator
d = (1+kappa*r.^2).^3; % Denominator
n = log(n2./d); % Gives values of number density of galaxies
plot(z,n,'r','LineWidth',1)
xlabel('\fontname{Times New Roman}Redshift (z)','FontSize',12)
ylabel('\fontname{Times New Roman}Log(n)','FontSize',11)
title('\fontname{Times New Roman}Number density against redshift (z) for k= 1','FontSize',11)
set(gca, 'XMinorTick','on', 'YMinorTick','on')
set(gca,'xtick',0:1:5)
set(gca, 'XMinorTick','on', 'YMinorTick','on')
hold on
% Case 2: rho=1.98*10^-23
% Defining constants
rho = 1.98*10^-23; % Upper density of the universe
c = 3*10^8;  % speed of light
R = 9*10^25; % cosmic scale factor equal to value of R(to)
G = 6.67*10^-11; % Gravitational constant
```

```
z =0:0.0001:5;
N = 1;
lambda = 1.19*10^-52;
kappa = 1; % the curvature parameter of the universe, gives value of k
beta = 8*pi*G*c^-4;
a=sqrt((beta*c^2*rho-lambda)/3);
a1 =a*R+sqrt(a^2*R^2-4*kappa);
a2 =a*R+sqrt(a^2*R^2-4*kappa*(1+z).^2);
n1 =2*(a1*(1+z)-a2);
d1 =a1*a2+4*kappa*(1+z);
r = n1./d1;
q = diff(r);
p = [0,q];
n2 = 4*pi*N*p.*r.^2; % Numerator
d = (1+kappa*r.^2).^3; % Denominator
n = log(n2./d); % Gives values of number density of galaxies
plot(z,n,'k','LineWidth',1)
% Case 3: rho=3.19*10^-26,
% Defining constants
rho = 3.19*10^-23; % Upper density of the universe
c = 3*10^8;  % speed of light
R = 9*10^25; % cosmic scale factor equal to value of R(to)
G = 6.67*10^-11; % Gravitational constant
z =0:0.0001:5;
N = 1;
lambda = 1.19*10^-52;
kappa = 1; % the curvature parameter of the universe, gives value of k
beta = 8*pi*G*c^-4;
a=sqrt((beta*c^2*rho-lambda)/3);
a1 =a*R+sqrt(a^2*R^2-4*kappa);
a2 =a*R+sqrt(a^2*R^2-4*kappa*(1+z).^2);
n1 =2*(a1*(1+z)-a2);
d1 =a1*a2+4*kappa*(1+z);
r = n1./d1;
q = diff(r);
p = [0,q];
n2 = 4*pi*N*p.*r.^2; % Numerator
d = (1+kappa*r.^2).^3; % Denominator
n = log(n2./d); % Gives values of number density of galaxies
plot(z,n,'g','LineWidth',1)
hold on
% Case 4: rho=6.23**10^-23,
% Defining constants
rho = 6.23*10^-23; % Upper density of the universe
c = 3*10^8;  % speed of light
R = 9*10^25; % cosmic scale factor equal to value of R(to)
```

```
G = 6.67*10^-11; % Gravitational constant
z =0:0.0001:5;
N = 1;
lambda = 1.19*10^-52;
kappa = 1; % the curvature parameter of the universe, gives value of k
beta = 8*pi*G*c^-4;
a=sqrt((beta*c^2*rho-lambda)/3);
a1 =a*R+sqrt(a^2*R^2-4*kappa);
a2 =a*R+sqrt(a^2*R^2-4*kappa*(1+z).^2);
n1 =2*(a1*(1+z)-a2);
d1 =a1*a2+4*kappa*(1+z);
r = n1./d1;
q = diff(r);
p = [0,q];
n2 = 4*pi*N*p.*r.^2; % Numerator
d = (1+kappa*r.^2).^3; % Denominator
n = log(n2./d); % Gives values of number density of galaxies
plot(z,n,'b','LineWidth',1)
legend('\rho= 8.78 × 10^{—24}','\rho= 1.98 × 10^{—23}','\rho= 3.19 × 10^{—
23}','\rho=6.23 × 10^{—23}','Location','NorthEast')
hold off
```

Appendix VIII: MATLAB code for number density against redshift for standard Friedmann redshift and approximate standard Friedmann redshift models comparison

MATLAB codes for comparing the standard Friedmann redshift model and approximate standard Friedmann redshift model models' effect of density on the evolution of light intensity with redshift (figures 23 and 24). $\lambda = 1.19 \times 10^{-52}$ and 0 was used to represent curves either with or without cosmological constant.

```
% Case 1: k=0, Flat Universe
rho = 3*10^(-27);
c = 3*10^8;  % speed of light
R = 9*10^25; % cosmic scale factor equal to value of R(to)
G = 6.67*10^-11; % Gravitational constant
z =0:0.0001:5;
N = 1;
kappa =0; % the curvature parameter of the universe, gives value of k
beta = 8*pi*G*c^-4;
alpha = rho*R^3;
a1 =beta*c^2*alpha-12*kappa*R;
a2 =((beta*c^2*alpha)*(1+z))-(12*kappa*R);
r=(sqrt(12*R)*(sqrt(a2)-sqrt(a1)))./(sqrt(a1*a2)+(12*kappa*R));
q = diff(r);
p = [0,q];
n2 = 4*pi*N*p.*r.^2; % Numerator
d = (1+kappa*r.^2).^3; % Denominator
n = log(n2./d); % Gives values of number density of galaxies
plot(z,n,'b','LineWidth',1)
xlabel('\fontname{Times New Roman}Redshift (z)','FontSize',12)
ylabel('\fontname{Times New Roman}Log(n)','FontSize',11)
title('\fontname{Times New Roman}Number density against redshift (z)','FontSize',12)
set(gca, 'XMinorTick','on', 'YMinorTick','on')
set(gca,'xtick',0:1:5)
set(gca, 'XMinorTick','on', 'YMinorTick','on')
hold on
% Case 2: k=-1, Open Universe
% Defining constants
rho = 5*10^-27; % Upper density of the universe
c = 3*10^8;  % speed of light
R = 9*10^25;  % cosmic scale factor equal to value of R(to)
G = 6.67*10^-11; % Gravitational constant
z =0:0.0001:5;
L = 1;
```

```
kappa=-1;  % the curvature parameter of the universe, gives value of k
beta = 8*pi*G*c^-4;
alpha = rho*R^3;
a1 =(beta*c^2*alpha)-(12*kappa*R);
a2 =((beta*c^2*alpha)*(1+z))-(12*kappa*R);
r=(sqrt(12*R)*(sqrt(a2)-sqrt(a1))./(sqrt(a1*a2)+(12*kappa*R));
q = diff(r);
p = [0,q];
n2 = 4*pi*N*p.*r.^2; % Numerator
d = (1+kappa*r.^2).^3; % Denominator
n = log(n2./d); % Gives values of number density of galaxies
plot(z,n,'g','LineWidth',1)
% Case 3: k=+1, Closed Universe
% Defining constants
rho = 8.78*10^-24; % Upper density of the universe
c = 3*10^8;  % speed of light
R = 9*10^25;  % cosmic scale factor equal to value of R(to)
G = 6.67*10^-11; % Gravitational constant
z =0:0.0001:5;
N = 1;
kappa=1;  % the curvature parameter of the universe, gives value of k
beta = 8*pi*G*c^-4;
alpha = rho*R^3;
a1 =(beta*c^2*alpha)-(12*kappa*R);
a2 = ((beta*c^2*alpha)*(1+z))-(12*kappa*R);
r=(sqrt(12*R)*(sqrt(a2)-sqrt(a1))./(sqrt(a1*a2)+(12*kappa*R));
q = diff(r);
p = [0,q];
n2 = 4*pi*N*p.*r.^2; % Numerator
d = (1+kappa*r.^2).^3; % Denominator
n = log(n2./d); % Gives values of number density of galaxies
plot(z,n,'r','LineWidth',1)
%standard
% Case 1: rho=8.78 *10^-24
rho = 3*10^(-27);
c = 3*10^8;  % speed of light
R = 9*10^25; % cosmic scale factor equal to value of R(to)
G = 6.67*10^-11; % Gravitational constant
z =0:0.0001:5;
L = 1;
lambda = 0;
kappa = 0; % the curvature parameter of the universe, gives value of k
beta = 8*pi*G*c^-4;
a=sqrt((beta*c^2*rho-lambda)/3);
a1 =a*R+sqrt(a^2*R^2-4*kappa);
a2 =a*R+sqrt(a^2*R^2-4*kappa*(1+z).^2);
```

```
n1 =2*(a1*(1+z)-a2);
d1 =a1*a2+4*kappa*(1+z);
r = n1./d1;
q = diff(r);
p = [0,q];
n2 = 4*pi*N*p.*r.^2; % Numerator
d = (1+kappa*r.^2).^3; % Denominator
n = log(n2./d); % Gives values of number density of galaxies
plot(z,n,'b--','LineWidth',1)
hold on
% Case 2: rho=1.98e-23,
% Defining constants
rho = 5*10^-27; % Upper density of the universe
c = 3*10^8;  % speed of light
R = 9*10^25; % cosmic scale factor equal to value of R(to)
G = 6.67*10^-11; % Gravitational constant
z =0:0.0001:5;
N = 1;
lambda = 0;
kappa = -1; % the curvature parameter of the universe, gives value of k
beta = 8*pi*G*c^-4;
a=sqrt((beta*c^2*rho-lambda)/3);
a1 =a*R+sqrt(a^2*R^2-4*kappa);
a2 =a*R+sqrt(a^2*R^2-4*kappa*(1+z).^2);
n1 =2*(a1*(1+z)-a2);
d1 =a1*a2+4*kappa*(1+z);
r = n1./d1;
q = diff(r);
p = [0,q];
n2 = 4*pi*N*p.*r.^2; % Numerator
d = (1+kappa*r.^2).^3; % Denominator
n = log(n2./d); % Gives values of number density of galaxies
plot(z,n,'g--','LineWidth',1)
% Case 3: rho=3.19*10^-23
% Defining constants
rho = 8.78*10^-24; % Upper density of the universe
c = 3*10^8;  % speed of light
R = 9*10^25; % cosmic scale factor equal to value of R(to)
G = 6.67*10^-11; % Gravitational constant
z =0:0.0001:5;
N = 1;
lambda = 0;
kappa = 1; % the curvature parameter of the universe, gives value of k
beta = 8*pi*G*c^-4;
a=sqrt((beta*c^2*rho-lambda)/3);
a1 =a*R+sqrt(a^2*R^2-4*kappa);
```

```
a2 =a*R+sqrt(a^2*R^2-4*kappa*(1+z).^2);
n1 =2*(a1*(1+z)-a2);
d1 =a1*a2+4*kappa*(1+z);
r = n1./d1;
q = diff(r);
p = [0,q];
n2 = 4*pi*N*p.*r.^2; % Numerator
d = (1+kappa*r.^2).^3; % Denominator
n = log(n2./d); % Gives values of number density of galaxies
plot(z,n,'r--','LineWidth',1)
legend('\rho= 3 × 10^{—27}, \kappa= 0','\rho=5 × 10^{—27}, \kappa= —1','\rho= 8.78
10^{—24}, \kappa= 1','\rho=3 ×10^{—27}, \kappa= 0','\rho=5 ×10^{—27}, \kappa= —
1','\rho= 8.78 ×10^{—24}, \kappa= 1','Location','SouthEast')
hold off
```

Appendix IX: MATLAB code for number density against redshift for standard Friedmann redshift and parametric models comparison

MATLAB codes for comparing the standard redshift model and parametric models' effect of density on the evolution of light intensity with redshift (figures 25 and 26). $\lambda = 1.19 \times 10^{-52}$ *and* 0 was used to represent curves either with or without cosmological constant.

```
% Case 1: k=0, Flat Universe
rho = 3*10^(-27);
c = 3*10^8;  % speed of light
R = 9*10^25; % cosmic scale factor equal to value of R(to)
G = 6.67*10^-11; % Gravitational constant
z =0:0.0001:5;
N = 1;
kappa =0; % the curvature parameter of the universe, gives value of k
beta = 8*pi*G*c^-4;
epsilon1 = 2.005;
epsilon2 = 0.005;
alpha = rho*R^3;
a1 =(beta*c^2*rho*alpha)-(12*kappa*rho*R);
a2 =((beta*c^2*rho*alpha)*(1+epsilon1*z+epsilon2*z.^2))-(12*kappa*rho*R);
r =((sqrt(12*rho*R)*(sqrt(a2)-sqrt(a1)))./(sqrt(a1*a2)+(12*kappa*rho*R)));
q = diff(r);
p = [0,q];
n2 = 4*pi*N*p.*r.^2; % Numerator
d = (1+kappa*r.^2).^3; % Denominator
n = log(n2./d); % Gives values of number density of galaxies
plot(z,n,'b','LineWidth',1)
xlabel('\fontname{Times New Roman}Redshift (z)','FontSize',12)
ylabel('\fontname{Times New Roman}Log(n)','FontSize',11)
title('\fontname{Times New Roman}Number density against redshift (z)','FontSize',12)
set(gca, 'XMinorTick','on', 'YMinorTick','on')
set(gca,'xtick',0:1:5)
set(gca, 'XMinorTick','on', 'YMinorTick','on')
hold on
% Case 2: k=-1, Open Universe
rho = 5*10^-27;
c = 3*10^8;  % speed of light
R = 9*10^25; % cosmic scale factor equal to value of R(to)
G = 6.67*10^-11; % Gravitational constant
z =0:0.0001:5;
N = 1;
epsilon1 = 2.005;
```

```
epsilon2 = 0.005;
kappa = -1;% the curvature parameter of the universe, gives value of k
beta = 8*pi*G*c^-4;
alpha = rho*R^3;
a1 = ((beta*c^2*rho*alpha)-(12*kappa*rho*R));
a2 = ((beta*c^2*rho*alpha)*(1+epsilon1*z+epsilon2*z.^2))-(12*kappa*rho*R);
r =((sqrt(12*R*rho)*(sqrt(a2)-sqrt(a1))./(sqrt(a1*a2)+(12*kappa*rho*R)));
q = diff(r);
p = [0,q];
n2 = 4*pi*N*p.*r.^2; % Numerator
d = (1+kappa*r.^2).^3; % Denominator
n = log(n2./d); % Gives values of number density of galaxies
plot(z,n,'g','LineWidth',1)
hold on
% Case 3: k=+1, Closed Universe
rho = 8.78*10^-24;
c = 3*10^8;  % speed of light
R = 9*10^25;% cosmic scale factor equal to value of R(to)
G = 6.67*10^-11; % Gravitational constant
z =0:0.0001:5;
N = 1;
epsilon1 = 2.005;
epsilon2 = 0.005;
kappa =1;% the curvature parameter of the universe, gives value of k
beta = 8*pi*G*c^-4;
alpha = rho*R^3;
a1 = (beta*c^2*rho*alpha)-(12*kappa*rho*R);
a2 = ((beta*c^2*rho*alpha)*(1+epsilon1*z+epsilon2*z.^2))-(12*rho*kappa*R);
r =((sqrt(12*rho*R)*(sqrt(a2)-sqrt(a1))./(sqrt(a1*a2)+(12*kappa*rho*R)));
q = diff(r);
p = [0,q];
n2 = 4*pi*N*p.*r.^2; % Numerator
d = (1+kappa*r.^2).^3; % Denominator
n = log(n2./d); % Gives values of number density of galaxies
plot(z,n,'r','LineWidth',1)
hold on
%standard
% Case 1: rho=8.78 *10^-24
rho = 3*10^(-27);
c = 3*10^8;  % speed of light
R = 9*10^25; % cosmic scale factor equal to value of R(to)
G = 6.67*10^-11; % Gravitational constant
z =0:0.0001:5;
N = 1;
lambda = 0;
kappa = 0; % the curvature parameter of the universe, gives value of k
```

```
beta = 8*pi*G*c^-4;
a=sqrt((beta*c^2*rho-lambda)/3);
a1 =a*R+sqrt(a^2*R^2-4*kappa);
a2 =a*R+sqrt(a^2*R^2-4*kappa*(1+z).^2);
n1 =2*(a1*(1+z)-a2);
d1 =a1*a2+4*kappa*(1+z);
r = n1./d1;
q = diff(r);
p = [0,q];
n2 = 4*pi*N*p.*r.^2; % Numerator
d = (1+kappa*r.^2).^3; % Denominator
n = log(n2./d); % Gives values of number density of galaxies
plot(z,n,'b--','LineWidth',1)
hold on
% Case 2: rho=1.98e-23,
% Defining constants
rho = 5*10^-27; % Upper density of the universe
c = 3*10^8;  % speed of light
R = 9*10^25; % cosmic scale factor equal to value of R(to)
G = 6.67*10^-11; % Gravitational constant
z =0:0.0001:5;
N = 1;
lambda = 0;
kappa = -1; % the curvature parameter of the universe, gives value of k
beta = 8*pi*G*c^-4;
a=sqrt((beta*c^2*rho-lambda)/3);
a1 =a*R+sqrt(a^2*R^2-4*kappa);
a2 =a*R+sqrt(a^2*R^2-4*kappa*(1+z).^2);
n1 =2*(a1*(1+z)-a2);
d1 =a1*a2+4*kappa*(1+z);
r = n1./d1;
q = diff(r);
p = [0,q];
n2 = 4*pi*N*p.*r.^2; % Numerator
d = (1+kappa*r.^2).^3; % Denominator
n = log(n2./d); % Gives values of number density of galaxies
plot(z,n,'g--','LineWidth',1)
% Case 3: rho=3.19*10^-23
% Defining constants
rho = 8.78*10^-24; % Upper density of the universe
c = 3*10^8;  % speed of light
R = 9*10^25; % cosmic scale factor equal to value of R(to)
G = 6.67*10^-11; % Gravitational constant
z =0:0.0001:5;
N = 1;
lambda = 0;
```

```
kappa = 1; % the curvature parameter of the universe, gives value of k
beta = 8*pi*G*c^-4;
a=sqrt((beta*c^2*rho-lambda)/3);
a1 =a*R+sqrt(a^2*R^2-4*kappa);
a2 =a*R+sqrt(a^2*R^2-4*kappa*(1+z).^2);
n1 =2*(a1*(1+z)-a2);
d1 =a1*a2+4*kappa*(1+z);
r = n1./d1;
q = diff(r);
p = [0,q];
n2 = 4*pi*N*p.*r.^2; % Numerator
d = (1+kappa*r.^2).^3; % Denominator
n = log(n2./d); % Gives values of number density of galaxies
plot(z,n,'r--','LineWidth',1)
legend('\rho= 3 × 10^{—27}, \kappa= 0','\rho=5 × 10^{—27}, \kappa= —1','\rho= 8.78
10^{—24}, \kappa= 1','\rho=3 ×10^{—27}, \kappa= 0','\rho=5 ×10^{—27}, \kappa= —
1','\rho= 8.78 ×10^{—24}, \kappa= 1','Location','SouthEast')
hold off
```

Appendix X: MATLAB code for number density against redshift for standard Friedmann redshift and non-parametric models comparison

MATLAB codes for comparing the standard redshift model and non-parametric models' effect of density on the evolution of light intensity with redshift (figures 27 and 28). $\lambda = 1.19 \times 10^{-52}$ *and* 0 was used to represent curves either with or without cosmological constant.

```
% Case 1: k=0, Flat Universe
rho = 3*10^(-27);
c = 3*10^8;  % speed of light
R = 9*10^25; % cosmic scale factor equal to value of R(to)
G = 6.67*10^-11; % Gravitational constant
z =0:0.0001:5;
N = 1;
kappa =0; % the curvature parameter of the universe, gives value of k
beta = 8*pi*G*c^-4;
alpha = rho*R^3;
delta=0.45;
a1 =beta*c^2*alpha-12*kappa*R;
a2 =((beta*c^2*alpha)*(1+z + delta^2.*z.^2))-(12*kappa*R);
r=(sqrt(12*R)*(sqrt(a2)-sqrt(a1)))./(sqrt(a1*a2)+(12*kappa*R));
q = diff(r);
p = [0,q];
n2 = 4*pi*N*p.*r.^2; % Numerator
d = (1+kappa*r.^2).^3; % Denominator
n = log(n2./d); % Gives values of number density of galaxies
plot(z,n,'b','LineWidth',1)
xlabel('\fontname{Times New Roman}Redshift (z)','FontSize',12)
ylabel('\fontname{Times New Roman}Log(n)','FontSize',11)
title('\fontname{Times New Roman}Number density against redshift (z)','FontSize',12)
set(gca, 'XMinorTick','on', 'YMinorTick','on')
set(gca,'xtick',0:1:5)
set(gca, 'XMinorTick','on', 'YMinorTick','on')
hold on
% Case 2: k=-1, Open Universe
% Defining constants
rho = 5*10^-27; % Upper density of the universe
c = 3*10^8;  % speed of light
R = 9*10^25;  % cosmic scale factor equal to value of R(to)
G = 6.67*10^-11; % Gravitational constant
z =0:0.0001:5;
```

```
N = 1;
kappa=-1;  % the curvature parameter of the universe, gives value of k
beta = 8*pi*G*c^-4;
alpha = rho*R^3;
a1 =(beta*c^2*alpha)-(12*kappa*R);
a2 =((beta*c^2*alpha)*(1+z+delta^2.*z.^2))-(12*kappa*R);
r=(sqrt(12*R)*(sqrt(a2)-sqrt(a1)))./(sqrt(a1*a2)+(12*kappa*R));
q = diff(r);
p = [0,q];
n2 = 4*pi*N*p.*r.^2; % Numerator
d = (1+kappa*r.^2).^3; % Denominator
n = log(n2./d); % Gives values of number density of galaxies
plot(z,n,'g','LineWidth',1)
% Case 3: k=+1, Closed Universe
% Defining constants
rho = 8.78*10^-24; % Upper density of the universe
c = 3*10^8;  % speed of light
R = 9*10^25;  % cosmic scale factor equal to value of R(to)
G = 6.67*10^-11; % Gravitational constant
z =0:0.0001:5;
N = 1;
kappa=1;  % the curvature parameter of the universe, gives value of k
beta = 8*pi*G*c^-4;
alpha = rho*R^3;
a1 =(beta*c^2*alpha)-(12*kappa*R);
a2 = ((beta*c^2*alpha)*(1+z+delta^2.*z.^2))-(12*kappa*R);
r=(sqrt(12*R)*(sqrt(a2)-sqrt(a1)))./(sqrt(a1*a2)+(12*kappa*R));
q = diff(r);
p = [0,q];
n2 = 4*pi*N*p.*r.^2; % Numerator
d = (1+kappa*r.^2).^3; % Denominator
n = log(n2./d); % Gives values of number density of galaxies
plot(z,n,'r','LineWidth',1)
%standard
% Case 1: rho=8.78 *10^-24
rho = 3*10^(-27);
c = 3*10^8;  % speed of light
R = 9*10^25; % cosmic scale factor equal to value of R(to)
G = 6.67*10^-11; % Gravitational constant
z =0:0.0001:5;
L = 1;
lambda = 1.19*10^-52;
kappa = 0; % the curvature parameter of the universe, gives value of k
beta = 8*pi*G*c^-4;
a=sqrt((beta*c^2*rho-lambda)/3);
a1 =a*R+sqrt(a^2*R^2-4*kappa);
```

```
a2 =a*R+sqrt(a^2*R^2-4*kappa*(1+z).^2);
n1 =2*(a1*(1+z)-a2);
d1 =a1*a2+4*kappa*(1+z);
r = n1./d1;
q = diff(r);
p = [0,q];
n2 = 4*pi*N*p.*r.^2; % Numerator
d = (1+kappa*r.^2).^3; % Denominator
n = log(n2./d); % Gives values of number density of galaxies
plot(z,n,'b--','LineWidth',1)
hold on
% Case 2: rho=1.98e-23,
% Defining constants
rho = 5*10^-27; % Upper density of the universe
c = 3*10^8;  % speed of light
R = 9*10^25; % cosmic scale factor equal to value of R(to)
G = 6.67*10^-11; % Gravitational constant
z =0:0.0001:5;
N = 1;
lambda = 1.19*10^-52;
kappa = -1; % the curvature parameter of the universe, gives value of k
beta = 8*pi*G*c^-4;
a=sqrt((beta*c^2*rho-lambda)/3);
a1 =a*R+sqrt(a^2*R^2-4*kappa);
a2 =a*R+sqrt(a^2*R^2-4*kappa*(1+z).^2);
n1 =2*(a1*(1+z)-a2);
d1 =a1*a2+4*kappa*(1+z);
r = n1./d1;
q = diff(r);
p = [0,q];
n2 = 4*pi*N*p.*r.^2; % Numerator
d = (1+kappa*r.^2).^3; % Denominator
n = log(n2./d); % Gives values of number density of galaxies
plot(z,n,'g--','LineWidth',1)
% Case 3: rho=3.19*10^-23
% Defining constants
rho = 8.78*10^-24; % Upper density of the universe
c = 3*10^8;  % speed of light
R = 9*10^25; % cosmic scale factor equal to value of R(to)
G = 6.67*10^-11; % Gravitational constant
z =0:0.0001:5;
N = 1;
lambda = 1.19*10^-52;
kappa = 1; % the curvature parameter of the universe, gives value of k
beta = 8*pi*G*c^-4;
a=sqrt((beta*c^2*rho-lambda)/3);
```

```
a1 =a*R+sqrt(a^2*R^2-4*kappa);
a2 =a*R+sqrt(a^2*R^2-4*kappa*(1+z).^2);
n1 =2*(a1*(1+z)-a2);
d1 =a1*a2+4*kappa*(1+z);
r = n1./d1;
q = diff(r);
p = [0,q];
n2 = 4*pi*N*p.*r.^2; % Numerator
d = (1+kappa*r.^2).^3; % Denominator
n = log(n2./d); % Gives values of number density of galaxies
plot(z,n,'r--','LineWidth',1)
legend('\rho= 3 × 10^{—27}, \kappa= 0','\rho=5 × 10^{—27}, \kappa= —1','\rho= 8.78
10^{—24}, \kappa= 1','\rho=3 ×10^{—27}, \kappa= 0','\rho=5 ×10^{—27}, \kappa= —
1','\rho= 8.78 ×10^{—24}, \kappa= 1','Location','SouthEast')
hold off
```

Appendix XI: Publication

European Journal of Applied Physics
Vol 7 | Issue 2 | March 2025
ISSN 2684-4451

REVIEW

Probing Cosmic Expansion: The Cosmological Implications of Redshift

Kennedy Konga[1], Dismas Wamalwa[1,*], Dickson Mwenda[1,2], and Daniel Maitethia[1]

ABSTRACT

Understanding the stretching of light wavelengths, or redshift, is essential for unraveling cosmic expansion and the structure of the universe. This paper investigates three redshift mechanisms: Doppler, cosmological, and relativistic redshift in the context of general relativity. While Doppler redshift applies primarily to nearby objects, cosmological redshift, governed by the expansion of the universe within the Friedmann-Lemaître-Robertson-Walker (FLRW) metric, becomes essential at cosmological distances, supporting the Big Bang model. The work of Edwin Hubble, which linked galaxy recessional velocities to their distances in what is now known as the Hubble-Lemaître law, provided a framework for measuring the expansion rate of the universe. Persistent discrepancies in this rate termed the "Hubble tension," continue to inspire debate and investigation. Additionally, this paper highlights essential distance measurement methods used in redshift analysis. Technological advancements, including the James Webb Space Telescope (JWST) and the Dark Energy Spectroscopic Instrument (DESI), are enhancing redshift accuracy, fostering new insights into dark matter, dark energy, and galaxy evolution, as well as probing the fundamental questions of the universe.

Submitted: November 09, 2024
Published: March 25, 2025
10.24018/ejphysics.2025.7.2.355

[1] *Department of Physical Sciences, Meru University of Science and Technology, Kenya.*
[2] *Department of Pure and Applied Science, Kirinyaga University, Kenya.*

* ***Corresponding Author:***
e-mail: dismasw@yahoo.com

Keywords: Cosmological, Redshift, relativistic, telescopes.

I. Introduction

Redshift is a fundamental concept in cosmology and astrophysics, referring to the observed increase in wavelength (or decrease in frequency) of light from an object moving away from the observer. This shift in light serves as key evidence for the universe's expansion, and it plays a critical role in understanding the large-scale structure and dynamics of the cosmos. The redshift-distance relation describes how this redshift correlates with the distance of celestial objects from Earth, providing deep insights into the universe's structure and expansion.

The foundation of this relationship was laid by Edwin Hubble in the late 1920s. His pioneering work, combined with Georges Lemaître's contributions, established what is now known as the Hubble-Lemaître Law. This law connects the velocity of galaxies (derived from their redshifts) to their distance from the observer, with the proportionality constant known as the Hubble constant, which symbolizes the rate of the universe's expansion [1], [2]. The redshift-distance relation remains central to modern cosmology, forming the cornerstone of the Lambda Cold Dark Matter model, which describes the universe's structure, composition, and evolution [3], [4].

Traditional methods of measuring cosmic distances, such as parallax and Cepheid variable stars, were used before the advent of redshift studies to map local regions of the universe. Parallax involves observing the apparent shift in a star's position against distant background stars as Earth orbits the Sun. For more distant objects, astronomers have relied on Cepheid variables, a type of star whose brightness varies predictably, making them reliable standard candles for measuring distances [5].

In more recent decades, several modern methods have further refined the accuracy of cosmic distance measurements, especially for distant galaxies. One such method is the use of Type Ia supernovae, which are standardized by their consistent peak luminosity. These supernovae were instrumental in discovering the universe's accelerated expansion, revealing the presence of dark energy [6], [7]. Baryon